NTNU
Norwegian University of
Science and Technology

Evaluation of Seakeeping Capabilities of a Floating Solar Plant

Trine Aas-Hansen

MASTER THESIS IN MARINE TECHNOLOGY

SPRING 2018

FOR

Trine Aas-Hansen

Evaluation of seakeeping capabilities of a floating solar plant

The company Ocean Sun has developed a concept for floating solar plants based on the use of circular floating collar used for conventional open fish farming plants. Inside the circular floating collar, a membrane is spread out on the water surface, and a large number of rectangular stiff solar panels of conventional construction are mounted. A drainage is arranged in the middle of the membrane to remove occasional water. While the glass-based panels are stiff, and can endure only limited bending loads, the entire collar and membrane structure is very flexible. Thus, wave motions will at least partly, pass through the structure. It is of interest to observe how large the wave motions and damping effect will be for different wave lengths and wave heights. Also it is of interest to observe to which degree water enters the top side of the membrane.

The core activity of the master thesis is a model test in the large towing tank at the Marine Technology Centre in Trondheim, with a 3 m diameter model of such a floating solar plant. The model test is to be performed in cooperation with master students Sindre Selvik and Henrik Markhus, where Selvik and Markhus will focus on forces and deformations of the solar panels using strain gauges, while Aas-Hansen will focus on seakeeping, hydrodynamics and hydroelastic response of the plant in general.

Therefore, the objectives of the master thesis are to:

- Give a general evaluation of the seakeeping properties of the plant, with focus on expected issues like water entering the membrane and excessive deformations

- Evaluate the response of the structure to waves, which might be expressed as a kind of frequency-dependent transfer function

- Evaluate if the presence of the panels influence the wave-induced motions of the structure, including membrane

- Discuss how the results of the model tests can be used to predict the response and seaworthiness in other sea conditions (frequency and amplitude dependence, linearity, effect of panel configuration, …)

- Give recommendations to improvement of the concept, if possible.

In the thesis the candidate shall present his personal contribution to the resolution of problem within the scope of the thesis work.

Theories and conclusions shall be based on mathematical derivations and/or logic reasoning identifying the various steps in the deduction.

The thesis work shall be based on the current state of knowledge in the field of study. The current state of knowledge shall be established through a thorough literature study, the results of this study shall be written into the thesis. The candidate should utilize the existing possibilities for obtaining relevant literature.

The thesis shall be organized in a rational manner to give a clear exposition of results, assessments, and conclusions. The text should be brief and to the point, with a clear language. Telegraphic language should be avoided.

The thesis shall contain the following elements: A text defining the scope, preface, list of contents, summary, main body of thesis, conclusions with recommendations for further work, list of symbols and acronyms, reference and (optional) appendices. All figures, tables and equations shall be numerated.

The supervisor may require that the candidate, in an early stage of the work, present a written plan for the completion of the work. The plan shall include a budget for the use of laboratory or other resources that will be charged to the department. Overruns shall be reported to the supervisor.

The original contribution of the candidate and material taken from other sources shall be clearly defined. Work from other sources shall be properly referenced using an acknowledged referencing system.

The thesis shall be submitted electronically (pdf) in DAIM:
  - Signed by the candidate
  - The text defining the scope (this text) (signed by the supervisor) included
  - Computer code, input files, videos and other electronic appendages can be uploaded in a zip-file in DAIM. Any electronic appendages shall be listed in the main thesis.

The candidate will receive a printed copy of the thesis.

Supervisor   : Professor Sverre Steen
Start   : 12.02.2018
Deadline   : 11.07.2018

Trondheim, 26.02.2018

Sverre Steen
Supervisor

Preface

This master's thesis is written at the Department of Marine Technology at the Norwegian University of Science and Technology during the spring of 2018.
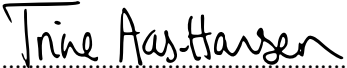
Doing experimental model tests in cooperation with the experienced people at SINTEF Ocean has been extremely educational, providing me with a more physical understanding of the theory I've learned through my studies at NTNU. Conducting the model test in collaboration with two students from the mechanical department at NTNU made me aware of new sides to problems, and it was interesting to be in a situation of sharing knowledge from different areas of expertise. I want to dedicate a special thanks to the employees at SINTEF for their positivity when assisting in preparations and execution of the experiment, especially Henning Braaten, Jørn Jensen and Jens Åge Havmo, and Bjørn-Ola Berge for answering all my questions regarding post-processing.

I would also like to thank SINTEF for funding through the SINTEF-scholarship, and Ocean Sun, Børge Bjørneklett in particular, for their cooperation throughout the process.

My lack of experience in model testing has lead to seeing new aspects in hindsight, that could have been investigated more closely. However, through careful guidance by my supervisor, Sverre Steen, the most important conditions were tested. I am very grateful for the time he has spent on our weekly meetings, helping me understand difficult concepts and guiding my work.

Last but not least, my family, fellow students and friends has made the process of writing this thesis a pleasure through motivating discussions when problems were faced and encouragement in more stressful times.

Trondheim, 29.06.2018

Trine Aas-Hansen

Abstract

The Norwegian company Ocean Sun has proposed a concept of a floating solar plant as an alternative to conventional land-based installations. This thesis reports the results from a model test on the suggested concept, based on double semi-submerged circular HDPE tubes similar to those of gravity fish cages. In the inner basin of these tori, a membrane is fastened to serve as support for solar panels. Three different model configurations were tested: one *without solar panels* on the membrane, one *with solar panels* and one with solar panels *rotated 30°* relative to the incoming waves, all based on the same floating collar and mooring configuration. The models were tested in both regular and irregular waves with the purpose of investigating the seakeeping capabilities of the suggested installation.

The results presented in this thesis include response amplitudes in the frequency domain, mean mooring loads and visual observations of the model's general behavior in waves with focus on wash, deformations and radiated waves. A thorough presentation of error sources in the experiment is included.

The floating solar plant is flexible and contours long period waves. In shorter waves the floating collar is too stiff to fully follow the wave elevation, and the vertical response decreases. The response plots does not show resonance frequencies within the range of tested waves.

Through visual observations the limiting factor for what waves the structure can withstand is considered to be wash from waves breaking over the structure. Significant amounts of water over-topped the installation in steep waves, which may affect the installation in terms of sloshing loads, corrosion and coverage of panels leading to decreased efficiency.

It is suggested to do a model test dedicated to determining the extreme limits of what weather the installation can withstand, with a focus on modeling the strength of the structure accurately. Furthermore, finding mooring load estimations for a specific area and associated weather condition is recommended.

Sammendrag

Det norske firmaet Ocean Sun har foreslått et konsept for et flytende solcelleanlegg som alternativ til konvensjonelle landbaserte installasjoner. Denne oppgaven viser resultatene fra en modelltest som ble utført på dette konseptet som er basert på to flytende HDPE-ringer like de som brukes i fiskemerder. En duk er spent opp i den indre sirkelen av disse flytende ringene, som solcellepaneler skal festes på. Tre forskjellige modellkonfigurasjoner er testet: en *uten paneler* på duken, en *med paneler* og en med paneler *rotert 30°* relativt til innkommende bølger. Alle modellene er basert på den samme flytekragen og den samme fortøyningen. Både regulære og irregulære bølger har blitt testet på alle tre modellkonfigurasjoner. Målet med denne modelltesten har vært å kartlegge respons og bevegelsesmønstrene til det foreslåtte konseptet i bølger.

Resultatene i oppgaven presenterer responsamplituder i frekvensdomenet, midlere fortøyningskrefter og visuelle observasjoner av den typiske oppførselen til modellen, med fokus på overskylling av bølger, deformasjoner og effekten av bølger generert av konstruksjonens bevegelser. En grundig gjennomgang av feilkilder i eksperimentet er inkludert.

Det flytende solcelleanlegget er fleksibelt og følger vannoverflaten i lange bølger. I kortere bølger er flytekragen for stiv til å følge overflatehevingen fullstendig, og den vertikale bevegelsen til modellen avtar. De presenterte responsplottene viser ingen tegn til resonans innenfor det testede intervallet av bølgefrekvenser.

Gjennom visuelle observasjoner er bølger som slår over installasjonen vurdert som den begrensende faktoren for hvilke sjøtilstander anlegget kan tåle. Betydelige mengder vann endte opp på membranen, noe som kan påvirke anlegget ved å innføre krefter av bevegelsene til disse store vannmengdene som virker på anlegget, gi høyere risiko for korrosjonsskader samt føre til nedsatt effekt av solcellene på grunn av vann og eventuelt salt som dekker dem til.

Det er foreslått å foreta en modelltest dedikert til å undersøke hvor ekstreme forhold anlegget kan stå imot, med et fokus på å modellere konstruksjonens styrke presist. Videre anbefales det å finne et estimat på fortøyningskrefter i et gitt område med tilhørende værforhold.

Table of Contents

List of Tables

List of Figures

Nomenclature

General parameters

kW$_p$	Kilowatt peak, measured effect in standard conditions
λ	Scale factor
λ_W	Wave length [m]
H	Wave height [m]
H_s	Significant wave height, used to describe irregular sea [m]
ω	Wave frequency [rad/s]
f	Wave frequency [Hz]
T	Wave period [s]
T_p	Peak period, used to describe irregular sea [s]
ζ_a	Wave amplitude [m]
η_{1a}	Amplitude of motion in surge [m]
η_{3a}	Amplitude of motion in heave [m]
std	Standard deviation
x	Horizontal coordinate, positive in direction of wave propagation [m]
z	Vertical coordinate, positive upwards [m]
N	Newton = kgm/s^2
F_N	Froude number
Re	Reynolds number
$H(f)$	Transfer function
U	Velocity [m/s]
g	Gravitational acceleration [m/s^2]
ν	Kinematic viscosity[m^2/s]
k	Wave number [m^{-1}]
γ	input parameter in JONSWAP spectrum

$S(f)$	Spectral density
f_s	Sampling frequency
f_n	Nyquist frequency

Abbreviations

PV	Photovoltaic
RAO	Response Amplitude Operator
JONSWAP	Joint North Sea Wave Project
HDPE	High Density Polyethylene

Commonly used expressions

Test x000	One test series including several runs
Run xxxx	One run on of the test, leading to one set of measurements
M01-M24	Marker number
z01-z24	Vertical motion for given marker location
x01-x24	Horizontal motion for given marker location
Steepness	Wave height to wave length ratio, H/λ
Model test	The full test performed
Experiment	The full test performed
Model without panels	The tested model with a membrane but without modeled solar panels
Model with panels	The tested model with a membrane and modeled solar panels
Model with rotated panels	The tested model with a membrane and modeled solar panels rotated 30 ° relative to incoming waves

Introduction

1.1 Background and Motivation

Photovoltaic (PV) modules, better known as solar panels, are a source of renewable energy by transforming solar irradiation into electricity. Globally, photovoltaics cover 1.8% of the electricity demand, and in Europe alone they cover 4% (Masson & Brunisholz 2016). Through the Paris Agreement, 195 countries have promised to work towards limiting the global increase of average temperature by decreasing their CO_2-emissions (United Nations 2015). With the world's growing demand for a reduction of greenhouse gas emissions, it is important to look for ways to increase the efficiency and use of renewable energy sources, like photovoltaic plants.

The efficiency of solar panels is dependent on many factors. The study by Rahman et al. (2015) investigates the effect of different parameters on the efficiency of the PV module: level of irradiation, dust on the module, humidity, flow of cooling water and the cell temperature. By keeping the surroundings stable and only changing one parameter at the time, they could measure the dependency of each of them. Through these experiments, it was found that the electrical efficiency decreased by 0.06 % for every 1°C increase in cell temperature for all irradiation intensities. Dubey et al. (2013) also reports a linear decrease in electrical efficiency and power generation with an increasing cell temperature. In other words, a low temperature on the panels is an important factor to ensure the best possible efficiency of the solar plant.

In an article in the magazine Power PV Tech (Reindl 2018), the growing field of floating solar plants is presented, and several benefits listed. According to this article, the beneficial

sides of putting the solar panels on water include:

- No reduced land area where available agricultural land is scarce.
- The cooling effect of the water yields improved effect of 10 to 25% compared to land-based plants.
- Less shading as they are located in open spaces.
- Reduced evaporation if put on water reservoirs.
- Big potential in combination with hydropower as the two energy sources have complimentary weather dependency. The water reservoir used for hydropower will work as a battery for rainy and cloudy days.

Due to these clear benefits, several floating installations have been developed through projects aiming to find good solutions for placing solar plants on water. Through a review of floating photovoltaic installations between 2007 and 2013, Trapani & Redón Santafé (2015) presents several existing projects ranging from small plants of 4kW by Osesol in Vendée, France, to larger ones like the 1157kW installation in Okegawa in Japan from 2012. Some are placed on small water reservoirs, for example in Far Niente Wineries in California where the installation supplies the farm's irrigation system with electricity. This project was one of the first to install solar panels on water, with the motivation of not occupying land used for growing grapes. Santafé et al. (2014) presents a concept like this, using floating photovoltaic modules as a cover on irrigation reservoirs. This idea has several benefits: First of all, the photovoltaic modules provides electricity to the irrigation systems, which is a power demanding process. Secondly, by having the modules float on a reservoir, they will not use the precious agricultural land. Thirdly, the PV-modules will work as a cover on the reservoir, limiting the evaporation of water. Other projects are located on larger lakes, like the grid connected plant by Byro in Bubano, Italy. The developers of this project claim 20-25% increase in power output due to the cooling effect from placing it on water (Trapani & Redón Santafé 2015).

As mentioned, floating photovoltaic installations can make it possible to switch to renewable energy in areas with little available land area, such as islands. Because of their location, the Maltese islands have a high level of daily insolation, which is advantageous for producing solar energy. However, the island is small, and has little land area to spare for an onshore solar plant, and because of this, Trapani & Millar (2013) suggests the use of offshore photovoltaic systems as a source of renewable energy. This project is the first to focus on less protected areas, i.e. not on reservoirs and lakes, and the potential for lower cost and reduction of CO_2-emissions is significant.

Trapani et al. (2013) evaluated floating photovoltaic plants as an alternative to the conventional offshore renewable energy sources: wind, wave and tidal power. The evaluated solar plants consisted of crystalline PV-panels on pontoon type floating structures, which resulted in a simple structure without moving parts. In addition, a flexible thin film solar plant that float on the surface is proposed. These alternatives for floating photovoltaics are compared from a technological and economical perspective: the total area occupied, risk and consequence of collision, how much is produced and the cost of the system. According to this study, the oldest technology, tidal barrages, is the cheapest source of energy with offshore wind as a close competitor. The suggested thin film PV installation is at the same

level as the wind energy, producing the same amount of energy at a smaller geographical footprint. The study confirms that floating photovoltaic plants are able to compete with the existing renewable energy sources and should be investigated more closely.

The Norwegian company Ocean Sun has suggested a concept for a floating solar plant using simple and mostly existing technology. The floating structure consists of a conventional circular high-density polyethylene (HDPE) fish cage, with a flexible membrane fastened to this floating collar (see Figure 1.1). On this thin membrane the solar panels will be attached with the help from aluminum frames. The idea is that since the panels are only separated from the cool water surface by this thin membrane, the heat from the solar cells will be transported through the aluminum frame to the water, ensuring a simple but effective cooling. This concept forms the basis for this thesis.

Figure 1.1: *Demo installation by Ocean sun in Sørfjorden outside Bergen. Photo credit: Ocean Sun*

The concept developed by Ocean Sun, if proved to fulfill their predictions, may be beneficial in developing tomorrows solar plants. The solution is simple and the fact that the concept utilizes standard parts and require little design work and special production, gives it potential for lower investment costs. The natural cooling from the sea surface is a simple way to ensure a stable and low temperature in the solar cells, and the floating structure will solve the problem with space in areas where the electricity production compete with agriculture for land areas.

1.2 Research Questions

When considering the suggested concept presented above, there are several questions that are interesting to address in order to investigate the potential for such an installation, and to know more about its working limits. How does such a structure behave in waves? How is the response affected by the membrane and the solar panels? And is there a risk of water washing over the membrane, leaving salt on the modules and affecting the motion? How large are the loads on the panels, and could they result in high strain values damaging the solar cells? It will also be important to know more about the mooring loads and optimal mooring configurations for such a structure. All of these aspects are important when considering the choice of location for this floating solar plant.

1.3 Previous Work

To the authors knowledge, there is not much literature describing the exact structure suggested by Ocean Sun. However, this installation is based on the same type of floating collar as the one used for gravity fish cages. Because of this, it is natural to investigate what work has previously been done analyzing the response and dynamic behavior of this type of fish cage.

The gravity fish cage typically consists of a floating collar made up from two HDPE tubes, a fish net, a bottom ring with sinking weights and mooring lines. Several experimental and numerical analyses have been performed to learn more about the response of fish cages, and the forces affecting it in waves and current.

Colbourne & Allen (2001) did measurements of the wave motion and the mooring loads on a full-scale fish cage like the one described above in relatively bad weather conditions. They found no apparent correlation between the sea state and the mooring loads and concluded that the mooring loads must be dominated by current and wind loads. This structure had a 5-meter-deep net cage under the surface, making it more exposed to current loads than the floating solar plant presented by Ocean Sun, which has its full structure on the sea surface. In the same study, Colbourne & Allen (2001) also did a model test on a suggested fish cage design for more exposed areas. This model test resulted in response plots in both surge and heave for different mooring configurations, showing a distinct reduction in heave motion for one of their mooring configurations at the cost of larger surge motion for long wave periods. This should be kept in mind when considering how the floating solar plant shall be moored to the sea floor: Which motions are more critical for the structure and its environments? This also indicate that if the chosen mooring configuration in a model test deviates from the full-scale configuration, this might be an significant error source when evaluating the structure's response in waves.

Newman (1977) analyzed the motion of a floating slender torus in waves small compared to the torus radius. He found that the presence of an internal basin resulted in standing waves with a dominating effect on the hydrodynamics of the structure, resulting in oscillating motions for some wave frequencies. These effects may change in a model test through viscous and nonlinear effects which were neglected in Newman's calculations. In addition, his studies were restricted to very short waves. A floating solar plant will experience short waves, but the response in longer waves also needs to be investigated when evaluating the seakeeping abilities of such a structure. Also, short waves will be more affected by the membrane with panels, making Newman's analysis less relevant.

Dong et al. (2010) and Xu et al. (2011) have both simulated the response of a gravity cage in regular and irregular waves. These fish cages included the floating rings, net cage, moorings and weights. Mooring line tension and heave and surge motion was calculated, and transfer functions developed. In addition, the numerical calculations were validated by model tests. Figures 1.2a and 1.2b show the resulting transfer functions in heave from their numerical and experimental tests.

Through a numerical simulation of a semi-submerged floater and fish cage system, Li et al. (2013) draw several conclusions about the motions of the system in regular waves as well
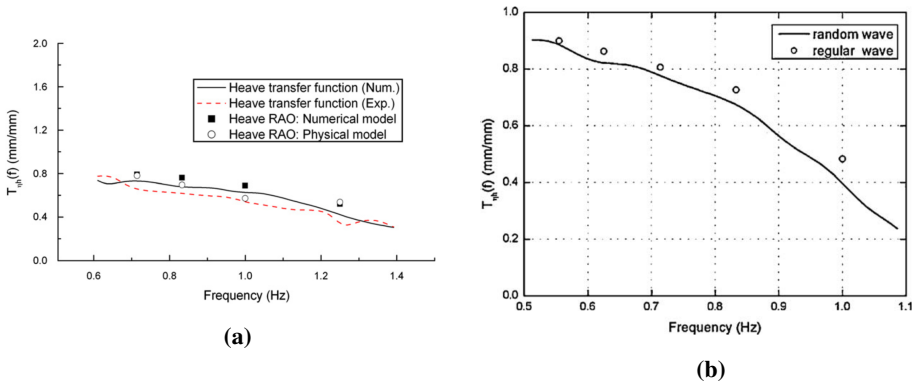
Figure 1.2: *Heave transfer functions from Xu et al. (2011) (1.2a) and Dong et al. (2010) (1.2b)*

as in current. First of all, for the tested waves it was observed that the floater follows the water particle motion, which means large deformations of the floater in waves. However, when testing how the floater was affected by the net cage, the vertical motion decreased as a result of the extra weight of the system. The horizontal motions were also affected by the net, but these were enhanced by the forces from the moving underwater net. This may indicate that the vertical motion for the presented solar plant may be larger than that of a fish cage, and the horizontal motions smaller. The current mostly affects the net, and the net will then affect the floater. Without the net cage, as in the concept by Ocean sun, it is reasonable to assume that the current loads will be considerably reduced.

Kristiansen & Faltinsen (2015) did experimental and numerical simulations of a circular fish cage in order to test the sensitivity of different parameters. The model test was also in this study done to validate numerical simulations, which again was used to test the sensitivity of different parameters in order to answer which factors that are important when modeling such an installation in waves and current. For instance, they tested the sensitivity to changes in cross-sectional diameter, net depth and stiffness of the cage as well as other model dimensions. They checked how numerical parameters like mesh size and number of modes affected the results and they performed simulations with different loads. Their conclusion said that the mooring loads are not affected significantly by most variations. The two exceptions that were found was when the floater was modeled as rigid, and when the nylon for the net cage had an unrealistically low stiffness. These results indicate that the stiffness of the floating collar is more important to model correctly than other parameters.

The studies related to the doctoral thesis of Li (2017) compares model tests with low-frequency slender body theory and numerical simulations of a floating flexible torus with horizontal moorings in regular deep-water waves. The study showed good agreement between the different sets of results for the first harmonic component. Figure 1.3 shows the calculated heave amplitude transfer function through low-frequency slender body theory with and without Haskind relationship, and results from WAMIT using higher order Boundary Element method. It can be seen that the response of the torus is dependent on the different positions on the model. $\beta = \pi$ is in front of the model, towards the incoming

waves. Here, the value of the transfer function is close to one for all tested wavelengths, which indicates that the vertical response amplitude is equal to the wave elevation, and the structure is following the waves in front. At $\beta = \pi/2$ or 90 degrees, the response is quite different, it goes to zero as the waves become shorter. When moving backwards on the model to $\beta = 0$, the higher order results from WAMIT shows larger oscillatory motions.
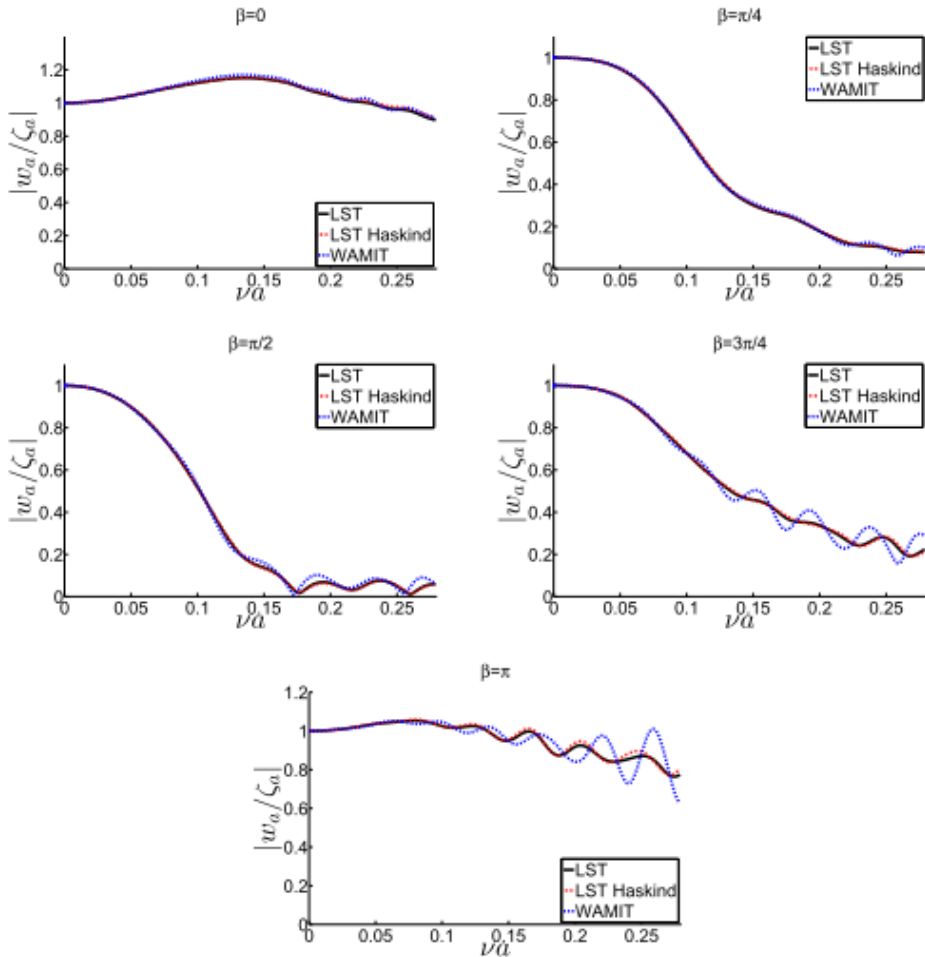
Figure 1.3: *Plots from Li (2017) showing vertical amplitude transfer function plotted against the non-dimensional wave number ν at different points on the floating torus showed by the β-angles.*

In this study, only the floating torus is considered, without the net cage and weights below the surface. This is similar to the suggested structure by Ocean Sun since both are surface structures. Because of this, results presented in this thesis is especially interesting when considering the response of the floating solar plant in waves.

1.4 Objectives for the Current Thesis

As discussed above, many studies have been performed in order to investigate the response of fish cages in waves. However, a thorough model test of a concept like Ocean Sun's solar plant seem to be missing. A lot of the discussed previous work done on similar structures may prove valuable for this type of installation as well, but a model test dedicated for this particular structure is still necessary to identify the main differences from previous tested models.

As an attempt to fill this gap in knowledge, this thesis presents such a model test and results gained from it. A model test is suitable for exploring new concepts where little is known about the expected response. It is a good tool for obtaining a better understanding of physical phenomena which may be difficult to capture using alternative methods like numerical solvers. A model test is well suited for investigating complicated situations when it is not known which anomalies that will occur (Steen 2014). In addition, a well performed and realistic model test is considered reliable and credible compared to numerical models which may neglect phenomena and contain human errors.

The main drawbacks to model testing is that it is not very flexible in terms of changing parameters throughout experiments. To make a model accurately is expensive in terms of both time and money, and whereas numerical models may easily be adjusted, physical model parameters must be thoroughly planned and well justified as they are more difficult to alter at a later time.

This thesis will *evaluate the seakeeping capabilities of a floating solar plant when exposed to regular and irregular waves*, with seakeeping capabilities meaning hydrodynamic response, mooring load and general behavior of the structure. This will be evaluated through a model test in the towing tank at SINTEF Ocean in Trondheim, Norway. More specifically, the objectives of the thesis are:

- To present the response of the structure for regular waves of different period and steepness, as well as for two irregular sea states.
- To evaluate how the response is affected by the membrane and the solar panels.
- To do a visual evaluation of the response, looking for deformations and wash from waves.
- To discuss how the results from this experiment can be used to evaluate other sea states.
- To suggest improvements to Ocean Sun's concept if detected.

Questions related to the deformation and strain of the solar panels for different wave conditions will be investigated in the master thesis by Henrik Markhus and Sindre Selvig at the department of Mechanical Engineering at NTNU. Their work is based on the same model test as the results presented in this thesis but will look closer at measuring deformations of solar panels, determining the stress rate and range of stress present in the panels and determining the most important wave parameters affecting the panel deformation. Panel deformation and strain is undesired as it can lead to lower efficiency of the solar cells.

1.4.1   Main Contributions

This thesis investigates a new type of floating solar plant. It presents model test results of a floating torus with a flexible, inelastic membrane in the center. This model is tested both with and without modeled solar panels, thus leading to increased knowledge of the influence a membrane with and without the weight and stiffness of solar panels has on the response of a moored floating torus. This differs from previous model tests done on floating tori, as the membrane and panels has not been included in earlier studies.

1.5   Thesis Structure

The thesis started by presenting relevant previous work. The focus on this part was on previous studies analyzing the motion and response in waves of similar structures as the one suggested by Ocean Sun. Mostly, these are numerical and experimental investigations of gravity fish cages subjected to deep water waves.

The next chapter presents the current model test. The physical model and the test facilities used as well as the experimental setup is described, and the scaling parameters are presented. Further, the test conditions of the different experiments are discussed, as well as the instrumentation and sensors used. Finally the procedure for post processing of measurement data is described.

Chapter 3 presents results and observations obtained during the experiment. They are presented through plots and figures, and important aspects are described in the text. This chapter also includes an analysis of the wave stability as well as the uncertainty found in repeated tests. Results are presented in full scale.

The discussion of the presented results is found in Chapter 4. Here, the errors and uncertainties of the model test is presented, and based on this, the results from Chapter 3 are discussed. This chapter also includes suggestions to improvements of the concept.

Finally, concluding remarks are given, and further work suggested in Chapter 5.

Model Test

The purpose of the model test was to investigate the response of a circular floating structure similar to the one suggested by Ocean Sun, when exposed to regular and irregular deep-water waves. This test was done on a floating collar with a membrane without and with aluminum plates imitating solar panels. The model was subjected to a wide range of waves, both regular waves with varying period and steepness and irregular sea states. The following chapter will describe in detail how this experiment was performed, including the physical modeling, description of test conditions, instrumentation and post-processing.

2.1 Test Facilities

The model tests were performed in SINTEF Oceans towing tank in Trondheim between the 26.02.2018 and 06.03.2018. The dimensions of the tank are presented in Table 2.1. The 260-meter-long tank can be divided into two parts, which was the case in this experiment. The shortest section of the tank, at 85 meters, was used for this model test. In this part, the tank is 10 meters deep and 10.5 meters wide. The tank is equipped with a double flap wave maker and a wave beach to absorb the wave energy and minimize the reflected waves and the time to wait for calm water between tests.

The tank has a carriage where the model is connected and from which the experiments are run, called the seakeeping carriage. From this carriage, all waves, instrumentation and measurements are controlled. The carriage is also equipped with video cameras to obtain footage of the experiment from two directions. This is particularly useful to further investigate unexpected measurements and results.

Table 2.1: *Information about the towing tank at SINTEF Ocean, (SINTEF Ocean 2014)*

Parameter	Value
Length	85 m
Width	10.5 m
Depth	10 m
Wave maker	Double flap
Maximum wave height	0.9m
Wave period range	0.8-5s
Maximum wave steepness	$^{1}/_{10}$

2.2 Model

The floating collar used in this experiment is based on an already existing fish cage model used by SINTEF Ocean in previous experiments, see Appendix A.1. Therefore, this model will not be entirely equal to Ocean Sun's full size structure. Dimensions of the model can be seen in Table 2.2, while scaling to full scale and comparison with the suggested design by Ocean Sun will be discussed in Section 2.4. The floating torus is made by a PVC tube to ensure correct stiffness and enclosed by pieces of divenycell to give buoyancy and the correctly scaled diameter. It is also equipped with 40 plastic brackets and railings made from a plastic tube.

Table 2.2: *Test model properties, model scale*

	Unit	Model scale
Inner diameter	m	3.13
Pipe diameter	mm	32.5
Height railing	mm	80
Bending stiffness, pipe	Nm^2	1.7
Solar panel size	mm	104x62
Panel thickness	mm	0.3
Weight panels	g	5.42
Panel stiffness	Nmm^2	9346
Number of panels	-	736
Membrane weight	g/m^2	95

The membrane is modeled by using tent canvas, made from silicone covered polyethylene. This fabric is light, durable and waterproof, which are important qualities to imitate. The weight of the fabric is not correctly scaled, as other properties were more important in the choice of membrane: The focus was to find a fabric which was almost inelastic to ensure a realistic behavior, and durable enough to endure the experiment. The scaled values can be seen in Table 2.4. The fabric was lightly sanded to give it better adhesiveness, so that panels could be glued on. The membrane was custom sewn with nylon loops which were used to fasten the membrane to the floating collar using cable ties, as shown in Figure 2.1. The same figure shows how the membrane is extended up to the railings working as

freeboard to protect the installation from waves washing over it.

Figure 2.1: *Close-up showing how the membrane is fastened to the floating collar, as well as the brackets and the railing.*

The solar panels are imitated by thin aluminum plates, ensuring a correctly scaled size and weight, at the cost of having a too high stiffness compared to full scale. However, in the full-scale installation, the panels will have to be stiff enough to avoid high values of strain and will be reinforced by aluminum frames to a higher stiffness. This justifies the choice of having stiffer panels than the actual scaled value to ensure the correct weight, and also make the total stiffness and response more realistic.
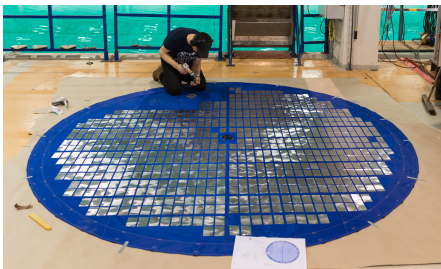
(a)   (b)

Figure 2.2: *Gluing the panels to the membrane of the model, before fastening it to the floating collar. Photo credit: SINTEF Ocean*

The panels where sanded and glued on to the membrane using epoxy glue in a pattern inspired by Ocean Suns concept. This pattern includes walkways between the panels,

ensuring accessibility of all solar panels, see figures 2.2 and 2.3. Four selected panels are made from plastic, this will ensure a more realistic stiffness and they are used for the strain measurements done by Markhus and Selvig.
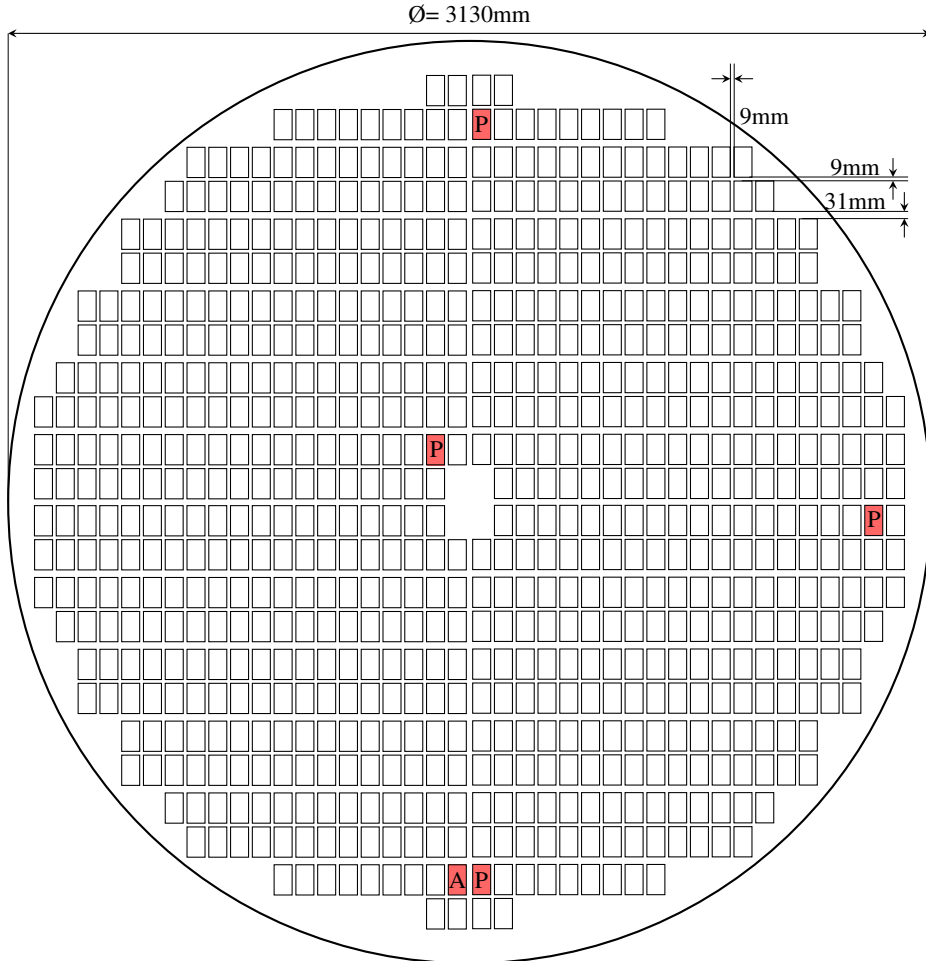
Figure 2.3: *Drawing of the model membrane, showing the position of panels, with dimensions. The red panels are equipped with strain gages, P = Plastic panel, A = Aluminum panel.*

2.3   Experimental Setup

The floating structure was fastened in the middle of the seakeeping carriage, with four horizontal mooring lines as shown in Figure 2.4. The mooring lines were two-point (crow feet) fastened in loops in the outer ring of the floating collar, and the other end through

pulleys and vertically up to load cells connected to springs. The springs ensured pre-tension in the lines, keeping the model in place while measuring forces and avoiding slack in the mooring lines during the experiment. The springs had a stiffness of 30N/m in all directions and a pre-tension of about 44-47N in the direction of the wave propagation, and 10-13N in the transverse direction for all tests.

The carriage was stationary at 34.5 meters from the wavemaker. It is important that the model is close enough to the wavemaker so that the waves do not get unstable, at the same time as it cannot be too close, because the waves need time to fully develop. According to a report from MARINTEK, now SINTEF Ocean (Stansberg 1993), showing the spatial variations of waves of different period and steepness, most of the tested regular waves in this report are stable at 40 meters from the wavemaker.
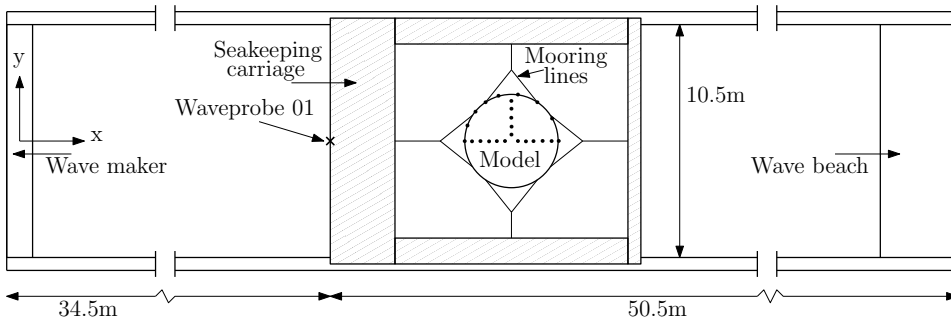
Figure 2.4: *Test setup for the experiment, top view*
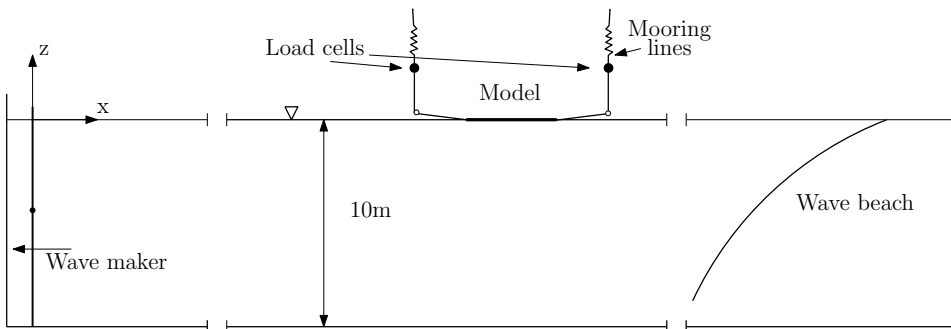
Figure 2.5: *Test setup for the experiment, side view. Seakeeping carriage excluded for clarity.*

There was a wave probe installed on the seakeeping carriage (called WAVE_01), closest to the wavemaker, which measured the actual incoming waves in front of the model. During the wave check one was also placed at the position where the model is illustrated in Figure 2.4 (called WAVE_02).

Figure 2.4 also shows the position of the markers used for optical measurements, more closely explained in Section 2.7.1. The marker positions are the points where response

was measured, and the positions were chosen to give an image of how the response varies at different locations of the structure. Symmetry was assumed about the x-axis, so the markers were focused on one side of the model.

Figure 2.5 shows a side view of the test setup, where the horizontal mooring is illustrated. Only the front and back mooring lines are shown, but the side ones are configured the same way. The positions of the mooring line load cells are also shown.

2.4 Scaling

Complete similarity between model and full scale is only achieved if the model and full-scale structure has *geometrical*, *kinematic* and *dynamic* similarity (Steen 2014). The geometrical similarity ensures the same shape of the two structures. All linear dimensions must be scaled using the same scaling factor, $\lambda = L_F/L_M$. Geometric similarity also applies to the surrounding environment and elastic deformations. Kinematic similarity means that the velocities are similar, and the flow will follow geometrically similar paths. The ratios between velocities in model scale has to be equal to the same ratios in full scale. Dynamic similarity ensures equal force ratios in model and full scale. To ensure similarity in gravity forces, the non-dimensional Froude Number has to be equal for full scale and model scale. This will however not ensure similarity for viscous forces, which require equal Reynolds Number. For other force components like elastic forces, surface tension and drag, other dimensionless numbers must be used. An equal Froude or Reynolds number will result in a model velocity defined by Equations 2.1 and 2.2:

$$F_{N_M} = F_{N_F}$$
$$\frac{U_M}{\sqrt{gL_M}} = \frac{U_F}{\sqrt{gL_F}} \tag{2.1}$$
$$U_M = \frac{U_F}{\sqrt{\lambda}}$$

$$Re_M = Re_F$$
$$\frac{U_M L_M}{\nu_M} = \frac{U_F L_F}{\nu_F} \tag{2.2}$$
$$U_M = U_F \lambda \frac{\nu_M}{\nu_F}$$

Where F_N is the Froude number, U is velocity, g is gravitational forces and L is the characteristic length. Re is Reynolds number, ν is kinematic viscosity and λ is the scaling factor. Subscripts M and F indicates model scale and full scale respectively. These expressions yield different definitions of the model velocity. The kinematic viscosity can in theory be changed in model scale to make the two expressions equal, but this is practically

impossible. Thus it is not possible to ensure that both Reynolds and Froude Numbers are equal in model and full scale, and one has to choose what forces are the most important. For most offshore structures, Froude scaling is applied, as it is the gravitational forces that controls the elevation of the sea surface in waves (Steen 2014). This was assumed to be the most important component in the present experiment as well, and therefore, Froude scaling was applied for this model test. Table 2.3 shows some scaling factors when using Froude scaling. The ratio between the water density in model and full scale, $\frac{\rho_F}{\rho_M}$, is assumed to be $\frac{1025}{1000} = 1.025$.

Table 2.3: *Scaling factors, Froude scaling.*

Parameter	Scaling factor	Unit
Length	$L_F = \lambda L_M$	m
Time	$t_F = \sqrt{\lambda} t_M$	s
Structural mass	$m_F = \frac{\rho_F}{\rho_M} \lambda^3 m_M$	kg
Volume	$V_F = \lambda^3 V_M$	m^3
Force	$F_F = \frac{\rho_F}{\rho_M} \lambda^3 F_M$	N

When planning of this experiment started, the model floating collar was thought to be scaled with a factor of 16, both in terms of dimensions and bending stiffness. The size, weight and stiffness of the panels were therefore scaled accordingly. However, after more thorough investigation, it was discovered the scaling factor was actually 20, mainly meaning that the bending stiffness of the floating collar was too high throughout the tests. Due to this, some key parameters will be presented in both scale factor $\lambda = 16$ and 20, see Table 2.4.

Table 2.4: *Test model properties presented in model scale and upscaled with a scale factor of $\lambda = 16$ and 20, together with parameters from the suggested concept by Ocean Sun.*

Parameter	Unit	Scaling	Model	$\lambda = 16$	$\lambda = 20$	Ocean Sun
Inner diameter	m	λ	3.13	50.08	62.6	49.60
Pipe diameter	mm	λ	32.5	520	650	500
Height railing	mm	λ	80	1280	1600	-
Bending stiff., pipe	Nm^2	λ^5	1.7	1 782 579	5 440 000	1 339 870
Solar panel size	mm	λ	104x62	1664x992	2080x1240	1658x997
Panel thickness	mm	λ	0.3	4.8	6.0	-
Weight panels	g	$\frac{\rho_F}{\rho_M} \lambda^3$	5.42	22800	44400	18500
Panel stiff.	Nmm^2	λ^5	9346	98.00x10^8	299.07x10^8	1.99x10^8
Number of panels	-	-	736	736	736	720
Membrane weight	g/m^2	$\frac{\rho_F}{\rho_M} \lambda$	95	1558	1948	900

Based on the values in the table above, a scale factor of $\lambda = 16$ yields parameters closer to Ocean Suns concept values and will be used further in this report. If it is desired to analyze the results for another scaling factor, the full scaled results presented later in this thesis can be scaled to other sizes using the rules presented in Table 2.3.

2.5 Test Conditions

In this model test, four tests have been carried out with the same wave conditions, in addition to one towing test, see Table 2.5. The first test was done without a model present (test 8000), only to test the stability of the waves and make measurements of wave motion at the location where the model was later placed. One wave probe was located in the position of the model (WAVE_02), and one in front, closer to the wavemaker (WAVE_01). The second test (test 2000) tested the model without solar panels in the same waves. The third (test 3000) and fourth test (test 4000) were done to investigate the model with solar panels with the short edge facing the waves and turned approximately 30 degrees respectively. Figure 2.6 shows photos of the model setup for tests 2000, 3000 and 4000.

Table 2.5: *Test condition numbering from the experiment.*

Test numbering	Test description
2000-series	Tests of model without panels.
3000-series	Tests of model with panels. Short edge facing the incoming waves.
4000-series	Tests of model with panels. Rotated approximately 30 degrees compared to 3000-series, facing the waves diagonally.
5000-series	Towing test of model with panels.
8000-series	Test of wave stability without model present.
9000-series	Test runs used for calibration, testing etc.

Tests 2000, 3000 and 4000 are the ones that will contribute to answering the main objectives presented in Section 1.4. By testing the model both with and without solar panels, it allows for comparing the responses and saying something about how the structure is affected by the panels, both because of extra weight and additional stiffness of the system. The only difference between test 3000 and 4000 is the direction of the panels relative to the incoming waves. By doing both of these, the test will answer whether or not the direction of the incoming waves is important for the response, which can be helpful when positioning the full-scale installation relative to the main wave direction.

The experiment mainly consisted of regular waves of different period and wave steepness. Each regular wave was run for an amount of time ensuring that at least ten stable waves passed the structure, after the waves were fully developed and before the model was hit by reflected waves. In addition to the regular waves, two irregular sea states were tested for a longer amount of time. In total, each model configuration has been subjected to 22 regular waves and two irregular sea states. The water was allowed to completely calm down between each run to minimize the noise contamination from the remaining motion of the water surface. This meant waiting 15-25 minutes depending on the type of wave. A zero measurement was done before each new run. Some parameters like water level and temperature might change throughout the model test, and by resetting reference level before each run, the measurements are as accurate as possible. The full test log describing details of the model test can be found in Appendix B.1.
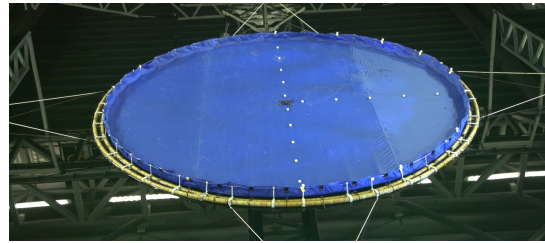
(a) *Test setup 2000*
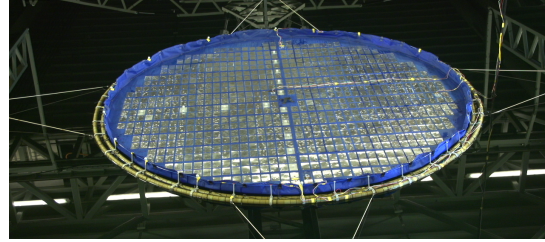
(b) *Test setup 3000*
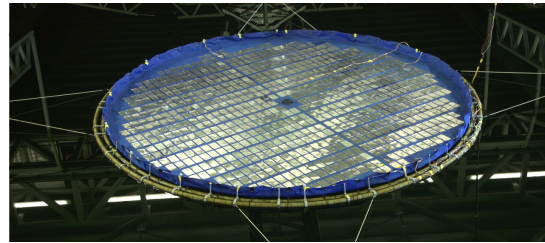
(c) *Test setup 4000*

Figure 2.6: *Model setup with/without panels for the three response tests, seen from the front.*

2.5.1 Waves

Regular Waves

In linear wave theory, as described by Faltinsen (1990), the surface elevation in regular deep water waves is described by a sinusoidal expression:

$$\zeta(x,t) = \zeta_a sin(\omega t - kx) \tag{2.3}$$

Where ζ_a is the wave amplitude, $\omega = 2\pi/T$ where T is the wave period is the angular frequency, and the phase shift is described by the the x-coordinate and the wave number, $k = 2\pi/\lambda_W$ where λ_W is the wavelength (see Figure 2.7).

The wave lengths range from a little more than two times the diameter of the structure (λ_W = 2D+16), to one third of the diameter. These were the wavelengths that were considered
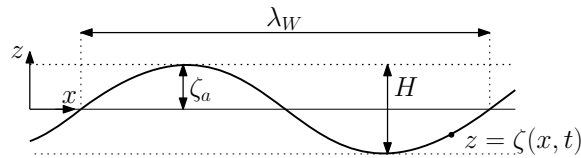
Figure 2.7: *Parameters of regular wave*

to be the most relevant for the model test, as longer waves are believed to only make the structure move up and down with the water rising, and shorter waves can easily become unstable. Wave heights were decided from three chosen values for wave steepness, H/λ_W, of $1/50$, $1/30$ and $1/15$. However, the two shortest waves were left out for the largest steepness, due to instability of these waves in the wave tank. The wavemaker has limits for how short and steep waves that can be made, depending on the location of the model in the tank. The shorter the waves, the shorter they can travel down the tank before they become unstable and polluted with other frequencies. Table 2.6 shows the waves used in all tests. The numbering goes from 8010 to 8220 for the regular waves, and each run in the experiment is named after the test series and this wave number, for instance 3010 to 3220 for test 3000. Repeated runs of the same wave are numbered by the last digit, for instance would 3011, 3012, 3013 be repetitions of test 3010.

Table 2.6: *Regular waves, full scale. The two empty spots in the matrix are left out due to instability of waves in the tank. D is the diameter of the floating collar, H is wave height, λ_w is the wavelength.*

Wavelength	Period	**Weather number** (wave height) per steepness H/λ_W		
		1/50	1/30	1/15
$\lambda_W = 2D+16$	8.63s	**8010** (H = 2.30m)	**8090** (H = 3.87m)	**8170** (H = 7.74m)
$\lambda_W = 2D$	8.01s	**8020** (H = 2.00m)	**8100** (H = 3.34m)	**8180** (H = 6.68m)
$\lambda_W = 1.5D$	6.94s	**8030** (H = 1.50m)	**8110** (H = 2.50m)	**8190** (H = 5.01m)
$\lambda_W = D$	5.66s	**8040** (H = 1.00m)	**8120** (H = 1.67m)	**8200** (H = 3.34m)
$\lambda_W = D/1.5$	4.62s	**8050** (H = 0.67m)	**8130** (H = 1.11m)	**8210** (H = 2.23m)
$\lambda_W = D/2$	4.00s	**8060** (H = 0.50m)	**8140** (H = 0.83m)	**8220** (H = 1.67m)
$\lambda_W = D/2.5$	3.58s	**8070** (H = 0.40m)	**8150** (H = 0.67m)	-
$\lambda_W = D/3$	3.27s	**8080** (H = 0.33m)	**8160** (H = 0.56m)	-

The wavemaker in the towing tank makes a numerical wave based on a wave height H and period T. These are transformed to a motion pattern of the wave flap. The correspondence between the input parameters and the outputted waves is discussed later in this thesis (Section 3.1). The wave height and period of the waves are generated from the desired wave lengths and steepnesses discussed above, using the dispersion relationship for deep-water waves:

$$\omega^2 = kg \tag{2.4}$$

Where ω is the wave frequency, k is the wave number and g is gravity. According to

Faltinsen (1990), the dynamic pressure decreases exponentially with depth, and at half a wavelengths depth the dynamic pressure is only 4% of the value it has at the water surface. The water depth at the towing tank is 10 meters, while half the longest wavelength is 3.63 meters. With this in mind, the bottom of the wave tank will have negligible effect on the waves, and the assumption of deep water is justified.

Irregular Sea State

When considering irregular waves, the sea surface will be described statistically. In linear wave theory it is assumed that the irregular sea state can be divided up into a series of regular waves with varying length and height, and with a uniformly distributed phase angle ϵ between 0 and 2π (Faltinsen 1990). The wave elevation is then the sum of all the regular wave components:

$$\zeta(x,t) = \sum_{j=1}^{N} \zeta_{aj} sin(\omega_j t - k_j x + \epsilon_j) \tag{2.5}$$

When considering an irregular sea state, it is common to assume that the wave process is stationary in an interval between 20 minutes and 3 hours (Myrhaug & Lian 2009), which means that the statistical parameters like mean value and variance are constant. In order to ensure a stationary process, the irregular sea states in this test are run for about 25 minutes in model scale, which in full scale is well within this interval.

A wave spectrum is defined so that the area within a small frequency interval is equal to the energy of all wave components of the sea state that is within this interval (Myrhaug & Lian 2009). The wave spectrum of $\zeta(t)$ is denoted $S(\omega)$:

$$\frac{1}{2}\zeta_{aj}^2 = S(\omega_j)\Delta\omega \tag{2.6}$$

Where the left side of the equation represents the energy of the wave components within the interval $\Delta\omega$. The total energy of the sea state is the sum of all these intervals.

The irregular sea states in this model test are generated using the JONSWAP-spectrum (Joint North Sea Wave Project), which is recommended for dimensioning of floating fish cages by the Norwegian Standard (Norwegian standard 2003). The sea states are defined based on previous model tests done by SINTEF Ocean to test the response of a fish cage built around the same floating collar. The choice of wave height has also been based on the work by Lader et al. (2017) to find typical sea states. This work presents a method for estimating the wind-generated waves for fish farm locations in Norway, which is representative for locations relevant for Ocean Sun's concept for a floating solar plant. The study does not consider swell, but because Ocean Sun's plans do not include placing the installation offshore, only in confined waters. The maximum values of a 50 year significant wave height of about 2.5 meters from this study should represent some of the worst sea states that could be experienced by the structure. The chosen irregular sea states are presented

in Table 2.7, where H_s is the significant wave height, T_p is the peak period of the sea state and γ is the peakedness parameter.

Table 2.7: *Irregular waves in full scale, $\lambda = 16$*

Weather number	H_s	T_p	γ
8520	2.50m	6.00s	2.00
8530	1.50m	4.50s	2.00

Figure 2.8 shows the measured wave spectrum for weather number 8520 and 8530 plotted together with the corresponding theoretical JONSWAP-spectra calculated through Equation 2.7 (Myrhaug & Lian 2009).

$$S(f) = \alpha g^2 (2\pi)^{-4} f^{-5} exp[-\frac{5}{4}(T_p f)^{-4}] \gamma^{exp\left[-\frac{(T_p f - 1)^2}{2\sigma^2}\right]}$$

$$\alpha = 0.036 - 0.0056 \frac{T_p}{\sqrt{H_s}}$$

$$\sigma = \begin{cases} 0.07, & f \leq f_p \\ 0.09, & f > f_p \end{cases}$$

(2.7)

Where T_p, H_s and γ are as described above, g is the gravitational acceleration, α determines the spectrum shape for high frequencies and σ is the standard deviation.
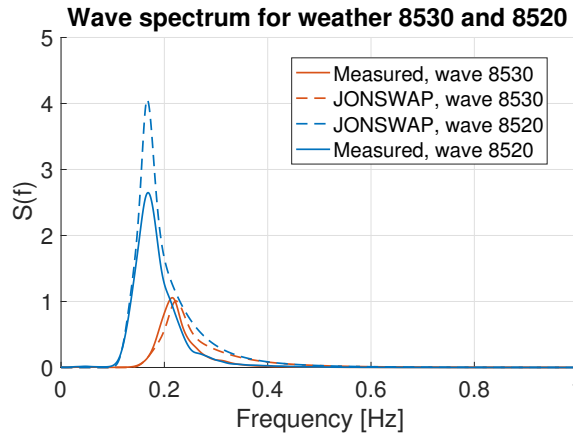
Figure 2.8: *Measured wave spectrum for irregular sea state 8520: $H_s = 1.5m$, $T_p = 4.5s$, $f_p = 1/T_p = 0.22Hz$, and 8530: $H_s = 2.5m$, $T_p = 6.0s$, $f_p = 1/T_p = 0.17Hz$, in addition to the inputted JONSWAP spectrum for each sea state (dotted lines).*

2.6 Towing Test

After all wave tests were completed, a towing test was performed (test 5000). The results from this test can be used to find the necessary towing force of the structure, or the resistance, but also to estimate forces working on the installation in current. The test is done by letting the seakeeping carriage run at known speeds while measuring the load in the front and aft mooring line. Since it was the last test performed during the experiment, the model was kept as in test 4000, rotated with panels. The only alteration done to the test setup was that the side mooring lines were removed such that only the lines in the direction of motion was kept. This was done in order to make sure the full towing force was transfered through the two mooring lines in line with the motion

The model was tested in full scale velocities 1, 2 and 3 knots, see Table 2.8. In one run, the model was tested at two speeds, which was possible because of the length of the towing tank. The carriage was started at the lowest speed, and when it was visually observed from the measurements that the mooring load had stabilized, the velocity was increased to the next level. When stable measurements were achieved again, and the end of the tank met, the carriage was taken back to the starting position. The waiting time between runs were in the order of the waiting time during the wave tests to make sure the water was calm and the measurements reliable. A zero measurement was done before each new run.

Table 2.8: *Full scale velocities in the towing test*

Test number	Speed [knots]	Speed [m/s]
5010	1 and 2	0.514 and 1.029
5020	2 and 3	1.029 and 1.543

2.7 Instrumentation

In this section the sensors used to obtain measurements are presented, along with an explanation of how they work and why they are included. Table 2.9 shows most important channels of measurements used in the model test, while the full channel list for all tests can be found in Appendix A.3. In addition to these measurements, the water temperature was logged regularly. All parts of the instrumentation process, choice of sensors, setup and calibration are done with the help of Jens Åge Havmo at SINTEF Ocean.

Table 2.9: *Channel list for most important measurements in the experiment. The sample frequency was changed for some channels after tests 8000 and 2000, due to overload of information in the system for long tests when all channels were used. Where two sampling frequencies are listed, it means before/after this change. A detailed channel list for each test can be found in Appendix A.3*

Channel name	Sample frequency [Hz]	Explanation
DAQ time stamps SR2	200	Time stamps for 200 Hz measurements
DAQ time stamps	50/25	Time stamps for 50/25 Hz measurements
WAVE_01	200/25	Wave probe 1 in front of model
WAVE_02	200/25	Wave probe 2. 8000: at model position, 3000 and 4000: next to WAVE_01
x01-x24	50/25	x-position of markers M01-M24
y01-y24	50/25	y-position of markers M01-M24
z01-z24	50/25	z-position of markers M01-M24
res01-res24	50/25	Residual for markers M01-M24
line0_Z8758	200	Tension fore mooring line
line90_Z8759	200	Tension left mooring line
line180_Z8760	200	Tension aft mooring line
line270_Z8763	200	Tension right mooring line

2.7.1 Optical Measurements

The software Qualisys Track Manager has been used to do optical motion tracking during the model test. This is how the response of the model is measured. Small reflective markers have been placed on strategic positions on the model, and special cameras in the four corners of the test area track the motion of these points, and thus also the movement and deformation of the model.

The cameras send out infrared signals that are reflected from the markers spread out on the test section. These reflections are seen by the cameras. When setting up the system, the makers on the model can be identified manually, and other points that may also reflect the infrared light, can be ignored. The cameras are calibrated in relation to each other, and when two or more cameras can see the same reflected point, this is identified as an object. Through triangulation, the position of these chosen markers in x-, y- and z-direction is always traced, and through this, a measurement of the response at different points is obtained.

The optical measurement setup in the Towing Tank allows for 24 markers to be inputed. As it is desired to have as much information as possible of the motions of the model, it was decided to use all 24 channels. Figure 2.9 shows the location of all the 24 markers, with numbering. The markers are placed to capture three main variations in the response:

- Evenly spaced along the center line of the model to see how the waves are propagating through the model and capture potential damping.
- In the transverse direction relative to the incoming waves. The markers are focused on one side of the model due to assumed symmetry and evenly spaced from the center and out.

• On the floating collar, spread out to see differences along it, and in relation to the motions of the membrane. The markers on the floating collar are not evenly spaced, as Qualisys needs the markers to be spread unevenly to know the orientation of the model.

Epoxy glue and double-sided tape is used to fasten the spheres on the membrane, while those on the floating collar are fixed to the railings with screws.

The optical measurement system is calibrated by moving a rigid rod with a marker in both ends around in the measurement area. The markers have a known distance between them, and the program can then calibrate its measurements to match the actual distance.

(a) *Test 2000, without panels* **(b)** *Test 3000, with panels* **(c)** *Test 4000, rotated panels*
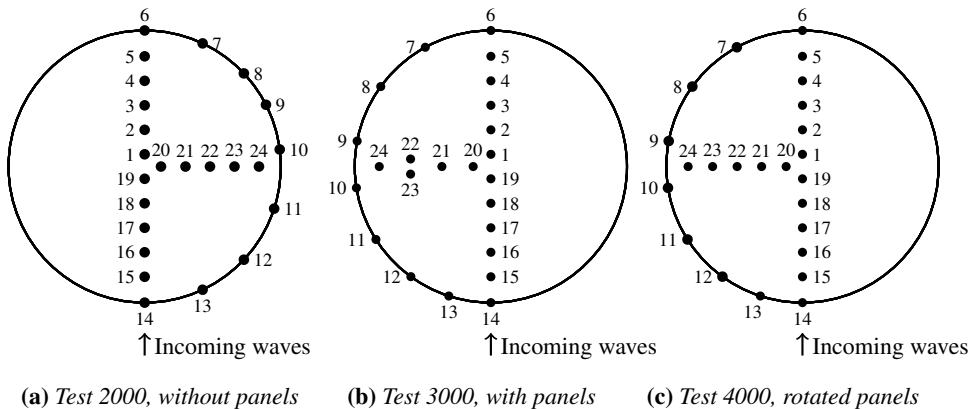
Figure 2.9: *Approximate placement of markers for the three tests. Exact placement with dimensions can be seen in Appendix A.2.*

The general pattern of the marker positions is the same for all tests, but for practical reasons there are small variations between them. The model configuration in test 2000 was made first. When the model for test 3000 was set up, chords from the strain gages were placed on the right side. In order to limit the interference between the chords and the field of view of the cameras, the markers were moved to the left side of the structure. In addition, two markers were placed on the same panel to investigate the local motion on this, mostly for the work by Markhus and Selvig who investigate deformation of the panels.

2.7.2 Wave Probes

In test 8000, where the waves were tested, two wave probes were used to measure the wave elevation. One placed on the seakeeping carriage, in front of the model location, while the other at approximately the center position of the model. The one in front of the model had the same position throughout all tests. The wave probes consist of two parallel rods partly submerged under the water surface. Voltage is applied to the rods, and the degree of submergence and hence the wave elevation, will affect the current across these rods. By measuring this electric current, the wave elevation is known.

Calibration of the wave probes are done by submerging the probes to known depths while measuring the signal from the probes. These measurements are used to determine the calibration factor. Plots from the calibration process can be seen in Appendix A.4.1.

2.7.3 Mooring

The structure is held in place by four horizontal mooring lines which measure the force in the lines at all times. Two lines are in the wave propagation direction, in the front and back, and the other two are fastened transverse of the incoming waves. The mooring lines are made from light, thin rope, in order not to add additional weight to the load cells. Each line is fastened at two points, see Figure 2.4, going through pulleys and are fastened to load cells which are able to measure the mooring forces in the lines as the waves hit the structure.

The load cells are calibrated by applying known loads and tested after installation. The plot from testing the calibration factors is shown in Appendix A.4.2, and shows a measuring error of less than $\pm 1\%$.

2.7.4 Strain Gages

Five panels are equipped with strain gages to measure strain in the solar panels in three directions, $0°$ and $\pm 45°$. The panels are located two in the front, one in the middle, one on the side and one in the aft of the structure (see Figure 2.3). Four of these panels are made from thin plastic, which has a stiffness closer to that of a solar panel. The fifth panel that is measured, is one of aluminum, like the rest. This panel is measured because it may be closer to the stiffness of a panel with a strengthening aluminum frame that will be used in the full-scale installation.

The reason for the strain measurement is to know how large the panel strain is in waves. The performance of solar panels can be severely affected by the presence of micro cracks, which can be caused by high strain. According to Dolara et al. (2014), the yearly energy production may be reduced by up to 32% compared to a panel with no cell cracks. This part of the experiment will be further discussed in the master thesis by Markhus and Selvig.

2.7.5 Sensor Calibration

The input signal from the wave probes, strain gages and load cells are in millivolts, and had to be converted to the correct physical units. This was done through the calibration process. The first step is to apply known loads to the transducer and plotting a calibration curve from the measured voltage and the known load or size. From this curve, one can see the linear relationship and determine the calibration factor from the slope. This calibration factor is used to transform the output voltage to the desired measurement unit.

If calibration is performed before mounting the transducer on the test location, it can be beneficial to check that the calibration factors are still providing reasonable measurements. This had to be done for both the wave probes and the load cells in the mooring lines, and both provide reasonable readings. Plots from the factor check can be seen in Appendix A.4.

2.8 Repeated Tests to Estimate Uncertainty

The precision error of an experiment is a measure of the scatter or variation of results which is found by repeating a test with the exact same conditions. Due to a limited amount of time to perform the tests, this could not be done for each wave. However, to get an indication of the uncertainty, repeated tests were performed for one wave in test 3000 and 4000. In these cases, the same wave was run under the same conditions 5 or 6 times. Nothing was changed from one run to another, but the waiting time between waves was long enough to ensure calm water.

The calculation of the precision error was done as described by Steen (2014):

First, the vertical response amplitudes for the N runs were calculated, and the standard deviation, S_X of these measurements found. The precision limit of these measurements was then found as $P_X = S_X \cdot t_N$, where t_N is the weight for estimating a confidence interval in a Students-t distribution. The value of t was found through the built-in MATLAB-function *tinv*. By dividing the value of the precision limit by the average of the response amplitudes, the uncertainty of a single test was determined.

The runs in this experiment has only been done once for most waves, and the uncertainty of these will be assumed to be of the order of the calculated uncertainty for a single test. The preferred way to do an experiment in order to minimize the uncertainty, would be to always repeat the runs at least 5 times and use the mean value in further calculations. Unfortunately, this would be very time consuming and costly, and could not be performed in this experiment.

2.9 Analysis of Measured Data From the Tests

Every run from the model test leads to a separate file containing time series with the measurements described in the channel list above (Table 2.9). These files contain time series from when the wave maker starts until it is stopped. This means that they had to be processed before results could be presented. This process will be described in the following section. All post-processing has been done using MATLAB and a MATLAB program made by SINTEF Ocean called PlotMe.

2.9.1 Choice of Stable Time Series

Before the measurements were analyzed, the data series had to be cut to stable time intervals to avoid transient effects. This was done through visual inspection of the time series from each test run. The SINTEF-made tool PlotMe has been employed for this task as it offers an easy way to identify and cut the stable intervals. Each trimmed time series had at least ten waves passing, to ensure a representative selection of data. Figure 2.10 shows how the stable time interval of a time series was identified.
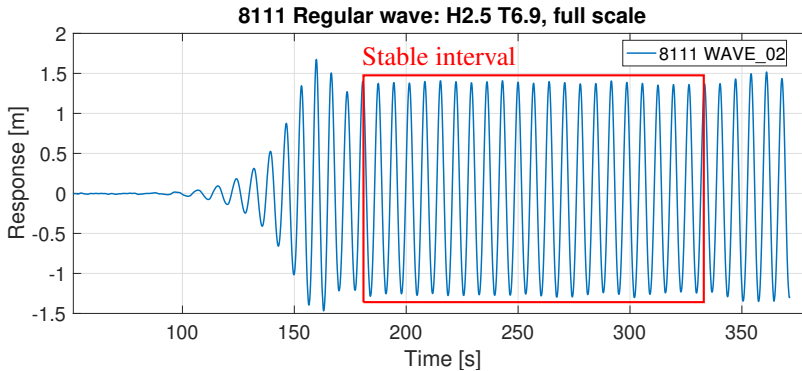
Figure 2.10: *Measurements of wave elevation at the position of the model in wave 8010. The red square illustrates how the stable time interval from the data series is chosen, avoiding the first unstable waves and the waves reflected from the wave beach in the tank seen at the end of the signal. Plotted through PlotMe by SINTEF Ocean.*

2.9.2 Sampling Frequency and Filtering

Filtering During Measurements

The sampling frequency of measurements is important as it determines the resolution of the signal. The higher the sampling frequency is, the higher resolution you get, but at the cost of a larger demand for storage capacity. This demand can be a motivating factor to limit the sampling frequency. The most important aspect is to choose a sampling rate which gives you all necessary information of the signal, since a too low sampling frequency can lead to erroneous frequencies measured, so-called aliasing, as illustrated in Figure 2.11. In aliasing, higher frequencies is folded back to appear as lower frequency signals.

The Nyquist frequency, f_n, determines the highest frequency which can be fully captured for a given sampling frequency, f_s, in order to prevent these new, erroneous frequencies from appearing in the measurements.

$$f_n = \frac{f_s}{2} \tag{2.8}$$
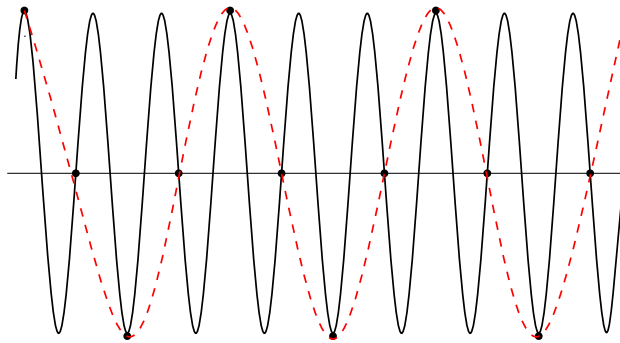
Figure 2.11: *Aliasing. The real signal (black line) is not captured but a new frequency (red dotted line) is introduced because of the sampling frequency being too low.*

This means that the sampling rate should be at least twice the highest frequency in the signal.

Most analog measurements in a model test like this will be contaminated by high-frequency noise. To remove these unwanted frequencies, and avoid aliasing, the signal is filtered through an analog lowpass filter before sampling. A lowpass filter lets low frequencies pass and removes frequencies above a chosen cutoff frequency from a signal. It is important that this cutoff frequency does not compromise the frequencies that are important in the measurement, thus it should be set well above these. In addition, the filter should remove frequencies well below the Nyquist frequency, meaning that the sampling rate has to be high. A recommended rule is to set the cutoff frequency to 1/10 of the sampling frequency (Steen 2014).

Wave measurements are important in this experiment and will now be used to exemplify how these frequencies should be decided. Waves usually lead to frequencies of interest below 2Hz. The filter cutoff frequency should thus be set well above the this, for instance at 20 Hz. As the sampling frequency should be ten times the cutoff frequency, it is recommended that it is set to 200Hz, which reflects is the normal practice at SINTEF Ocean.

The analog channels in this test were lowpass filtered at 20Hz to remove measurement noise as explained above, and in test 8000 and 2000, the sampling frequency of all these channels was 200Hz. However, during the longer time series from the irregular sea states, the measurement system experienced problems handling the amount of data from all channels, and it was decided to reduce the sampling frequency for the Oqus measurements (digital) from 50Hz to 25Hz. Due to an error unknown to the author, several of the analog channels were also affected by this change and had their sampling frequency reduced from 200Hz to 25Hz, while the cutoff frequency remained at 20Hz. The frequencies had these values for the rest of the experiment. This is an unfortunate mistake during the experiment which may have led to systematic errors in the measurements. However, the only affected channels are the wave measurements in tests 3000, 4000 and 5000. The response amplitude operator, further described in Section 2.9.3, is presented from wave measurements in test 8000, and response measurements from tests 2000, 3000 and 4000, non of which are

affected by the human error when changing the sampling rate. Further discussion of this will be done in Section 4.1.7.

Filtering During Post-processing

To detect the presence of unwanted frequencies from the measurements, the measured signal was transformed from time domain to frequency domain. By doing this, all frequencies present was made visible, and it was possible to evaluate whether the signal needed further filtering to remove unwanted frequencies.

To transform the time series to the frequency domain, a Fast Fourier Transform was used through the built-in MATLAB function *pwelch*. The function returns an estimate of the power spectral density of the inputed data series.

If unwanted frequencies are found in the measurements, these should be excluded through digital signal filtering before further calculations are performed.

The response in x and z direction and the wave measurements from the regular wave tests in this experiment has been filtered using a Butterworth bandpass filter in MATLAB. A bandpass filter allows the frequencies in the band set by the lower and higher cutoff frequencies to pass and remove frequencies outside this interval. The higher and lower cutoff frequencies are set depending on the frequency of the peak frequency, f_p for each wave. This peak is the frequency containing the most energy and corresponds to the frequency of the regular incoming wave. The lower cutoff frequency for regular waves was set to $f_{c,lower} = 0.5 f_p$ and the higher cutoff frequency is $f_{c,higher} = 1.7 f_p$. Results from the irregular sea states were not filtered after the analog filtering during the measurements.

Figures 2.12, 2.13 and 2.14 show the power spectral density of the horizontal (surge) and vertical (heave) response, as well as for the wave elevation respectively, for point 4 on the model with panels exposed to wave 8140 (run 3140). In this plot, both the unfiltered and the filtered signal are plotted, and it can clearly be seen that peaks outside the pass band are removed from the filtered signal, without affecting the signal amplitude.

The zoomed boxes in the plots show an interval of 5% of the maximum spectral value where other smaller frequency peaks are present in the time series. The plots show a presence of higher harmonic peaks like $2f_p$ and $3f_p$. It can be seen that the peaks of the higher harmonics relative to the peak of the filtered signal, are larger for the response i surge than for the heave response and wave elevation.
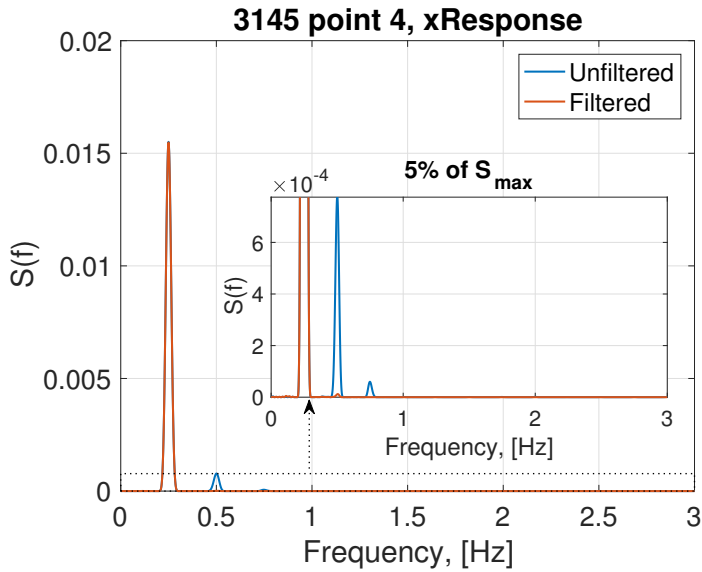
Figure 2.12: *Power spectral density of response in surge for model with panels in wave 8140. With zoomed window for clarity.*
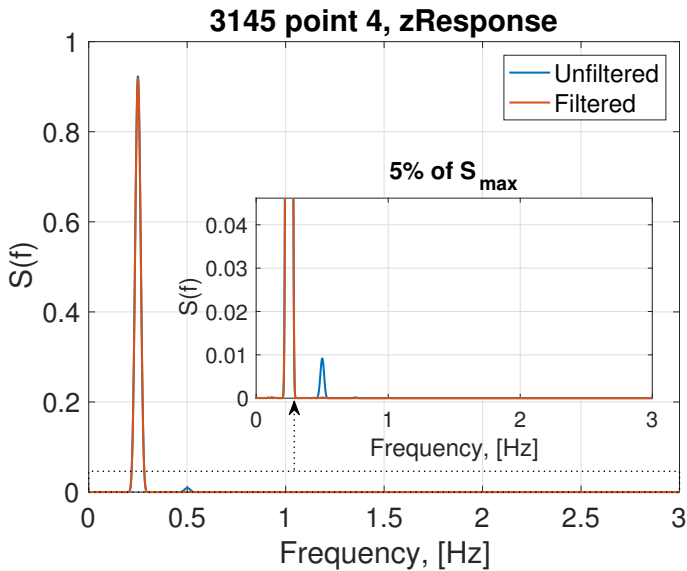
Figure 2.13: *Power spectral density of response in heave for model with panels in wave 8140. With zoomed window for clarity.*
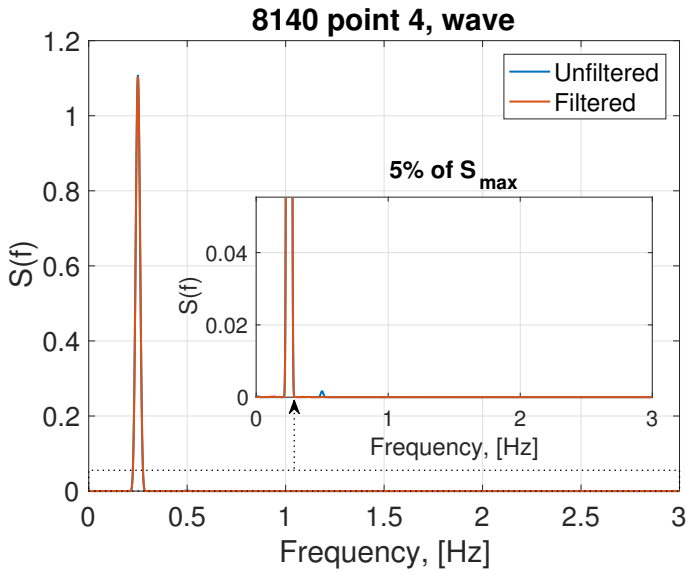
Figure 2.14: *Power spectral density of the wave elevation for model with panels in wave 8140. With zoomed window for clarity.*

2.9.3 Response Amplitude Operator

The response amplitude operator (RAO) is used to represent the response of different points on the model relative to the waves it is subjected to. It is defined as the ratio between the output amplitude, or the fundamental component of the measured amplitude of the response, and the input wave amplitude (Steen 2014). The RAO can also be defined as a transfer function, as it shows the relationship between the input signal and the output value.

$$RAO = \frac{\eta_a}{\zeta_a} \tag{2.9}$$

Where η_a is the response amplitude and ζ_a is the wave amplitude.

In theory, RAOs are calculated for all frequencies, but in this study they are calculated from the available wave frequencies from the test. Different RAOs are made from the response measured at different locations over the model, and the wave amplitude used is the one measured by the wave probe in the location of the model in test 8000. The measured wave and response amplitudes are found by using the formula:

$$x_a = \sqrt{2}std(x) \tag{2.10}$$

Where $std(x)$ is the standard deviation of the measured data x and subscript a means the signal amplitude.

For the irregular sea states, the linear transfer function between the response and the wave elevation is calculated from the response and wave spectra:

$$|H(f)| = \sqrt{\frac{S_{response}(f)}{S_{wave}(f)}} \tag{2.11}$$

Here, $|H(f)|$ is the transfer function or RAO and $S_{response}(f)$ and $S_{wave}(f)$ are the response and wave spectrum respectively, calculated from the measurements.

2.9.4 Mooring Forces

The forces in the mooring lines are oscillating in waves. The linear forces have a mean value of 0, so it will be interesting to know if there are second order effects causing the mean to deviate from zero. Figure 2.15 shows a typical timeseries of the mooring line loads in run 2190. It shows how the mooring forces reaches a peak when the first waves in the wave train hit the model before it stabilizes, oscillating around a mean value.
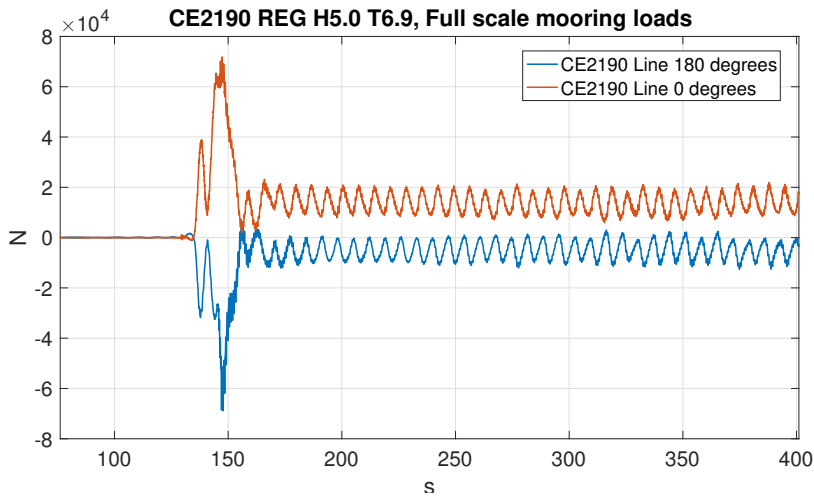
Figure 2.15: *Timeseries showing mooring loads in the front ($0°$) and aft ($180°$) mooring lines in full scale. H = 5.01m, T = 6.94s.*

The total mean force in the direction of wave motion is found by subtracting the load in the aft line from the front line:

$$F_{Mean,x} = mean(F_{Mooring,0°} - F_{Mooring,180°}) \tag{2.12}$$

CHAPTER 3

Results

This chapter will present selected results from the described model test. First, the wave test is presented in order to validate how close to the planned wave height and period the tested waves are. The vertical motion of different points on the model will be presented as response in the frequency domain. To fully explain the response in the frequency domain, both amplitude and phase should be included. However, no accurate position of the wave probe was logged, which makes it impossible to comment on the phase shift of the response, hence, only the amplitude is presented. Knowledge about the phase shift of the response could be used to predict the response in other parts of the structure, however, the amplitude of the response is measured at 24 different positions on the model, which gives a good picture of the response all over the model.

The horizontal motions are also presented through transfer functions, and the motion pattern in heave and surge is showed. Mooring loads will be analyzed by focusing on mean forces in different waves. Visual observations described through snapshots from the model tests are included to further enhance the knowledge of the seakeeping capabilities. Results from the towing test will be presented in order to give an image of loads in current or the towing force if the structure is to be moved.

Some comments will be given for all presented results, but the main discussion of these will follow in Chapter 4. All results are given in full scale with a scaling factor $\lambda = 16$.

3.1 Wave Stability Validation

Before the tests with the model started, all waves were run in the towing tank (test 8000). As mentioned before, two wave probes were used to measure the wave elevation: WAVE_01 was the wave probe placed on the seakeeping carriage, upstream of the model. WAVE_02 was positioned at approximately the place in the tank where the model was to be tested. Figure 3.1 shows the planned and measured wave height and period for the waves run in this test.
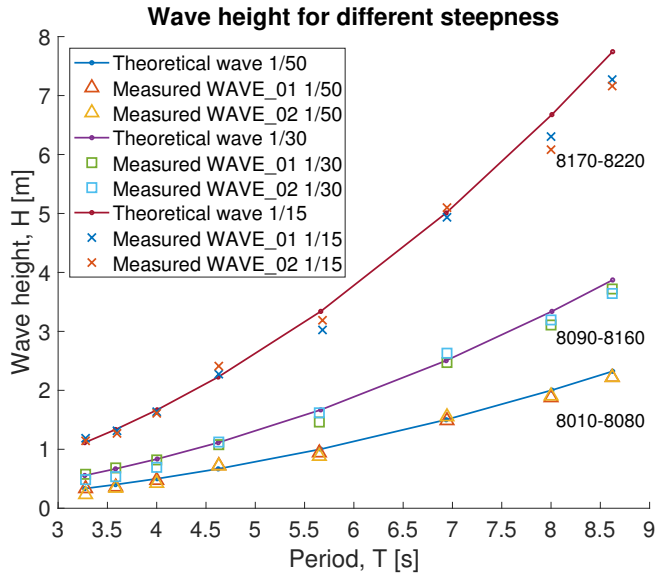
Figure 3.1: *Measured and theoretic wave height and periods in test 8000. Both wave probe WAVE_01 and WAVE_02 are included. The three lines represent waves of constant steepness.*

Figure 3.2 presents the the mean of the absolute relative error in the measurements at the two wave probes. This means that it can be used to investigate which steepness is best captured by the wavemaker. By investigating the errors presented in the plots, it can be seen that the period is well recreated by the wavemaker, with a maximum relative error of about 0.2%. The error in wave height is however larger, up to 10-15%. The relative error in the height of the waves increase with decreasing period, which is reasonable as the shorter waves has less energy and loose height when traveling in the tank.

The waves with steepness $H/\lambda = 1/15$ seems to have a low relative error, but as the shortest waves with this steepness became unstable, the waves with steepness $1/30$ where chosen to calculate the RAOs in the following section.
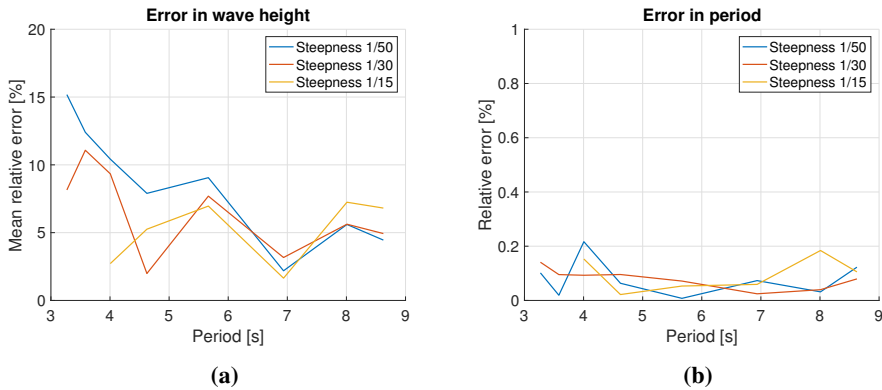
Figure 3.2: *The absolute relative error in wave height (a) and period (b) is presented as a function of the input period. The error is presented by the mean of the two absolute relative errors calculated from the measurements by the two wave probes.*

3.2 Vertical Response

In this section, the vertical response in waves at points of interest is presented. Most figures show results from the three different model configurations: test 2000, model with membrane but without panels, test 3000, model with panels and test 4000, model with panels rotated 30 degrees. Figure 3.3 shows an example of a time series showing the vertical response of a point on the model (marker M01, in the middle of the membrane) relative to the wave elevation at approximately the same position. This plot is only meant to illustrate the typical magnitude of the response. There is a phase shift between the model response and the incoming wave which is most likely due to the fact that the measurements are not done at the same time and not necessarily at the exact same position.
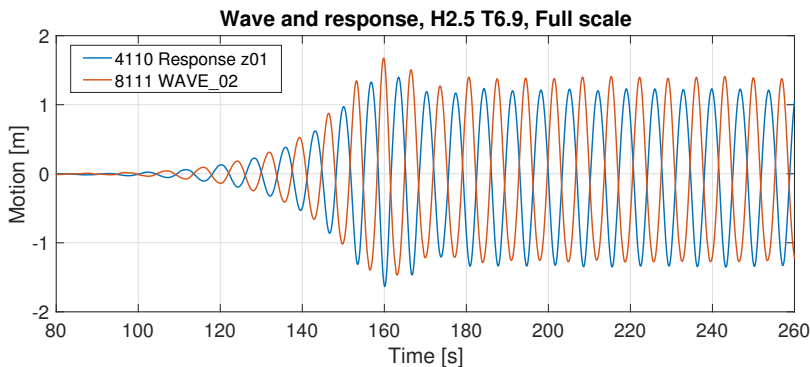
Figure 3.3: *Vertical response of marker M01 (blue line) and wave elevation (red line) at approximately the same position in wave 8110: H = 2.5m, T = 6.9s. Plotted through PlotMe by SINTEF Ocean.*

3.2.1 Vertical Response of All Points on Model

As explained in Section 2.5, all waves were run on the three different model setups. The response of all measured points on the model is gathered in Figure 3.4 to show the spread in motion relative to the wave input. It can be seen that for long-period waves, the entire model follows the vertical wave motion. The wave elevation and the vertical response are the same, leading to a RAO of approximately one. For shorter waves, the variation between points is larger. Some move a lot, resulting in a RAO of 0.8 to 0.9, while others have values going to zero, meaning no vertical response. Points 7 to 14 are located on the floating collar. It can be seen that these stand out as those of the lowest response, while the remaining points, located on the membrane, are have a higher and more uniform response.

It can be seen that the model without panels seem to reach a higher maximum response than the two tests including panels. There are also larger differences between each point in this test than what is experienced from the two tests with panels.

(a) *Model without panels.*

(b) *Model with panels.*

(c) *Model with rotated panels.*
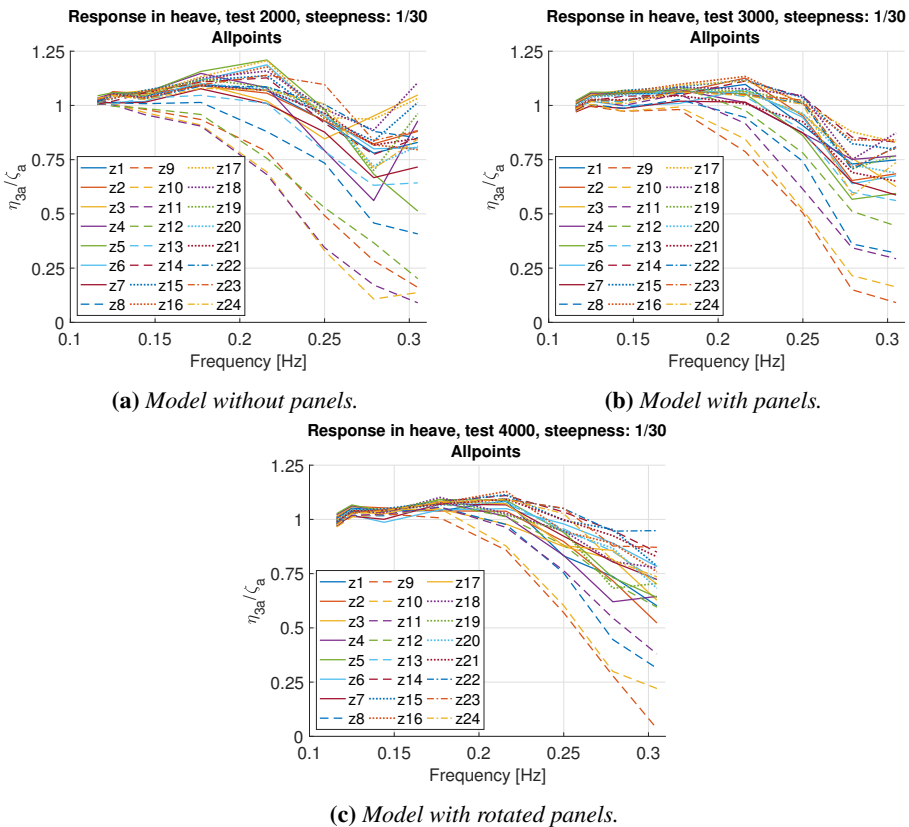
Figure 3.4: *Response plot in heave. Measurements from all 24 markers are included. The position of the markers M01-M24 can be seen in Figure 2.9. The z indicates that it is the vertical motion of the markers that has been considered.*

3.2.2 Vertical Response Along Centerline

Figure 3.5 shows the response of points located along the centerline of the membrane, in the wave direction. This plot may give information about how the response is damped when the wave travels through the structure. Point 15 is the first one the waves hits. Points 19 and 1 are located in the middle of the membrane, while point 5 is near the back wall of the model, also illustrated in the plots. As commented above, all points move along with the wave in long wave periods, while the response decreases when the waves get shorter. Points on the model without panels have larger variations between points, and seem to experience a slight increase in response for the shortest waves, which is also seen for some points in test 3000. No clear pattern on the motion of different points in relation to each other is seen, except that the point in the front, point 15, in general seem to have the largest motion amplitudes.

(a) *Model without panels.*

(b) *Model with panels.*

(c) *Model with rotated panels.*
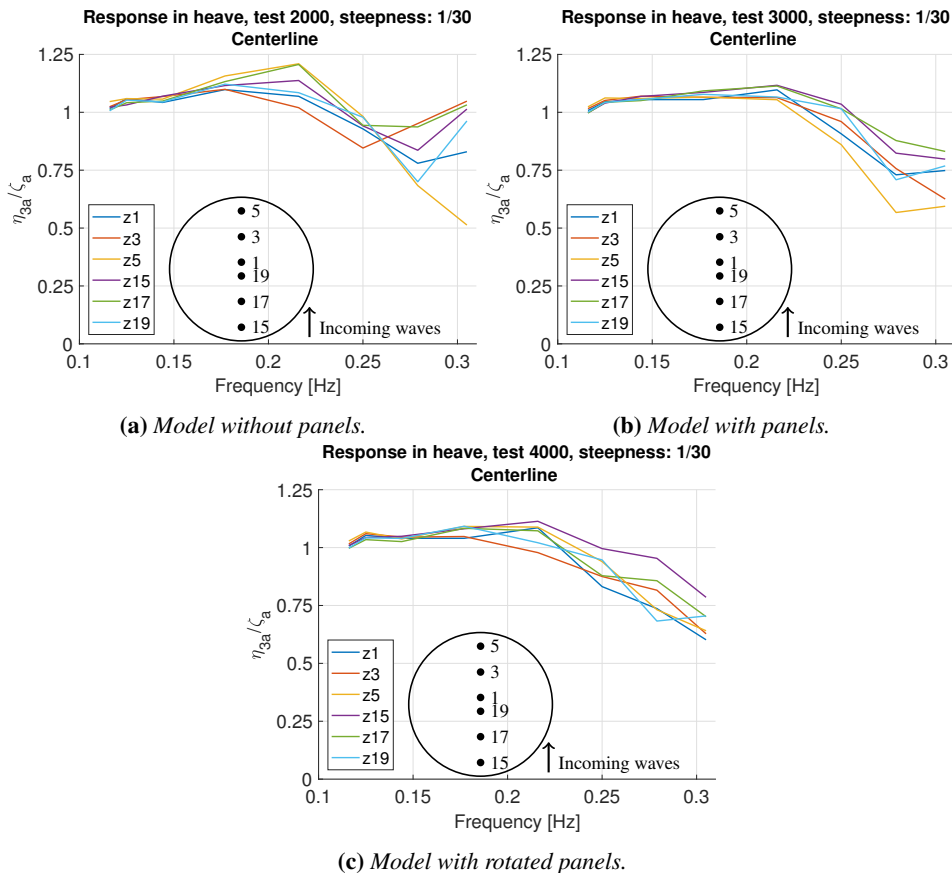
Figure 3.5: *Response plot in heave. Comparison of points along the centerline of the membrane. The locations of the points are illustrated in the plots.*

3.2.3 Vertical Response in the Transverse Direction

Figure 3.6 shows the response from the center point and out to the floating collar, transverse to the incoming waves. It can tell us something about how the motions vary in the transverse direction. Point 24 is the one closest to the wall, and in general, it seems to have lower response than the ones closer to the middle. The difference is however small and may be due to measurement uncertainties. In test 3000, points 22 and 23 are placed on the same panel, and as seen in plot 3.6b, they have almost the exact same response. In general it can be said that the motions are quite uniform along the middle of the model.

(a) *Model without panels.*

(b) *Model with panels.*

(c) *Model with rotated panels.*
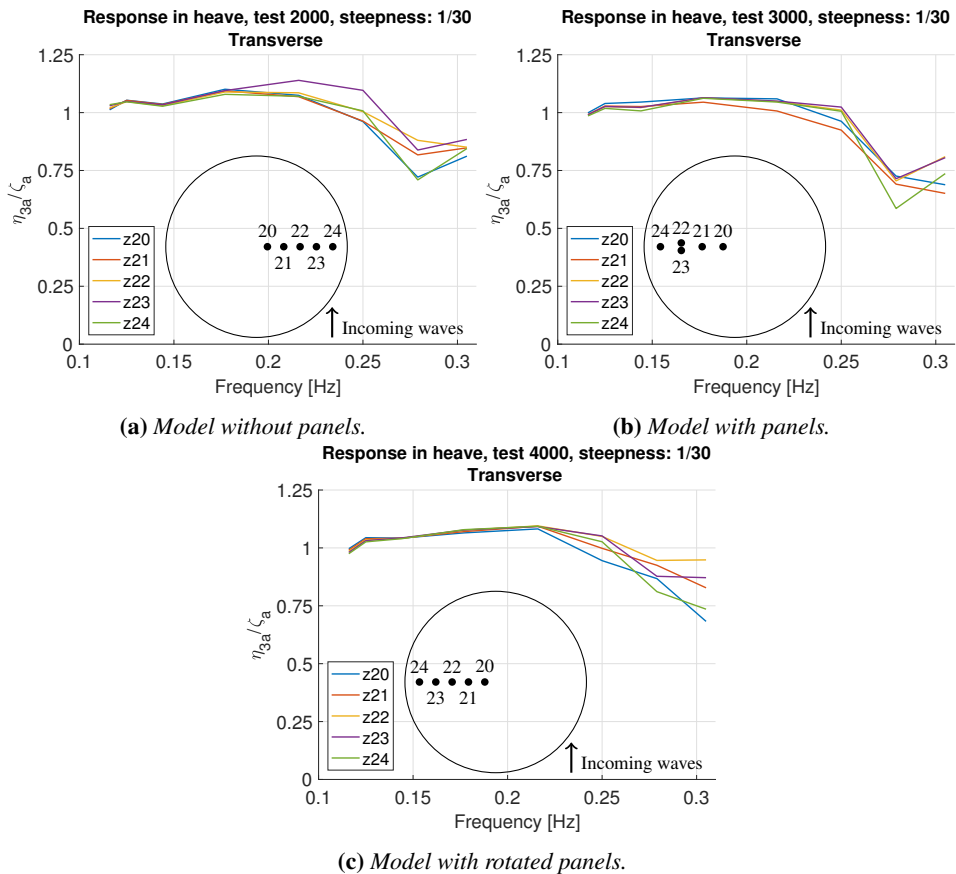
Figure 3.6: *Response plot in heave. Comparison of points on the membrane transverse of incoming waves, from the middle point and out. The locations of the points are illustrated in the plots.*

3.2.4 Vertical Response of the Floating Collar

The floating collar have a larger stiffness than the membrane, and the response varies more across it than it does on the membrane. The plots in Figure 3.7 show how different points

on the torus move in the vertical direction: Point 14 is in the front of the model, points 9, 10 and 11 are located at around 90 degrees and point 6 is at the far back of the model. The plots show a large difference in the response for short waves: while the points located at the side of the floating collar has little or no movement for the shortest waves, the points in the front and back move quite a lot. For tests 3000 and 4000, the point in the back also has less motion than the one in the front, indicating that the motion may be damped across the structure.

Because the marker placement for test 2000 is different from 3000 and 4000 (see Figure 2.9), both markers 9, 10 and 11 are included to represent the response of middle part of the floating collar. The location of point 10 in test 2000 corresponds to the location of point 9 in test 3000 and 4000, while point 11 in 2000 corresponds to point 10 in the results from tests 3000 and 4000. This should be kept in mind while studying the results from the floating collar in Figure 3.6.

(a) *Model without panels.* (b) *Model with panels.*

(c) *Model with rotated panels.*
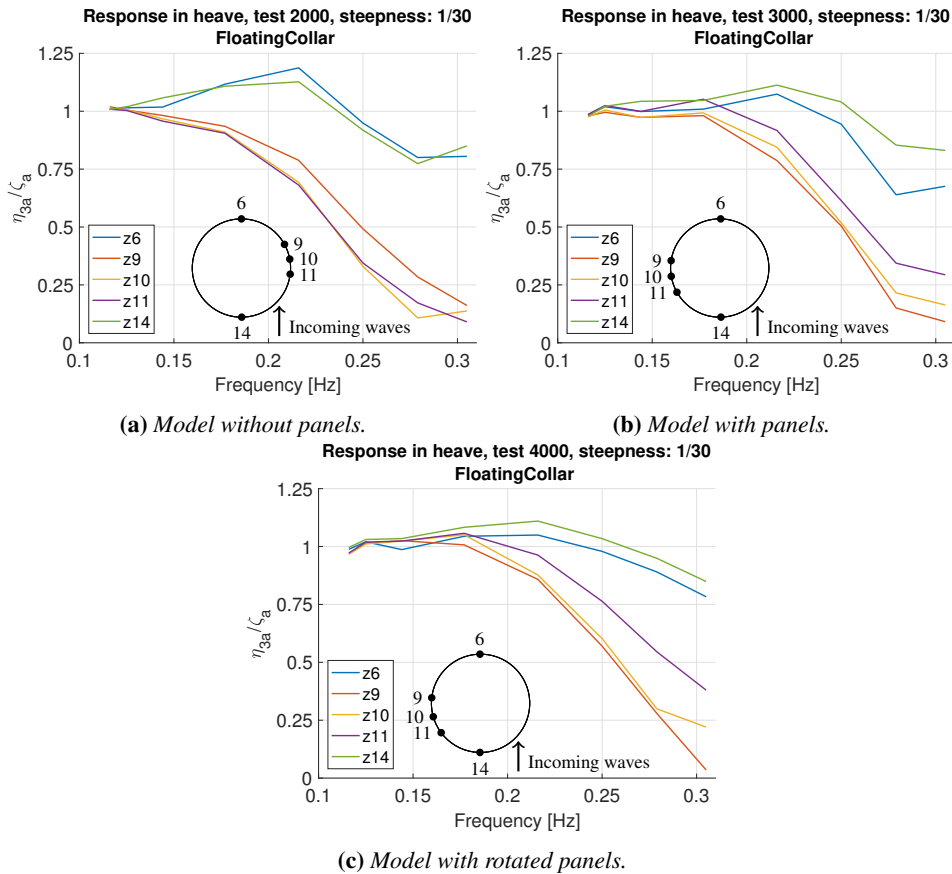
Figure 3.7: *Response plot in heave for points on the floating collar. The locations of the points are illustrated in the plots.*

3.2.5 Vertical Response in Irregular Waves

Figure 3.8 shows the transfer function $|H(f)|$ in heave for all points in the irregular sea state 8520, with $H_s = 2.5$m and $T_p = 6.0$s. The plots show similar trends as the response in regular waves, seen in Figure 3.4. For long waves, all parts of the model follow the waves, while for shorter waves the motion varies more. For some points the response amplitude decreases a lot as the waves get shorter, while for others it stays quite high. Points 7 to 14 are placed on the floating collar, and as for the RAO based on regular waves, the points with the lowest response amplitude are on the this collar.

(a) *Model without panels.*　　　　　　(b) *Model with panels.*

(c) *Model with rotated panels.*
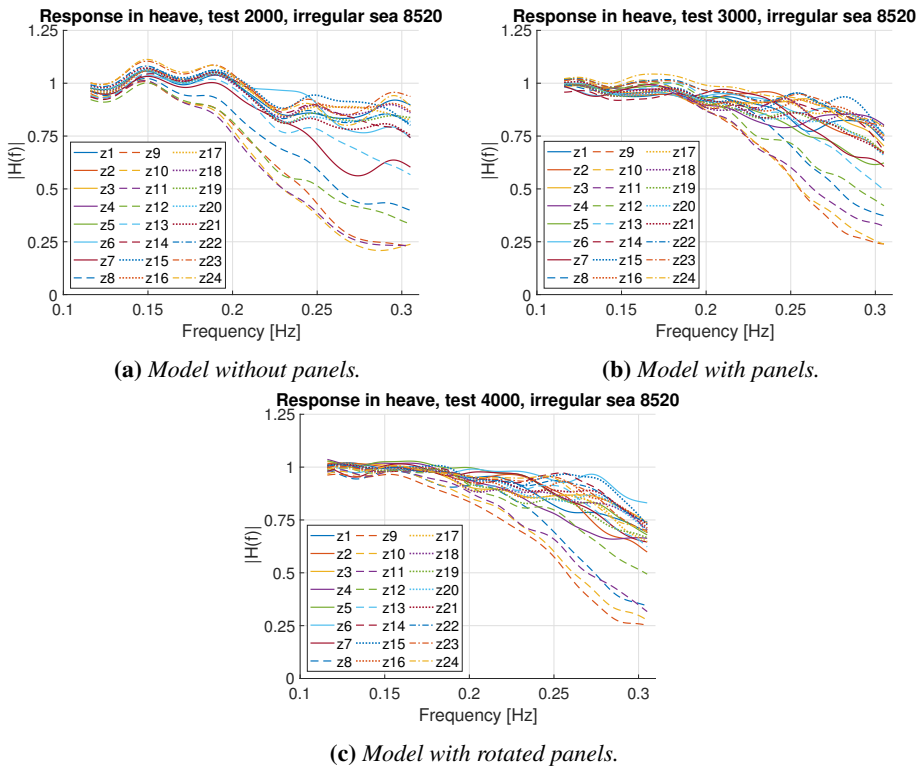
Figure 3.8: *Response plot in heave for irregular sea state 8520, $H_s = 2.5$m, $T_p = 6.0$s. Measurements from all 24 markers are included.*

3.2.6 Vertical Response Summarized

All the above presented plots show that the model follow long waves, with a response equal to the wave elevation. For shorter waves, the response decrease. The response of the membrane is quite similar at all points, while the response of the floating collar varies a lot between the front, aft and middle part. The plots show no signs of resonance behavior for the tested wave frequencies.

3.3 Comparisons

3.3.1 Variations With Steepness

Figure 3.9 shows how the response varies with wave steepness for four different points on the model. All results in this figure are from test 2000, the model without panels. Similar plots from tests 3000 and 4000 can be found in Appendix C.1. For the steepest waves, the shortest ones could not be run because they became unstable at the location of the model. This is why the RAO for the steepest waves (yellow) does not cover the same frequency interval as the two other lines. Four different points are tested for consistency: one in the middle of the membrane, one in the front and the aft, and one at about 90°.

(a) *Point in the middle of the membrane.* **(b)** *Point on membrane, at about 180 degrees.*

(c) *Point on floating collar, at about 90 degrees.* **(d)** *Point on floating collar, in the front, 0 degrees.*
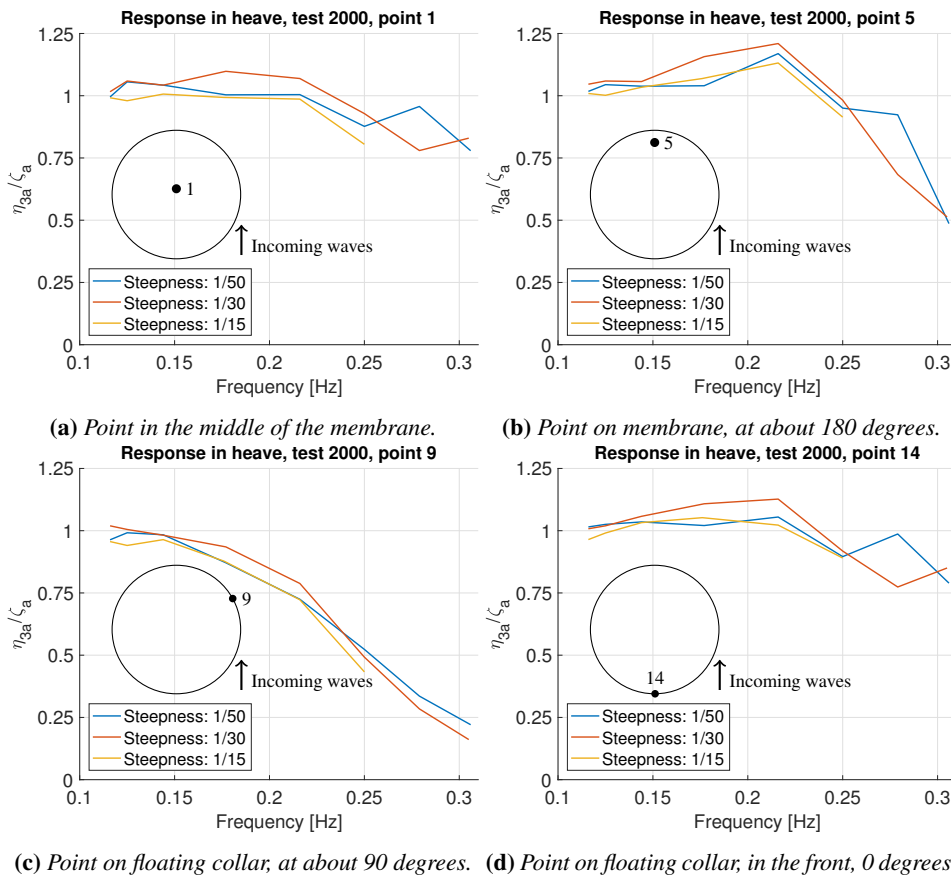
Figure 3.9: *Response plot in heave showing the variations with wave steepness for run 2000. The locations of the points are illustrated in the plots.*

All four plots show that the response amplitudes are similar for all three tested values for wave steepness, indicating that the response amplitude is quite linear for this structure.

3.3.2 Compared Response in Membrane and Floating Collar

(a) *Model without panels.*

(b) *Model with rotated panels.*

(c) *Model without panels.*

(d) *Model with rotated panels.*
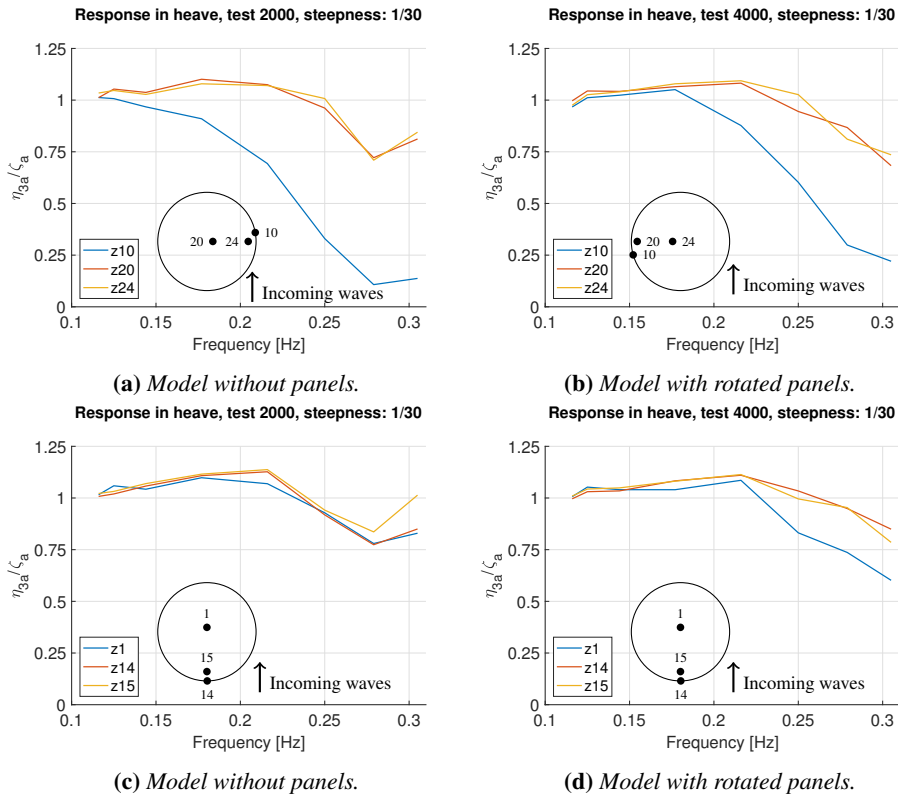
Figure 3.10: *The response of the membrane vs the response on the floating collar. a) and b) shows point 20 in the middle of the membrane, point 24 on the edge of the membrane, at about 90° and point 10 right next to point 24, but on the floating collar. c) and d) shows point 1 in the middle of the membrane, point 15 in the front of the membrane and point 14, right in front of it, on the floating collar. The locations of the points are illustrated in the plots.*

Figure 3.10 is meant to compare the motion of the membrane with the motion of the floating collar, in order to evaluate to what degree the motions of the membrane is affected by movements of the floating collar. The plots in 3.10a and 3.10b show the response of a point in the middle of the membrane (point 20), one on the edge of the membrane, at about 90° (point 24) and a point right next to it, but on the floating collar (point 10). It seems that the motions of the point close to the floating collar is no more affected by it than the point in the middle.

Figures 3.10c and 3.10d show equivalent plots for points along the centerline. Point 14 is on the floating collar, in front of the model, point 15 is right behind this, on the membrane and point 1 is in the middle of the membrane. These plots show the same, the point close to the floating collar does not seem to be affected by the motions of the floating collar.

3.3.3 Compared Response With and Without Membrane

As described in Section 1.3, Li (2017) investigated the vertical response of a floating collar with horizontal moorings. Figure 3.11 shows a small selection of results from this study, and corresponding results from the current model test of the model without panels. This comparison will hopefully show the effect of a membrane in such a floating collar. The plots show the vertical response at a point in the front (a), a point at about 90° (b) and a point in the aft of the model (c).

(a) *Front*   **(b)** *center*

(c) *Aft*
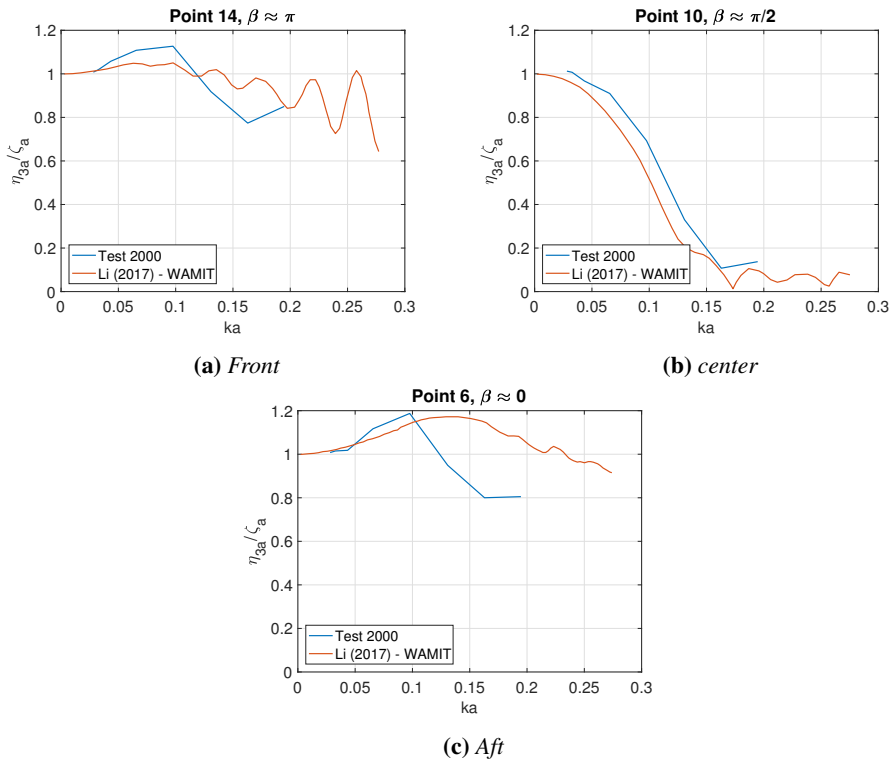
Figure 3.11: *Comparison between numerical simulations by Li (2017) on a floating torus and experimental results from the current study of a double-torus with a membrane. The numerical results are calculated using WAMIT. a) shows results from a point in the front of the floating collar, where the waves hit first, b) shows results from a point at about 90 degrees, and lastly, c) shows the transfer function in the aft of the model. The x-axes are wavenumber, k, multiplied by the tube diameter a.*

The trends are similar between the floating collar with and without a membrane, but especially the point in the back (c) seem to be affected by the membrane in shorter waves. This will be discussed further in Section 4.2.1.

3.3.4 Compared Response in Regular and Irregular Waves

Figure 3.12 shows the response of some selected points on the membrane and the floating collar, both in regular and irregular sea. The results are from the model configuration with panels (test 3000). The regular waves have steepness $1/30$ and the irregular sea state that leads to the plotted transfer function is weather 8520, with $H_s = 2.5$m and $T_p = 6.0$s. Each point has the same line type in regular and irregular sea. This plot, as the plots in Figure 3.8 showing response of all points in irregular sea, also shows that the trends in the response plots for regular and irregular waves are similar. Point 10 at about 90° on the floating collar has a significantly lower response in shorter waves than the other points, located at the front, middle and aft section of the model (See Figure 2.9). The response for these three points seem to in general be lower in the irregular sea than the results from the regular waves show up to a certain frequency where the transfer function based on regular waves drops quite abruptly.
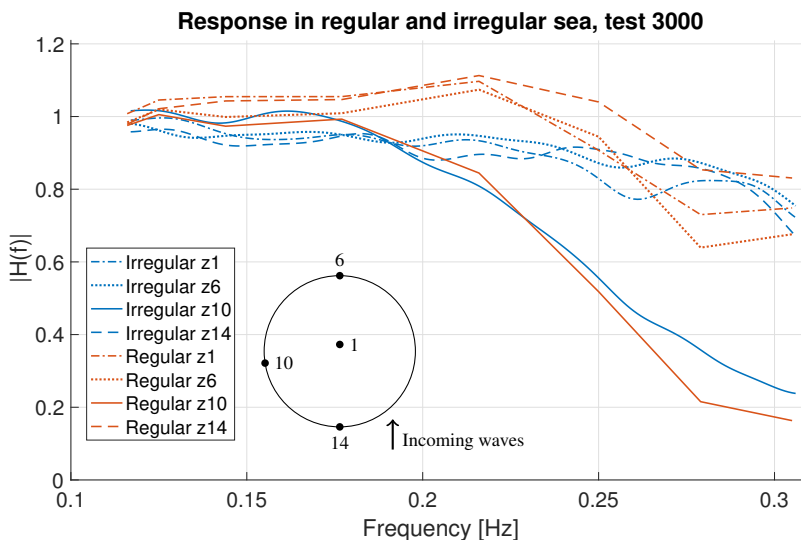
Figure 3.12: *Response of the same points in regular and irregular sea are plotted for comparison. The irregular sea state is 8520: $H_s = 2.5$m, $T_p = 6.0$s. The regular waves have steepness $1/30$. Blue lines represent the response in irregular sea, while the red lines represent response in regular sea. Each point have the same line type in regular and irregular sea. Positions of markers are illustrated in the plots.*

3.4 Horizontal Motion

Figure 3.13 shows the response amplitude operator in surge for all points on the model. All three model configurations are represented. The response in surge, the x-direction in the tank, is significantly smaller than the response in heave which was expected. For

most wave frequencies the amplitude of the surge motion is less than 25% of the wave amplitude. The exception is the longest wave for which the response is more than half the wave amplitude for all points. When the waves get shorter, the response decrease, and varies more. Markers M06 to M14 are on the floating collar, and in general the response of these vary a lot. The points on the membrane experience an almost identical response amplitude for all wave lengths. This trend is the same for all three model configurations, indicating that the horizontal motion is not affected by the presence of the panels of the direction of the incoming waves.

Point 24 is in the front of the model while point 6 is in the aft of the model. In all three plots the response of these two points seem to oscillate with a 180 degree phase shift: when the response in point 6 has a maximum, point 14 has a minimum and vice versa.

(a) *Model without panels.*

(b) *Model with panels.*

(c) *Model with rotated panels.*
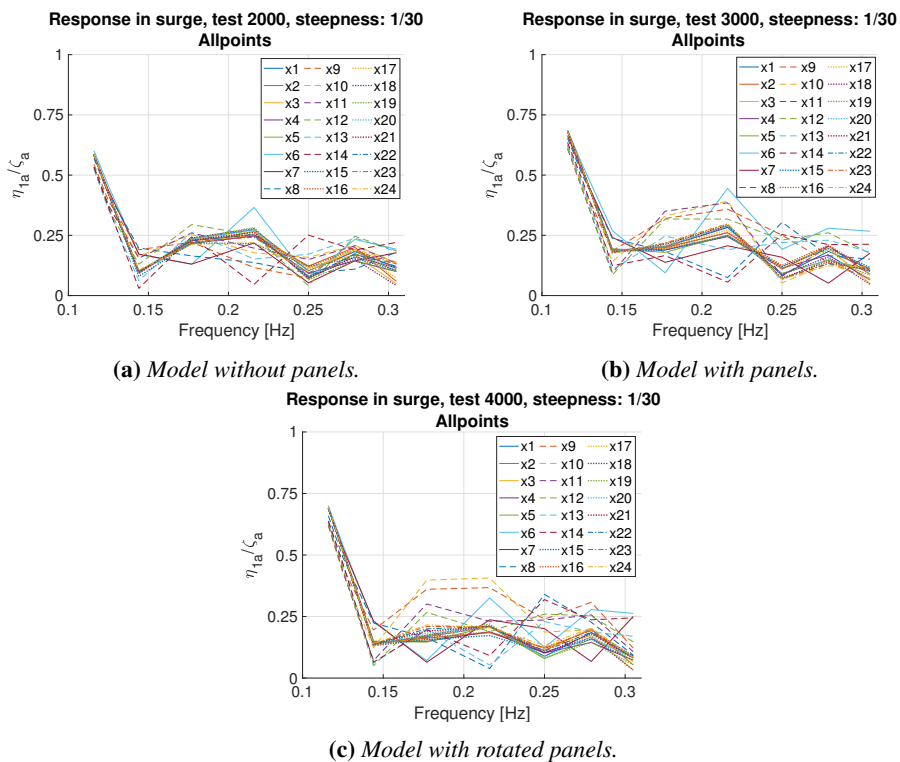
Figure 3.13: *Response plot in surge. Measurements from all 24 markers are included. The position of the markers M01-M24 can be seen in Figure 2.9. The x indicates that it is the vertical motion of the markers that has been considered.*

Figure 3.14 shows the vertical and horizontal response of four markers on the model without panels in wave 8170, normalized around zero. The points are placed on the middle of the membrane (M01), on the fore and aft of the floating collar (M14 and M06 respectively) and at about 90° (M11). The figure shows how the vertical motion has a phase

difference, which is natural due to the different locations . The horizontal motion has the same phase, indicating that the model moves as an unity in the horizontal direction. There are small differences in amplitude between the different points, which may be due to small deformations in the model.
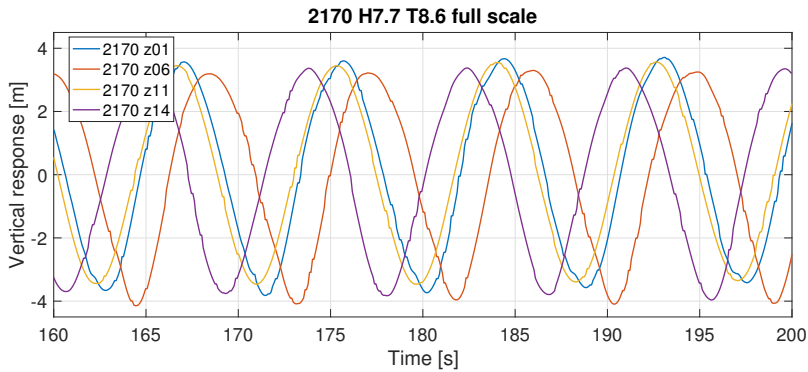
(a) *Vertical motion, normalized around zero.*
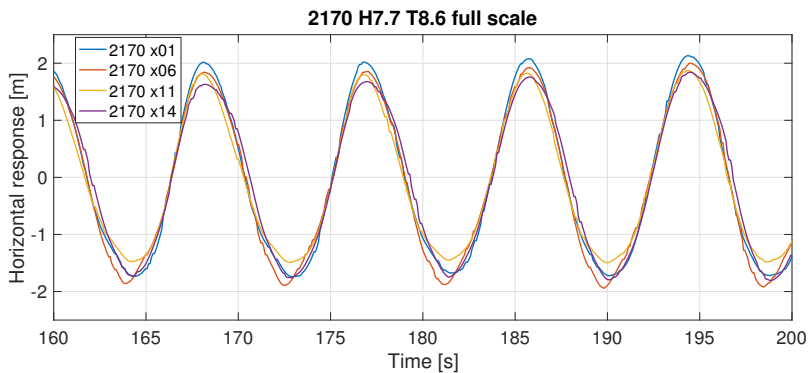
(b) *Horizontal motion, normalized around zero.*

Figure 3.14: *The plots show the vertical and horizontal motion of markers in the front (M14), aft (M06), middle (M01) and side (M11) of the model without panels in wave 8170: H = 7.7m, T = 8.6s.*

The plots in Figure 3.15 shows the motion pattern in vertical and longitudinal direction of these same four points. The location of point 11 in test 2000 corresponds to point 10 in test 3000 and 4000, which is the reason for the difference in the three plots. All three models have approximately the same motion amplitude in both x- and z-direction. In addition, the motion patterns are more or less the same. The latter does however vary with the different locations on the model. This will be further discussed in Section 4.2.2.

(a) *Model without panels.*

(b) *Model with panels.*

(c) *Model with rotated panels.*

(d) *Positions of markers.*
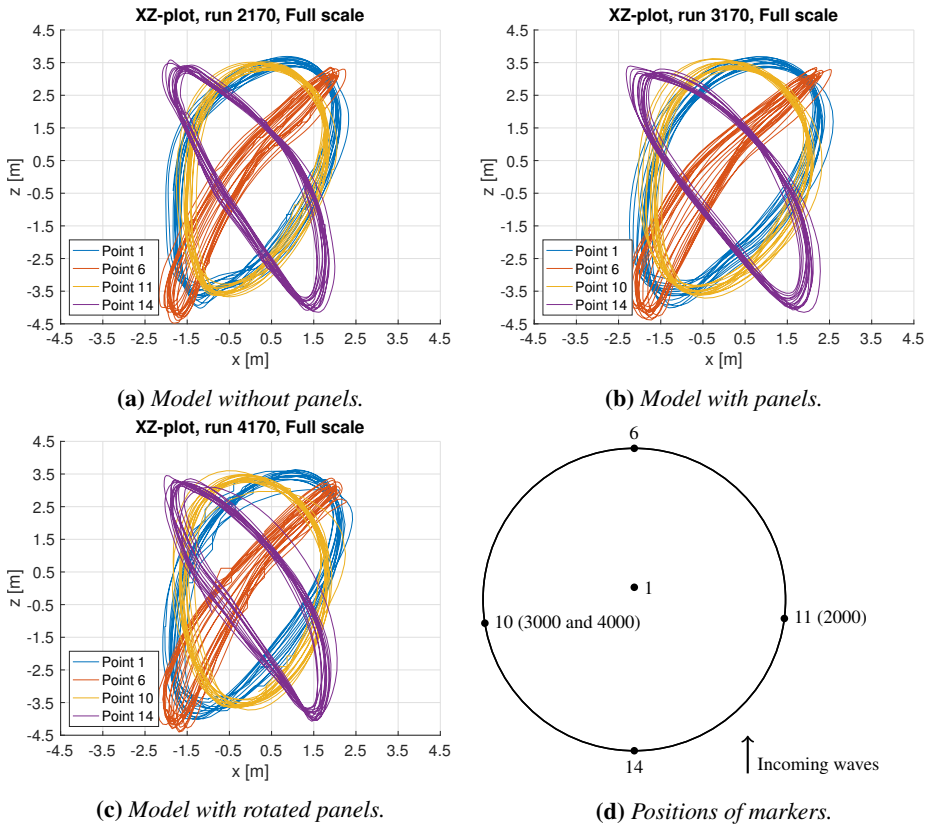
Figure 3.15: *Showing the motion in vertical and horizontal direction for the same points in the same wave on the three model configurations. Wave 8170: H = 7.7m, T = 8.6s. The locations of the points are illustrated in d).*

3.5   Mooring Forces

Figure 3.16 shows the mean force in the mooring lines in the direction of wave motion for each wave length tested. They are separated into the three values of steepness, and the plots show the three tests that are run, 2000, 3000 and 4000. The two least steep waves have low mean forces, close to zero. The steepest waves stand out, as the mean force in the mooring lines is much higher.

The mooring force for the steepest waves seem to be oscillating between higher and lower values as the wavelength changes. The tests of the model with panels seem to have a mean mooring force between 7 kN and 15 kN, while the model without panels have higher mean values varying between 12 kN and 20 kN. The plots show that the mean mooring loads is oscillating within a certain interval for the different wavelengths. These variations may be due to uncertainties in the measurements discovered while performing the towing test.

This will be further discussed in Section 4.2.3.

(a) *Model without panels.*

(b) *Model with panels.*

(c) *Model with rotated panels.*
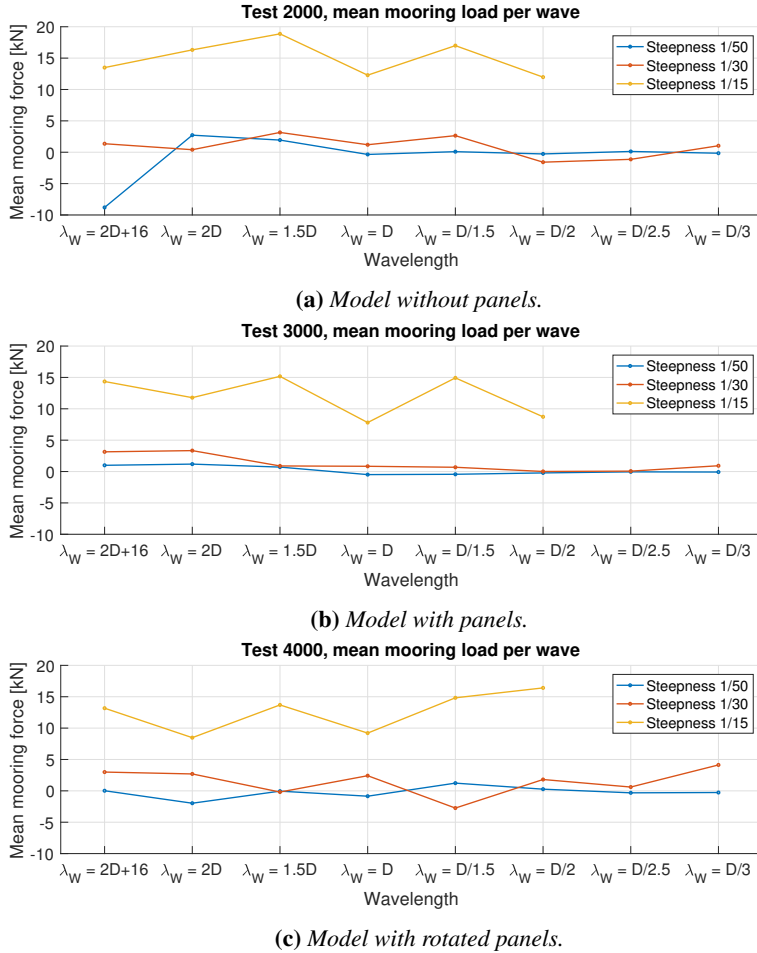
Figure 3.16: *Mean mooring force in direction of wave motion (x-direction) plotted for each tested wave, represented by its wavelength on the x-axis. The three plots represent the three model configurations, and all steepness values are plotted for each wavelength.*

Figure 3.17 shows the difference between the mean of the force peaks and the mean mooring force for all three tests. The steepness of the waves resulting in these plots is $1/30$. It can be seen that the maximum force decreases with decreasing steepness. Another aspect with these plots worth noticing is that the highest load value is lower for the model without panels (≈ 36 kN) than for the models with panels (≈ 44-45 kN).

(a) *Model without panels.*

(b) *Model with panels.*

(c) *Model with rotated panels.*
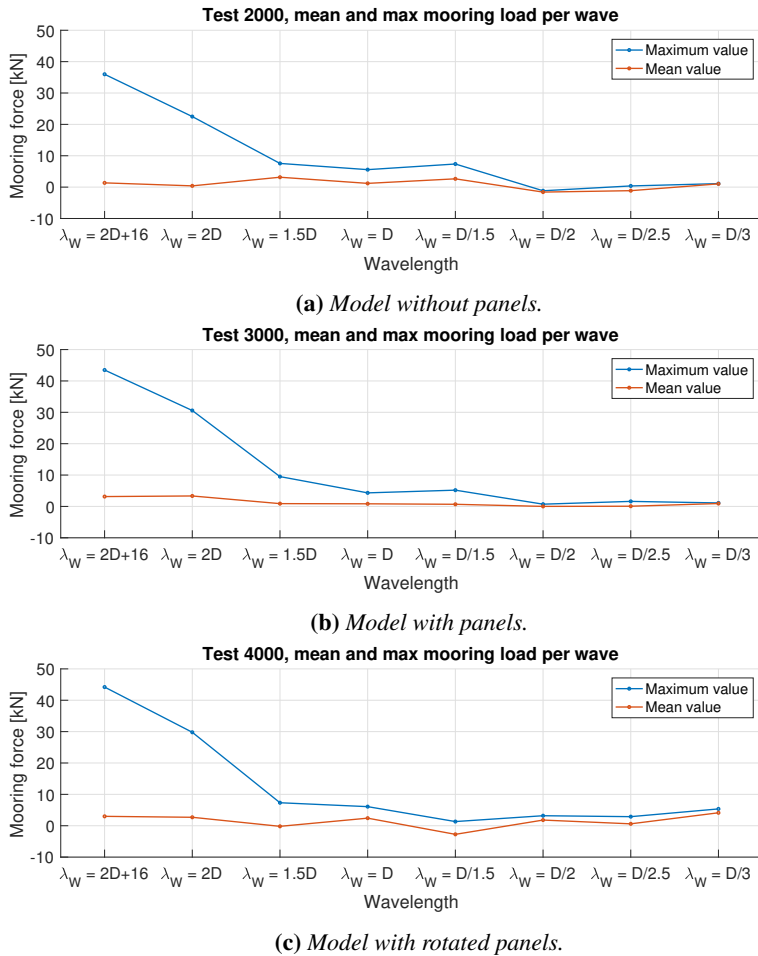
Figure 3.17: *Mean of oscillating force and maximum of force peaks in the direction of wave motion for steepness 1/30. The three tests 2000, 3000 and 4000 are shown. Plotted for each tested wave, represented by its wavelength on the x-axis.*

3.6 Visual Observations

This section will present snapshots from video footage of the model tests in order to describe observations of motion, deformation, wave making, waves over-topping the structure and other relevant phenomena noticed by visual investigation. Short relevant video clips can be found attached to this thesis.

3.6.1 Motion in Long Period Waves

Figure 3.18 shows the model with panels' motions throughout one wave period of the longest and steepest wave, wave 8170 with $H = 7.74m$, $T = 8.63s$ and steepness = $1/15$. The snapshots show how the model follows the wave elevation and contours the wave. The model travels back and forth with the oscillatory particle velocity on the surface. It clearly creates radiated waves traveling mostly in the x-direction, and not as much in the transverse (y-) direction. The water is over-topping the floating collar in the front and aft, but it is stopped from entering the membrane by the freeboard.

(a)

(b)

(c)
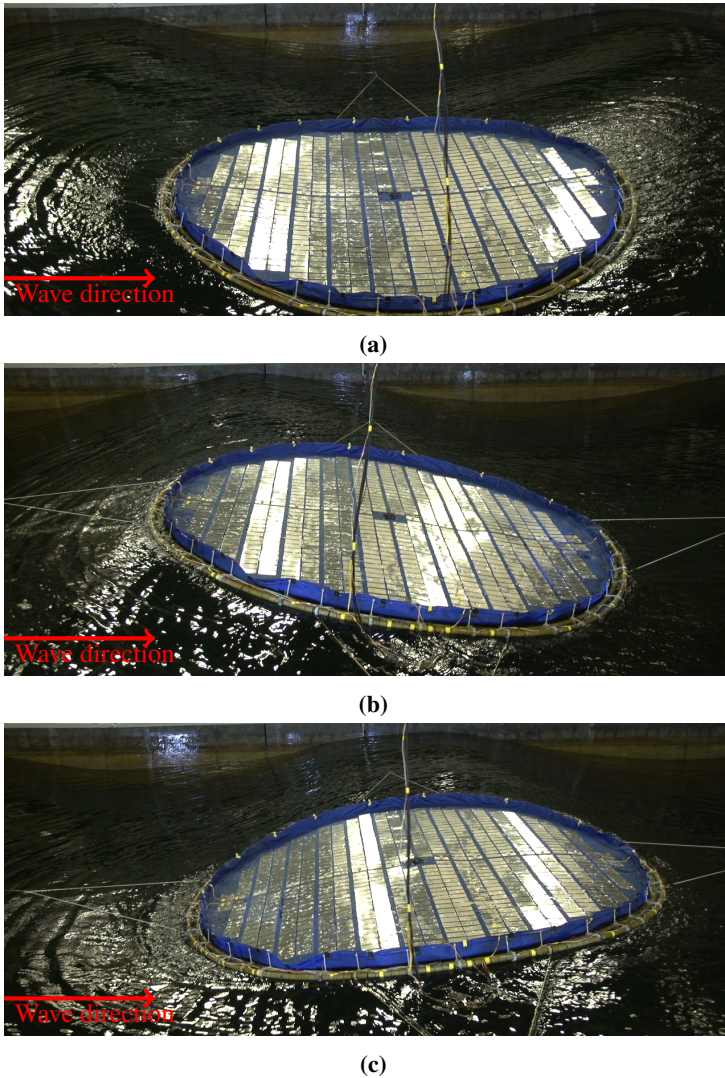
Figure 3.18: *Model in long period wave with large steepness. Run 3170.*

There are internal waves traveling across the inner section of the floating collar, seen by flapping motions in the membrane, better visualized on the model without panels in Figure 3.19.

(a)

(b)

(c)

(d)

(e)
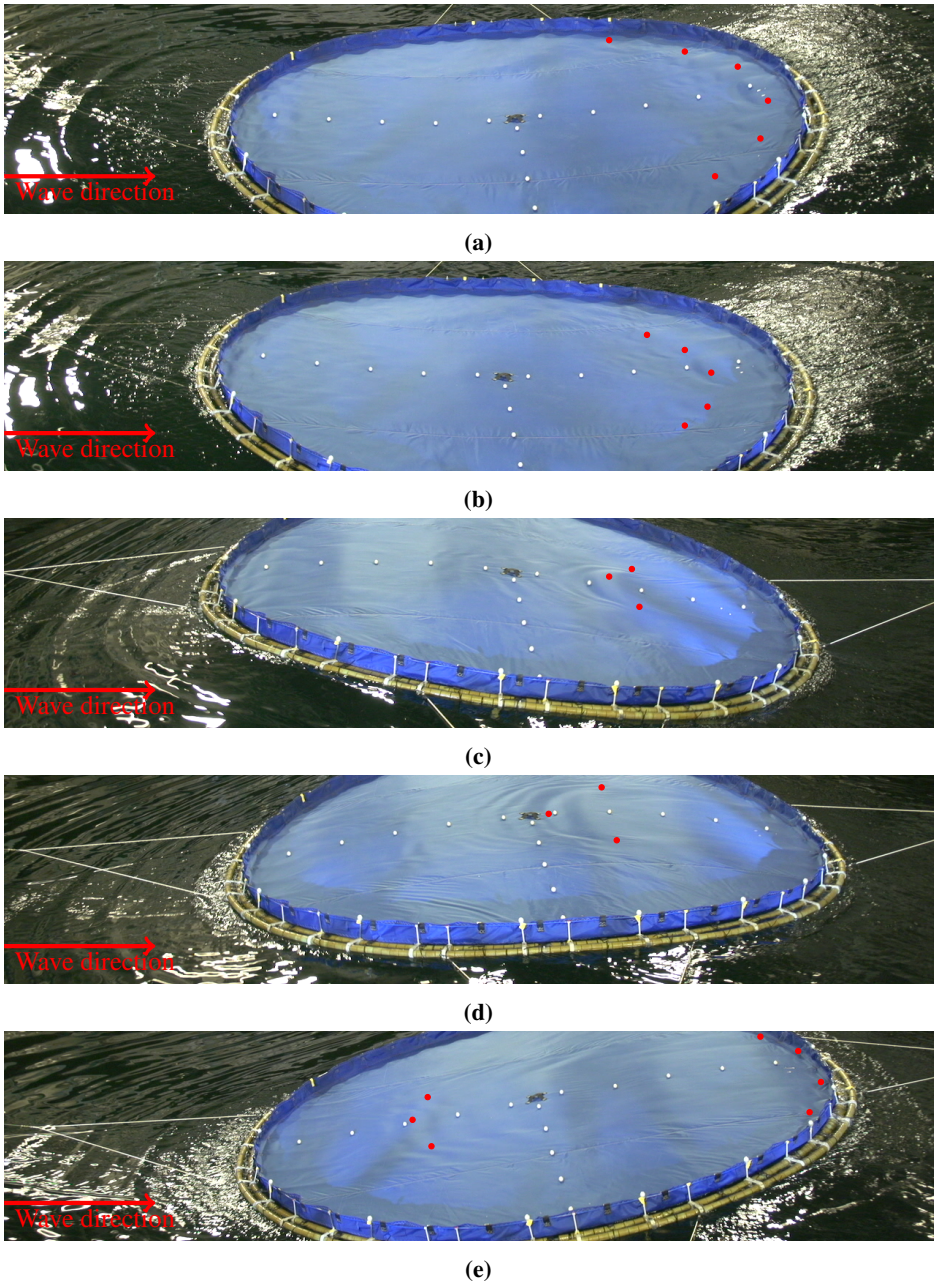
Figure 3.19: *Model in long period wave with large steepness. Run 2170.*

The red dots in Figure 3.19 follows the local wave motion inside the floating collar throughout one wave period of the incoming wave. These photos follow a full wave period, and by investigating the motion, it can be seen that these small waves are created with the same frequency as of the incoming wave but is traveling towards the wavemaker.

3.6.2 Motion in Short Period Waves

In short period waves, the model behaves quite differently. The wave travels through the membrane as it does in longer waves, but the floating collar is too stiff to fully contour the wave. The front and back moves up and down with the wave elevation, while the middle part of the collar has very little motion. This corresponds well with the RAOs showing the motion of the collar, Figure 3.7, as the value goes towards zero when the wave period decrease.
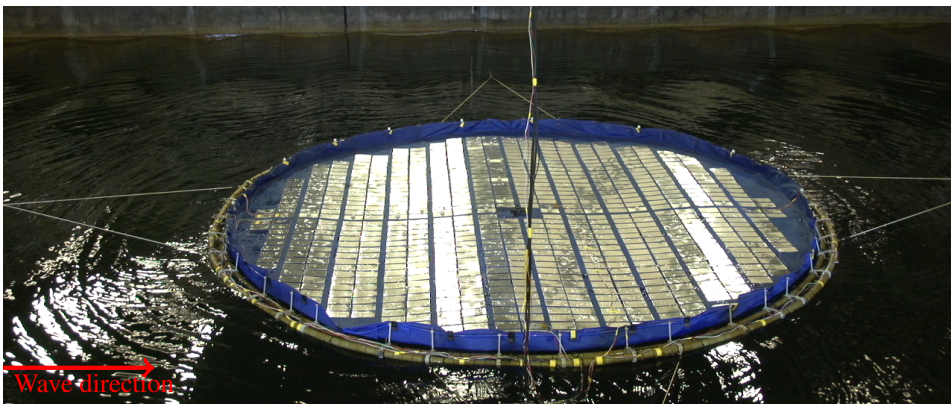
Figure 3.20: *Model with panels in short period wave with large steepness. Run 3160, $H = 0.56m$, $T = 3.27s$ and steepness = 1/30.*

The stiffness of the floating collar seems to prevent it from contouring the short waves. The result of this is that the collar experiences in and out of water motion as seen in Figure 3.21. This snapshot is taken from a wave that has a wavelength equal to half the model diameter, wave 8220. In some instances, water is pushed up along the freeboard. It is likely that without it water would have entered the membrane.

Figure 3.21: *Motion in short period waves. Run 3220, H = 1.67m, T = 4.00s and steepness = 1/15.*

For the shorter wavelengths the waves radiated from the model are also mostly traveling in the x-direction of the towing tank. Figure 3.22 shows how the front of the model is moving in and out of water for the short and steep wave 8220, creating radiated waves.
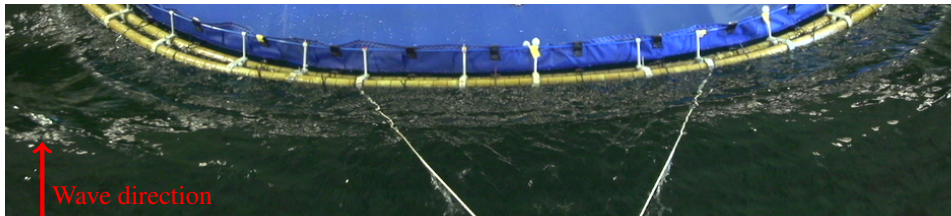
(a) *Floating collar going into the water before a wave crest.*
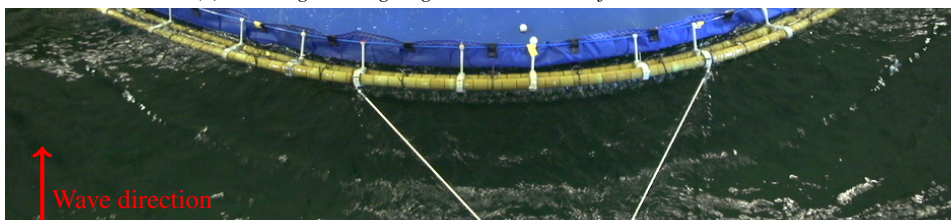
(b) *Floating collar going out of the water before a wave trough.*

Figure 3.22: *Motion in short period waves. Run 2220, H = 1.67m, T = 4.00s and steepness = ¹⁄₁₅. a) show when a wave crest approach the model and the floating collar goes into the water. b) is taken when the crest has passed and the floating collar goes out of the water.*

3.6.3   Waves Washing Over the Structure

There were several cases of waves washing over the model throughout the regular wave tests. This mainly happened for the steepest waves and was a result of the leading waves in the wave train being steeper than the stable ones coming after. However, it was during the irregular sea states that wash was considered a bigger problem.

Figure 3.23 shows snap shots from when some of the steepest waves of an irregular sea state hit the model without panels. This sea state was run for approximately 25 minutes, and afterwards, 14 liters of water was pumped from the model. Upscaled, this corresponds to more than 57 000 liters of water washing over the structure in 1 hour and 30 minutes. Some waves in this sea state were breaking, which indicate a local steepness of these waves close to ¹⁄₇.

Figure 3.24 shows how water can enter the membrane from the side of the model. The waves hit the model at the front side first, and then the wave builds up along the freeboard until it washes over at about 45 degrees from the front. It was also observed that without the freeboard, more water would be likely to wash over the membrane. The freeboard served as a wall in some cases when it was hit by the steep waves.

(a)

(b)

(c)
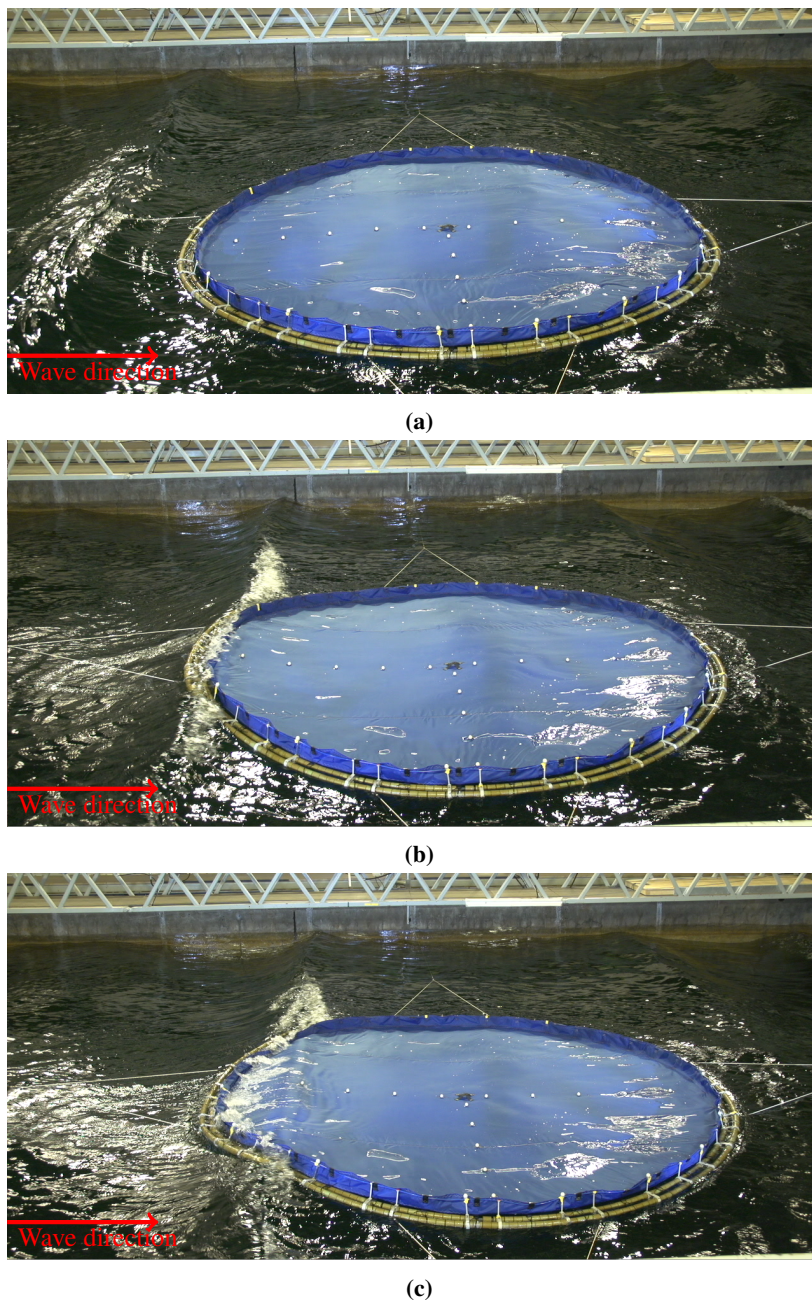
Figure 3.23: *Water entering the structure in the irregular sea. Run 2522, $H_s = 2.5m$ and $T_p = 6.0s$. A significant amount of water can be seen on the membrane. a) shows the steep wave closing in on the model, and b) is a photo taken as the wave breaks over the model. Here, it can be seen where the water enters from. c) is taken right after the wave washed over the structure and shows the amount of water that entered the membrane in one single wash.*

(a)

(b)

(c)

(d)
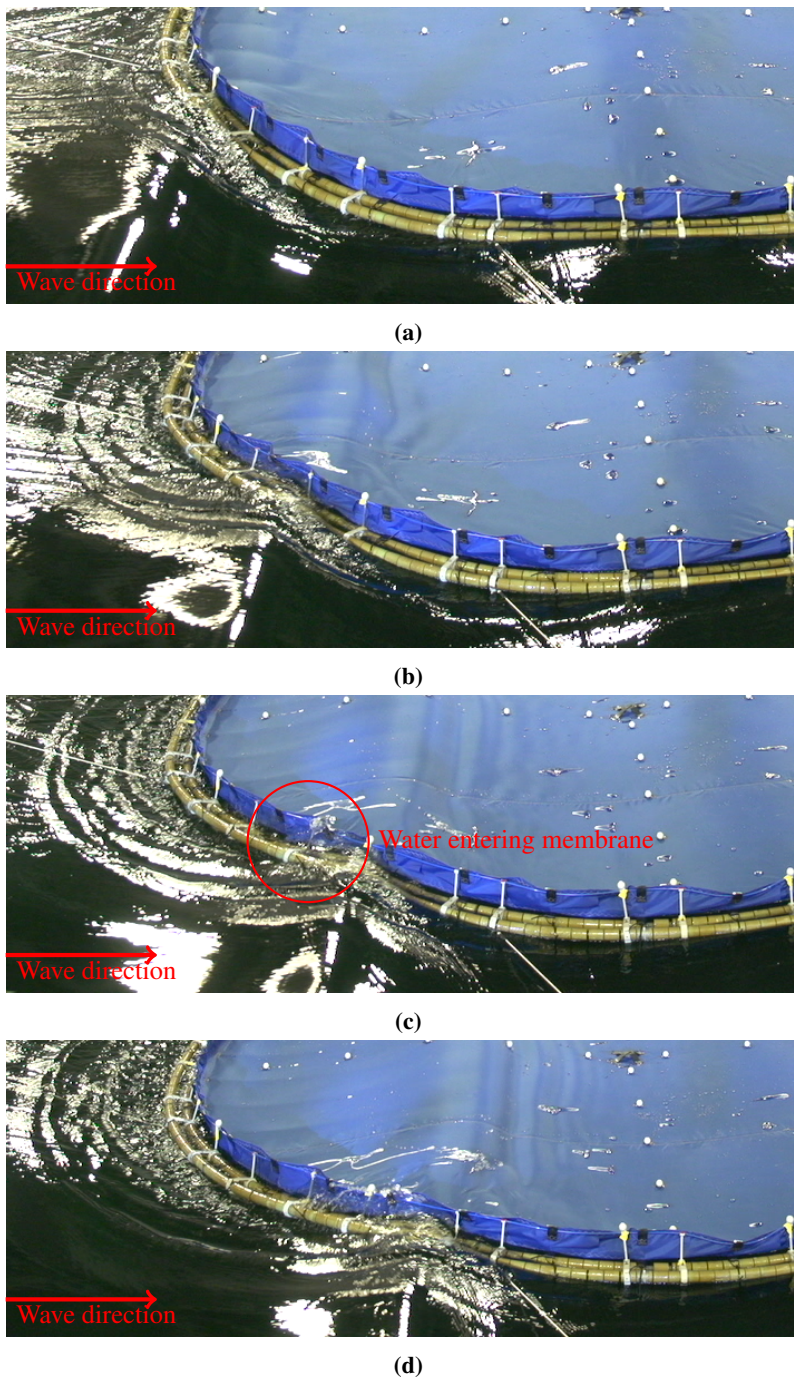
Figure 3.24: *Water entering the membrane from the side. Run 2220, H = 1.67m, T = 3.27s. One of the first waves in the wave train, probably steeper than the stable waves.*

3.7   Uncertainty Estimate From Repeated Measurements

To calculate the precision error for the measured response in the model test, one wave in test 3000 was run 6 times, and one from test 4000 was run 5 times. The calculated single point precision limit for a confidence interval of 95% will represent the uncertainty of each vertical response value. The uncertainty of the mean of the repeated test is also presented in the plot, but as the rest of the waves are only run once, this value will be too small to represent the uncertainty of the experiment. For test 3000, the uncertainty is calculated to be 15.9% and for test 4000 it is a bit lower, at 6.7%, both quite high uncertainties.

(a) *Model with panels, wave 8140.* **(b)** *Model with rotated panels, wave 8210.*
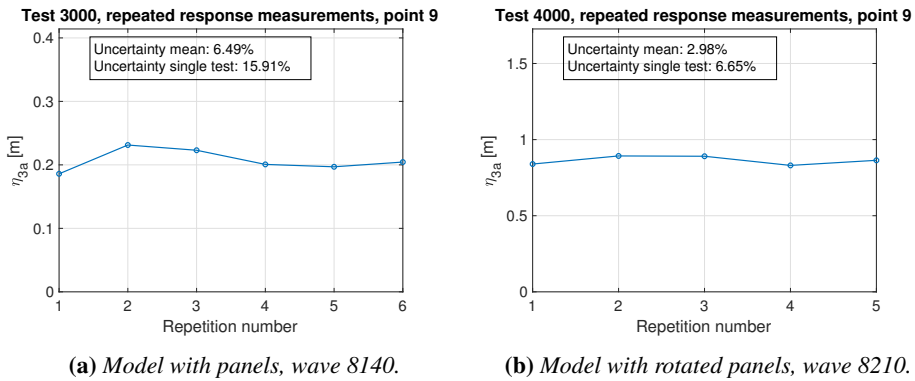
Figure 3.25: *Repeated tests for test 3000 and 4000*

3.8   Towing Tests

Figures 3.26 and 3.27 show the results from the towing test of the model for a full-scale towing speed of 1, 2 and 3 knots. As the plots show, there is a significant difference in the resistance at 0 knots velocity. The resistance should be zero as long as the model is not moving and there is no current. However, it is not, which indicate inaccurate measurements. Another aspect that decrease the credibility of this test is the large difference in measured resistance at 2 knots. In run 5012 the mean of the towing force is measured to be 2808N, while in run 5020 it is 7544N. Except for the towing speeds, nothing has changed between the two tests.

Repeated tests of both 5010 and 5020 are included as plots in Appendix C.2, and all values are summarized in Table 3.1. The summary shows large differences in towing forces between the different runs which points towards the measurements being unreliable. It is assumed that the uncertainties are a result of an unfortunate mooring configuration with pulleys which introduce friction that could have affected the measurements in the load cells. This will be discussed further in Section 4.2.3 in the next chapter.
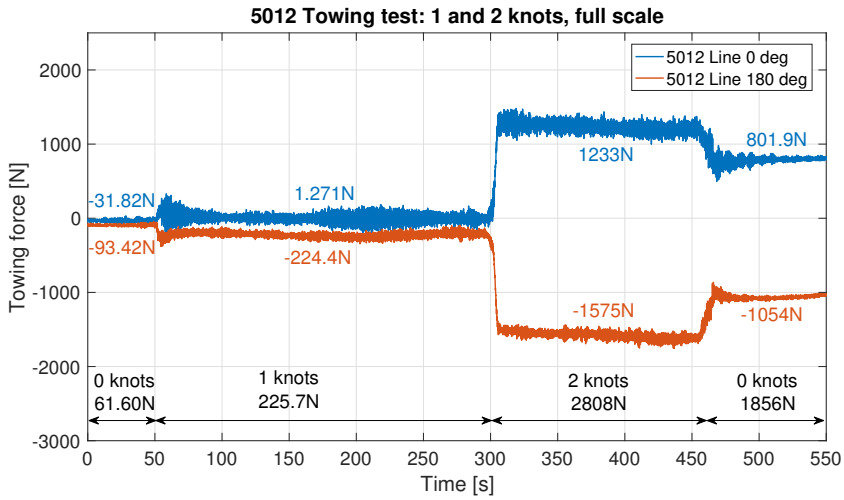
Figure 3.26: *Towing test to find resistance at 1 and 2 knots. Full scale resistance values for each velocity is mean towing force for the current speed.*
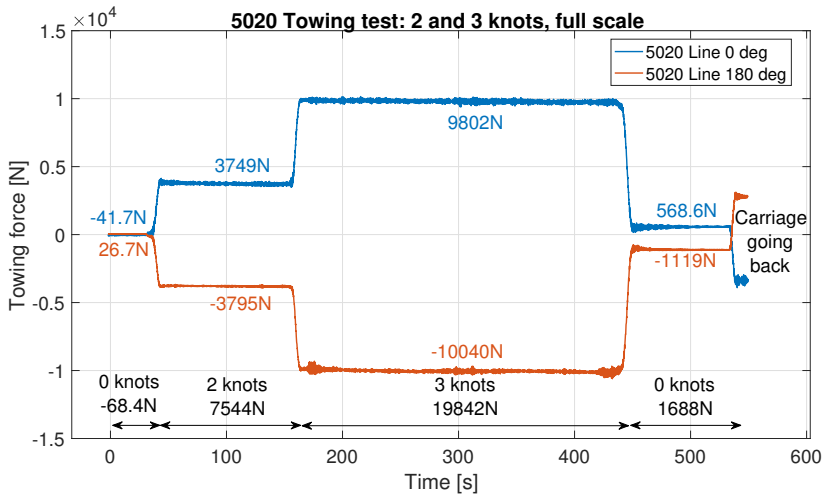
Figure 3.27: *Towing test to find resistance at 2 and 3 knots. Full scale resistance values for each velocity is mean towing force for the current speed.*

Table 3.1: *Towing forces from all runs summarized. Calculated mean force is also included, as well as the percentage difference between the maximum and minimum value for each towing speed, the maximum value being the reference value.*

	0 knots [N]		1 knot [N]	2 knots [N]	3 knots [N]
	Before	After			
Run 5011	-27	3109	59	4350	-
Run 5012	62	1856	226	2808	-
Run 5020	-68	1688	-	7544	19842
Run 5021	86	2425	-	8836	18723
Mean towing force	13	2270	143	5885	19283
Diff. between max and min	179%	46%	74%	68%	5.6%

Discussion

The following chapter will begin with a discussion of error sources in the experiment by trying to identify what sources that can be neglected, and which has to be accounted for when investigating the seakeeping capabilities of the structure. The most important observations from the presented results will then be summarized and discussed while the objectives of the thesis will be examined.

4.1 Errors and Uncertainties

When performing model tests there are many aspects that can affect the results. The measurements will most likely not represent the exact true value, and the difference between the measured value and the exact value is the error of the measurement. When the true value is unknown, as in most experiments, a statistical representation of the expected error can be made and is called the uncertainty of the measurement. In general, the errors are separated into *precision errors* which are variations in the measurements, and *systematic errors* or *bias errors* which can originate from different sources, more thoroughly discussed in this section.

4.1.1 Scaling

It is difficult to scale all parts correctly for model tests. The model in the current experiment has been Froude scaled, which leads to a too high Reynolds number in model scale

and hence incorrectly modeled viscous forces.

As mentioned in Chapter 1, Kristiansen & Faltinsen (2015) showed that a model with a too high stiffness affected the mooring forces of the structure. The stiffness of the model floating collar is a little too high compared to the full-scale collar in Ocean Sun's suggested structure as mentioned in Chapter 2. Based on this, the effect of the wrongly scaled stiffness may affect the results and should be kept in mind when investigating the results.

The membrane is assumed to be without elasticity and with a negligible bending stiffness. These assumptions are made to simplify the experiment and are based on the fact that the full-scale membrane is not very elastic, and it is only hand tightened to the circular frame, leaving it free to move instead of stretching. The mass of the membrane reached a lower limit when trying to find a material with the same strength and behavior as the one in full scale. Because of this, the weight is not properly scaled, and the membrane is too heavy compared to the suggested full-scale installation.

The stiffness of the modeled solar panels is also too high compared to the stiffness of a full-scale solar panel alone. However, to avoid high strain, the solar panels have to be reinforced in the full-scale installation to a point where they experience little to no deformation. This justifies the high stiffness of the model scale panels.

4.1.2   Model Inaccuracies

The floating circular structure is an already existing model SINTEF had available. Therefore, this will probably not be entirely equal to the full-size structure. However, the final design of the structure has not yet been finalized, and this study is more conceptional than finding the exact values for a specific structure. Some specific points are worth discussing, as they differ from the suggested concept:

- Due to human errors in the production, the model in this experiment has more panels than a corresponding sized full-scale structure is planned to have. This results in panels being placed closer to the floating collar, which may affect the stiffness of the whole structure, as well as the loads on the panels that are placed closest to the collar. However as mentioned, the design of the concept by Ocean Sun was not finalized when this experiment was performed, and this error is thus considered less important for the results, but something to keep in mind if the model test results is to be used for deciding the final design.
- The mooring system in the experiment is not realistic. In the model test, the model is moored horizontally, which in steep waves lifted the floating collar up from the water in wave troughs. As mentioned in Section 1.3, different mooring configurations can affect the response in both heave and surge (Colbourne & Allen 2001). This might be a significant error source when using model test result to predict response of the full-scale structure.
- Because it turned out to be the simplest solution, the membrane was fastened to the outer of the two rings in the floating collar. This was thought to not affect the model but turned out to slightly deform the position of the two floating tori in relation to each other which may again affect the behavior of the model.

- Throughout some of the wave tests, water would wash over the model in the first waves in the train, as these are steeper than the rest. This resulted in water on the membrane during the test interval, which may affect the response of parts of the membrane. It was observed that in some cases the water would gather around the reflective markers where the response was measured (see figure 4.1), which may have damped the response at these specific points. The real installation will most likely be equipped with pumps removing water due to rain and wash.
- The method Ocean Sun uses to fasten the solar panels to the membrane involves railings welded into the membrane which was considered too difficult to replicate in a model test. However, the difference between fastening them like this and gluing them on is assumed to be small in this scale and hence considered a less important source of error.
- The demo-installations by Ocean Sun has weights fastened to the middle of the membrane in order to create a slope in the canvas leading the water to the inlet of the pump. When testing the model this weight only created a pit in the middle and did not affect the inclination of the rest of the membrane. Due to this, and because the loads used in Ocean Sun's installation was arbitrarily chosen, this weight was taken off and not included in the model tests.
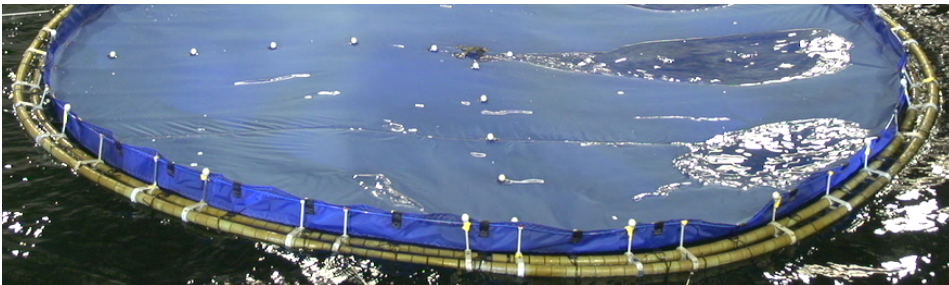
Figure 4.1: *Markers covered by water in run 2520.*

4.1.3   Errors in Test Setup

When creating waves in the towing tank, it is important that they stay stable past the point where the measurements are made. When waves become shorter and steeper, they will be able to travel a shorter distance before they get unstable and polluted by other wave frequencies. This means that in order to run short and steep waves on the model, it has to be placed as close as possible to the wavemaker, without risking that the waves are not fully developed. When testing the waves in run 8000, some waves showed unstable behavior and was taken out of the test matrix.

The opposite end of the tank was equipped with a wave beach to absorb the energy of the waves and minimize wave reflection. For long period wave trains traveling faster through the length of the tank, there are however wave reflections traveling in the opposite direction of the main waves. These reflections disturb the measurements when they hit the model.

Fortunately, for all waves it was possible to get a sufficient number of wavelengths before the reflected waves reached the model. This is still an argument for it being favorable to move the test section closer to the wavemaker and further from the wave beach (see Figure 2.4).

4.1.4 Errors in the Environmental Modeling

This model test is done to investigate how the structure acts when exposed to waves of different size and period. This means that it has not been tested for one specific location. At the time the experiment was performed, Ocean Sun did not have any specific location in mind, but was considering areas in different parts of the world, both in the ocean and on lakes and reservoirs. It was assumed that confined waters along the coast of Norway would represent the worst weather that was relevant for their concept. As the structure has many similarities with the gravity fish cages discussed in the introduction, and as the solar plant has been tested for serving these fish farming plants with electricity, locations where fish farms are placed has been used as basis for the choice of weather. Since the experiment was not performed for a specific area, errors in environmental modeling is considered less important.

A point where the experiment deviates from the realistic conditions is the lack of wind and current in combination with waves. However, this was not included in the scope of this thesis.

4.1.5 Tank Wall Effects

The model will be kept in the same place throughout the tests, which means that it will not outrun the waves made from the motion of the structure itself. In other words, it may be subject to radiated waves which are reflected by the tank walls. These may affect the motion of the structure that is to be analyzed, leading to erroneous results from the experiment. Ways to limit this error is by installing wave damping devices, by keeping the model small relative to the tank width, or by limiting the duration of the test. However, through visual observations these waves mostly travel in the direction of the waves, meaning that they do not hit the tank walls, and are in addition considered negligible in size compared to the incoming waves.

Parts of the waves made by the wavemaker was reflected back from the wave beach and towards the model. These disturbances can be clearly seen in the measurements when they hit the model. However, the time it takes for the waves to travel from the model to the beach and back again was sufficient to obtain a sufficient basis for the measurements, and this error source is neglected.

Blockage occur when a model is large compared to the tank and moving along it. The water will then gain an increased speed past the model. The model in the current experiment is not particularly large compared to the tank, and as it only lays on the surface, blockage is not considered to be a relevant error source in this model test.

4.1.6 Measurement Errors

The measurements from a model test is affected by the sensor accuracy. This accuracy is dependent on the calibration process, the measurement range, drift etc., and varies between different types of sensors.

The water temperature may affect the wave probe measurements, which is why the water temperature has been logged throughout the model testing. The logged water temperatures can be seen in Appendix B.2. The temperature varies between approximately 12.5°C and 14.5°C, i.e. $\approx$ 2°C variation. However, since zero measurements have been made regularly, drift due to water temperature variations is considered small. According to Steen (2014), the model accuracy of wave probes can roughly be assumed to be 1 mm.

The uncertainty of the optical measurement system Qualisys has been investigated by Jørn Jensen at SINTEF Ocean. After calibration of the system, there are still some variations in the measurements. Jensen reports a mean measurement error of 0.08 mm and a standard deviation of 0.5 mm, after calibrating a volume of 7m x 4.5m x 1m. This is the systematic error in the measurements. In addition, there are random errors in the system, found by measuring a stationary marker over time. This has through Jensen's investigations showed a standard deviation of 0.1mm. These uncertainties are statistically independent, and the total error in the measurements are thus equal to $\sqrt{0.5^2 + 0.1^2} \approx 0.5mm$. The fact that water in some cases covered the markers, as seen in Figure 4.1, may have affected the measurement accuracy, as the cameras could lose markers out of sight. By paying attention to the logging in Qualisys when there was a substantial amount of water on the membrane, it was observed that the cameras lost the markers out of sight for short time instances. However, this was only observed to happen when the model without panels was exposed to the irregular sea state 8520, and is not considered a problem for any of the other runs.

The check of the load cells in the mooring lines is presented in Figure A.6. The load cells were applied a known load of 1 kg after installation, and the measurements showed an error of less than $\pm 1\%$. However, the towing test showed inaccurate measurements which are suspected to come from pulley friction. More about this in Section 4.2.3

4.1.7 Human Error When Setting the Sampling Frequency

As mentioned in Section 2.9.2, a human error was made with regards to the sampling frequency of some of the measurement channels used in the model test. Some of the analog channels had their sampling frequency reduced from 200Hz to 25Hz between test 2000 and 3000, while the cutoff frequency of the lowpass analog filter remained at 20Hz. This is unfortunate, as the sampling frequency should be at least double the cutoff frequency to avoid aliasing in the signal. The wave measurements were the most important channels that were affected by this mistake. The sampling rate is still high enough to capture the waves with a frequency between 0 and 12.5Hz, but the noise with frequencies between 12.5Hz and the cutoff frequency of 20 Hz may be subject to aliasing, introducing more of the lower frequencies in the measurements. As the incoming waves in model scale are between 0.46Hz and 1.22Hz, these are well within the frequency range that is fully

captured. However, the presence of shorter waves (radiated waves, noise etc.) may lead to aliasing and thus erroneous amplitude measurements.

To investigate how this mistake affected the measurements, wave spectra was plotted for one wave measured with a sampling frequency of 200Hz and one sampled at 25Hz. The plots showed a significant difference in the amplitude of the two spectra for some waves, but the peak frequency was the same, and there were few other frequencies present. This was repeated for all waves, and as a general rule, the longer waves had similar amplitude, and the difference increased with decreasing wave length. This could be a result of the noise amplitude being relatively higher for shorter and smaller waves. Equation 2.6 shows the clear relation between the wave amplitude at a certain wave frequency and the spectrum value at this frequency indicating that the lowpass filter affected the wave amplitude measurements. Some examples of these plots are included in Appendix C.3.

The result is that the wave amplitudes from tests 3000 and 4000 are affected by the mistake in sampling frequency. There is a difference in the wave amplitudes measured at 200Hz and at 25Hz, but the wave frequency did not seem to be affected. The response measurements from these two tests are not affected as they are digital and not filtered before sampling. The results presented in this thesis is only based on wave measurements from test 8000, which were sampled at 200Hz and response measurements from tests 2000, 3000 and 4000.

As a concluding comment to the topic discussed in this subsection, the results presented in this thesis are not affected by the sampling error. However, if the measurements from this model test are to be further used, it should be kept in mind that some of the analog channels in tests 3000, 4000 and 5000 may by corrupted by this mistake.

4.1.8 Repeated Tests to Estimate Precision Error

The repeated tests showed large uncertainty in the experiments, 15.9 % in test 3000 and 6.7% in test 4000. The weight t from the students-t distribution decrease exponentially with the number of repeated tests. With few repetitions, the uncertainty is multiplied with a higher value of t to compensate for fewer repetitions. With this in mind, it would have been useful to base this uncertainty estimation on more measurements, however, lack of time made this difficult.

Another explanation for the high values of uncertainty, is that the author learned during the experiment that the waiting time in the first test was a little short, leading to uncalm water affecting the measured results in some cases.

4.2 General Discussion of Results

This section discusses the results presented in Chapter 3. Firstly, the most important aspects of the vertical response are considered, followed by the horizontal motion. Then the

mooring loads and towing test results are discussed and compared. Lastly, the importance of the visual observations done throughout the model test is examined.

4.2.1 Vertical Response

The vertical response of the different parts of the model is showed in Section 3.2. The response has been measured at different locations representing all the different parts of the structure (see Figure 2.9). From the response plots presented in this section, it can be seen that there are large variations of the response throughout the structure. For long waves, the whole model follows the wave, with a response that is close to the wave elevation. When the waves get shorter, some points experience a vertical response which is higher than the wave elevation. When the waves get even shorter, the response for all points decrease relative to the wave height, some more than others. The structure is elastic but seems to be too stiff to contour the water surface in the shortest waves. For long waves the model bend and follow the wave, while for shorter waves the floating collar does not move as much, probably because it is stiffer than the membrane. The front and back of the collar is more free to move up and down with the waves and has a higher response amplitude than the middle part of it. The membrane is more flexible and will bend with the shorter waves as well.

From the plot showing the response of only points on the floating collar, Figure 3.7, the points on the mid-section, i.e. 9,10 and 11, appear to have the least motion in shorter waves. This is also observed visually through video footage.

Effect of the Presence of a Membrane

The work by Li (2017) consisted of model tests and simulations of a floating flexible torus with horizontal moorings, more thoroughly described in Section 1.3. By comparing the results from this study with the results from the current model test, it is possible to look for differences between the plain torus and the torus with a membrane. In this way, the effect of a membrane in such a structure can be studied.

Figure 3.11 shows the vertical response calculated from WAMIT for a floating torus without a membrane plotted together with experimental results from torus with a membrane. The results from Li has been digitalized for better comparison. The trends of the response are similar, however, there are some distinct variations worth discussing.

Firstly, in the front part of the model, the experimental results show a higher response for long waves before it decreases drastically to a lower value. The model without a membrane, analyzed numerically, seems to have an oscillating response amplitude operator for the shortest waves

For the middle section of the collar, the decrease in RAO with decreasing wavelength seems to happen at a lower wave frequency for the model without a membrane. However, the model with a membrane show quite similar behavior.

For the measurements in the aft section of the model the differences between the motion is more or less the same for the longer waves. The model with a membrane seems to have lower response than the floating collar alone, especially for shorter waves. When the RAO of the experimental results reaches a value of 0.8, the floating collar alone still has a RAO of more than one. This means that its vertical motions are larger than the wave elevation whereas the membrane seem to dampen the motions of the model in the experiment significantly.

The results from Li (2017) are calculated by WAMIT, which is a computer program based on first and second order potential flow theory. Experimental investigation might include phenomena that are not captured by numerical solutions and may be the reason for some of the differences between the results presented in these plots. When using potential flow theory, viscous effects are not considered, which may introduce differences between the results. Another aspect that may affect the results is that the calculations without a membrane is based on a single HDPE tube, while the model test is done on a double-tube structure.

Seen in light of these uncertainties, the overall behavior is considered to be similar for both the model with and without a membrane.

Effect of Panels on the Membrane

When it comes to the effect the panels have on the wave-induced motions of the model, differences between the three tests has to be investigated. For the vertical response, it seems like a general trend that the model without panels has an increase in the RAO for the shortest wave. This sudden change in the decreasing trend is also seen in the model with panels and for some points in the model with the rotated panels, however less prominent and more damped than for the model without the more than 700 panels.

Another visible difference between the tests with and without panels is that the increased response for the middle length waves is largest for the model without panels. This seems like an additional indication that the presence of the panels increases the damping of the structure significantly. Also, the panels seem to affect the vertical motion of the floating collar for longer waves having the response of the collar follow the waves longer while the wavelength is decreasing and following the membrane's motion to a larger degree.

These observations point toward a higher damping for the model with panels. The floating collar is the same, so the difference must come from the presence of panels. The panels add a significant amount of weight to the structure, but also extra stiffness to the membrane and hence to the full structure which may be the reason for the differences. Also, membrane with and without panels were manufactured separately, and the fastening of the membranes to the floating collar was done without measuring the tension of the membrane. Hence, different pre-tension in the membrane for the two model configurations is also a possibility and may be a source of error.

4.2.2 Horizontal Motion

From the response amplitude operator in surge, Figure 3.13, it can be seen that the motions in surge are as expected smaller than in heave, and the whole membrane seem to be moving uniformly. The response of the floating collar varies a bit more, but for most of the wave frequency the surge amplitude for the whole model is less than 25% of the wave amplitude. There are little differences between the results from the three model setups.

The motion patterns at different points are shown through xz-plots in Figure 3.15. These plots confirm that there seem to be little differences between the model configurations, but the differences in motion patterns between points are clearly visible. The points in the middle of the structure show more or less circular motion patterns, while the points in front and aft have sharper oval motion patterns. Through visible inspection of the video footage the physical explanation for the motion pattern seem to be clearer. Because of little deformations in the horizontal direction, the whole structure seem to be moving horizontally as a unit, while vertically, all points can move separately. When a wave crest hits the front of the model, this point is forced to move upwards, but since the rest of the model have little motion in the horizontal direction, the same applies to the point in the front (point 14). When the wave reaches the middle of the model, it will pull the whole structure horizontally. The aft point will start by moving horizontally at this point in time, and then experience vertical motion when the crest reach the aft point of the model.

The presence of 2nd and 3rd harmonics in the response was briefly mentioned in Chapter 2. These components are relatively larger for the response in x-direction than for the vertical direction. It has not been part of the scope of this thesis to investigate these, but the importance of these components could be interesting to consider more closely to gain more knowledge about the surge motion of the model.

4.2.3 Mooring Loads During Waves and Towing

Figure 3.16 shows the mean mooring force measured for all waves. As briefly mentioned earlier, linear wave theory says that the mean force in waves should be zero (Faltinsen 1990). Linear wave theory assumes a small steepness, and it can be seen from the plot that the linear assumption of a mean force equal to zero is good for a steepness of $1/50$ and almost as good for a steepness of $1/30$. However, for the steepest waves presented in the experiment $H/\lambda_W = 1/15$, the nonlinear effects seem to be more prominent leading to a significantly higher mean force. Another thing to notice from these plots is how the mean force is oscillating when the wave length decrease.

The above described is the similar for all three model configurations that were tested, but with a small difference in value. The mean force for the steepest waves on the model without panels is slightly higher than for the model configurations with panels. When examining the plots in Figure 3.17 which show the mean mooring force in all tests, the maximum force experienced by the model is larger for the model with panels. These observations could be a result of the different stiffness of the models with and without panels, but the differences are small, and may also be due to measurement uncertainties.

The loads in the mooring lines during the towing tests are presented in Section 3.8 and are smaller than the maximum forces measured in the longest waves. For 1 and 2 knots, the forces are also smaller than the mean load in steep waves. As briefly discussed in Section 1.3, it was expected that the current forces would be less dominant compared with a fish cage since this structure is only on the surface. However, the measurements from the towing test show extreme variations between the different runs and are not considered reliable. In addition to the large difference in towing force for each towing speed, the results indicate a significant inaccuracy in the measurements as the resistance is not zero at zero velocity and current.

It is assumed that the main reason for the inaccurate measurements is friction in the pulleys used in the mooring configuration. The pulleys are placed between the load cells and the model, which means that they can affect the measured force in the mooring lines by introducing static friction in the tests. This means that a certain force must be overcome before the pulley can move, which is represented by the difference between the two zero-knots loads before and after the test given in Table 3.1.

If more accurate values for the towing resistance is to be obtained, the mooring configuration should be changed. One solution would be to change to frictionless pulleys, which might be difficult to find. Other measures to remove this error source would be to move the load cell to the model-side of the pulley, or to completely change the mooring configuration.

Because the results from the towing test show such clear signs of being unreliable, it is reasonable to keep in mind that this may also have affected the measured mooring loads in waves. It can be argued that the static friction has less impact on the mooring load measurements in waves, as the pulleys are continuously moving back and forth. However, when the pulleys are changing their scrolling direction, there will inevitably be a short stop, and the static friction of the pulleys may affect the measurements. The mean force in this test was as mentioned oscillating with the decreasing wave length. It would be reasonable that the pulley friction could lead to unexpected phenomena like this.

4.2.4 Visual Observations

In general, the model was observed to move flexibly and deform as the wave hit it. All waves could be seen traveling across the structure, but the shorter waves were more prominent in the membrane than in the floating collar. Apart from this, the most important visual observations were:

- Waves washing over the structure in steep and irregular waves.
- Water building up along the freeboard in a larger range of waves.
- Small waves in the internal basin radiated from the floating collar.

Waves washing over the structure is considered the most severe observed phenomenon. This was observed as the incoming waves got higher and steeper. The full-scale plant will be equipped with pumps to remove water from the membrane. However, these will mainly be meant to keep rain water away, not large amounts of water entering as a result of waves

over-topping the structure. It may lead to sloshing loads when the water is entering and moving around on the membrane, and in addition increase corrosion on the model. This is especially important to avoid if the model is installed in sea water, as the salt further accelerates corrosion. The studies by Rahman et al. (2015) showed that dust on a solar panel may reduce its performance by about 30%, and it is reasonable to think that this may also be the case if the panels are covered by a layer of salt. It would then be necessary to rinse the panels, resulting in extra maintenance. With this in mind, the limiting factor for tolerable sea states seems to be over-topping waves which again is strongly affected by the wave steepness. Wash was mostly seen in the irregular sea states where the steepness in some cases is high enough for waves to break.

The water that is building up along the freeboard illustrates the importance of a protective wall to limit the amount of water entering the membrane. This was seen for a larger range of waves than those that lead to water on the membrane.

Especially in larger waves, the floating collar tended to create radiated waves traveling outwards from the model, but also inwards inside the "pool" made by the torus. The small radiated waves from the structure lead to quite large motions of the solar panels. Through observation, these small waves was seen to have a significant effect on the panel movement. As these waves had a size in the order of the panels, they could contribute to deformation and strain of the panels, even though they may not have an equally important effect on the floating collar itself. It is important that the bending of the solar panels are kept to a minimum, to avoid large strain which can lead to micro cracks and a lower efficiency. These aspects will not be discussed more in this thesis but is thoroughly covered in the master thesis by Selvig and Markhus.

4.3 Trends of Results

The steepness comparison in Figure 3.9 indicates that the response shows linear behavior. The three different values of steepness show similar Response Amplitude Operators which indicate that the response is independent on wave steepness. This would mean that these results can be used to foresee the vertical motions of the structure in all kinds of waves. The fact that the transfer functions from irregular waves showed the same trends as those from the regular tests further support the assumption of linear behavior.

For longer waves than what has been tested in the present experiment, it is reasonable to believe that the transfer function of vertical response converges toward unity. The longer the waves are, the more will the model follow the wave elevation. For very short waves, the response is expected to go to zero. However, for the wavelength interval before this happens, the response can be more difficult to predict.

The model has shown to have similar behavior as the model without a membrane, tested by Li (2017), so one could assume that these results could be used to say something about the response of the present structure in shorter waves. Based on the plots for the response of different parts of the membrane versus the response of the floating collar (Figure 3.10)

the response amplitude of the floating collar, especially the middle section, is expected to go towards zero motion long before the response of the membrane.

As discussed above, the mooring loads show nonlinear behavior for the steepest waves. Hence, the mooring loads are more complex and harder to predict for other sea states.

4.4 Comments on Ocean Sun's Concept

The suggested concept by Ocean sun did not include a freeboard, this was only added to the model as it was considered interesting to investigate how it would work. It turned out to be effectful in limiting the amount of water washing over the membrane and panels as water was observed to build up along the edge in several instances. By extending the membrane up to the railings, a freeboard was achieved easily. However, the loads of waves hitting the freeboard may cause wear and tear of both membrane and railings, and other more durable solutions should be considered. In addition to this, it is recommended to further investigate the mooring configuration, depending on the location where the full-scale installation will be placed. More about this, and other suggested further work, in Section 5.2.

Conclusions

5.1 Concluding Remarks

This thesis has reported the results from a model test performed on a floating solar plant based on double semi-submerged circular HDPE tubes similar to those of gravity fish cages. In the inner basin of these tori, a membrane is fastened to serve as support for solar panels. Three different model configurations were tested: *without solar panels*, *with solar panels* and with solar panels *rotated 30°* relative to the incoming waves, all based on the same floating collar and mooring configuration. The models were tested in regular waves with a length ranging from a little more than twice to a third of the diameter of the floating collar. Each wavelength was tested for a steepness of $1/50$, $1/30$ and $1/15$. In addition, two irregular sea states based on the JONSWAP-spectrum were tested. The purpose of the model test has been to investigate the seakeeping capabilities of the suggested installation in waves.

The vertical motion has been presented in terms of response amplitudes in the frequency domain with a focus on identifying the effect the membrane and panels have on the motion of the installation. For all model configurations, the model followed the wave elevation in long waves. In shorter waves the model seemed to not be elastic enough to contour the water surface, leading to a decreasing response amplitude. There was a difference in this decrease in motion for the floating collar and the membrane. The motion of different points on the floating collar varied a lot, with points in the middle of the model going to zero for the shortest waves. The membrane is more elastic which allowed it to easily follow the waves, and the motion of all points on this showed the same trend. The models

with solar panels showed signs of higher damping, as there was a larger variation between the motion of different points on the model without panels. In some points the transfer function value rose slightly above unity, while others decreased. Except from this there did not seem to be signs of resonance behavior of the model in the tested waves. The vertical response also showed linear behavior.

In addition to the vertical response, the horizontal motion and mooring forces have been analyzed. The horizontal response showed little differences between the three model configurations. Unfortunately the mooring loads were observed to have high variations in results between runs, and were thus considered less reliable. In addition, the mooring line response showed nonlinear behavior.

The general behavior of the installation has also been evaluated through visual observations, both during the model test and by inspection of video footage afterwards. Snapshots from these are included for visualization. The observations showed that the steepest waves in the irregular sea states lead to substantial amounts of water washing over the structure and gathering on the membrane. This is considered the most severe observation and is after this model test considered the limiting factor for which waves the structure can withstand. In the interior basin of the floating collar, radiated waves caused flapping motions in the membrane. These were small and did not affect the motions of the floating collar notably, but as they had a size in the range of the solar panels, they might affect the strain and deformation of the panels.

As mentioned, the vertical response showed linear behavior for the tested waves, which indicate that the response plots presented in this thesis may be used to predict motion in waves of different steepness. The mooring force did however show nonlinear behavior, and may be more difficult to foresee.

Finally, the results from this model test suggest that a freeboard is necessary in order to limit the amount of water over-topping the structure. In this experiment, a freeboard was constructed by extending the membrane up to the railings of the floating collar. This was observed to prevent water from entering, and was a simple way of constructing a freeboard on the installation. However, it is unknown how large loads this configuration can handle and special attention should be made when choosing a possible layout for the freeboard of a full-scale structure.

5.2   Further Work

Reflecting on the model test in hindsight, some aspects are advised to further investigate if a new model test is to be performed, in order to get an even better insight in the seakeeping capabilities of the suggested floating solar plant.

Firstly, by testing the exact same floating collar and test-setup without a membrane, a better representation of the effect of a membrane could be obtained. The comparison with the results by Li (2017) provide an indication of the differences, but by keeping all

other parameters equal with and without a membrane, a more certain investigation may be performed.

The wave interval tested in this experiment was decided based on what was expected to be the most relevant wave lengths for such a structure. To verify the response at a specific location, the model should be tested in more precise wave conditions, both regular and irregular, based on wave data from this area. In addition, testing the model in even shorter waves could be interesting in order to see how the response amplitude is at higher frequencies. To make the environmental modeling as realistic as possible, wind and current could be introduced together with a relevant irregular sea state.

The model in this test was not pushed to determine extreme limits of the structure. The model test indicated that the problem of water washing over the structure occurred before extreme limits of what the structure itself could handle was reached, naming over-topping the limiting factor for allowable waves. However, when considering if a location is suitable for this installation, it could be highly relevant to be able to assess whether or not the structure can withstand the worst weather conditions seen in the suggested area. If reliable results should be expected, a different focus would have to be put into correct scaling of the membrane and its attachments to the floating collar, into mooring configuration and in general into the strength of all parts of the model. Getting a realistic picture of the extreme loads may be easier by including measurements of the load in the membrane and its attachments. In general, achieving a good indication of extreme limits would require a new dedicated model test.

Furthermore, if the phase shift of the response is to be investigated to obtain more information about the response of the structure, new model tests have to be performed with this in mind. As mentioned in Chapter 3, the exact positions of the wave probes were not logged in this model test, making it difficult to say anything regarding the phase shift of the response. Through a new test where this position in relation to the points where response is measured is logged, the phase shift may be found and the transfer functions complete.

The mooring line configuration in this experiment lead to inaccurate measurements, and the mooring force results presented showed signs of being unreliable and is advised to verify. However, these loads would be very beneficial to investigate in order to aid the design of mooring configuration when constructing a full-scale installation. It is suggested to investigate different mooring configurations with the goal of making the best full-scale mooring design, and avoid the problems with friction in the pulleys.

In addition to performing a new model test, a full-scale installation should eventually be tested. A demo installation has already been tested by Ocean Sun, but not of the size that this thesis is based on. Snow, waves from passing boats, bird droppings etc may introduce new challenges which is difficult to foresee without a full-scale test.

Bibliography

Colbourne, D. B. & Allen, J. H. (2001), 'Observations on motions and loads in aquaculture cages from full scale and model scale measurements', *Aquacultural Engineering* **24**, 129–148.

Dolara, A., Leva, S., Manzolini, G. & Ogliari, E. (2014), 'Investigation on performance decay on photovoltaic modules: Snail trails and cell microcracks', *IEEE Journal of Photovoltaics* **4**(5), 1204–1211.

Dong, G.-H., Xu, T.-J., Zhao, Y.-P., Li, Y.-C., Gui, F.-K. & Zhao, Y.-P. (2010), 'Numerical simulation of hydrodynamic behavior of gravity cage in irregular waves', *Aquacultural Engineering* **42**, 90–101.

Dubey, S., Sarvaiya, J. N. & Seshadri, B. (2013), 'Temperature Dependent Photovoltaic (PV) Efficiency and Its Effect on PV Production in the World A Review', *Energy Procedia* **33**, 311–321.

Faltinsen, O. M. (1990), *Sea loads on ships and offshore structures*, Cambridge University Press.

Kristiansen, T. & Faltinsen, O. M. (2015), 'Experimental and numerical study of an aquaculture net cage with floater in waves and current', *Journal of Fluids and Structures* **54**, 1–26.

Lader, P., Kristiansen, D., Alver, M., Bjelland, H. V. & Myrhaug, D. (2017), Classification of aquaculture locations in Norway with respect to wind wave exposure, *in* 'ASME 2017 36th International Conference on Ocean, Offshore and Arctic Engineering - OMAE2017-6165', pp. 1–10.

Li, L., Fu, S., Xu, Y., Wang, J. & Yang, J. (2013), 'Dynamic responses of floating fish cage in waves and current', *Ocean Engineering* **72**, 297–303.

Li, P. (2017), A Theoretical and Experimental Study of Wave-induced Hydroelastic Response of a Circular Floating Collar, PhD thesis, NTNU.

Masson, G. & Brunisholz, M. (2016), 2016 Snapshots of global photovoltaic markets, Technical report, International Energy Agency.

Myrhaug, D. & Lian, W. (2009), *Marine Dynamics, Irregular Waves*, Kompendieforlaget.

Newman, J. (1977), 'The motions of a floating slender torus', *J . Fluid Mech* **83**(4), 721–735.

Norwegian standard (2003), 'Norwegian standard NS 9415'.

Rahman, M., Hasanuzzaman, M. & Rahim, N. (2015), 'Effects of various parameters on PV-module power and efficiency', *Energy Conversion and Management* **103**, 348–358.

Reindl, T. (2018), 'At the heart of floating solar: Singapore', *Power PV Tech* **14**, 18–23.

Santafé, M. R., Ferrer Gisbert, P. S., Sánchez Romero, F. J., Torregrosa Soler, J. B., Ferrán Gozálvez, J. J. & Ferrer Gisbert, C. M. (2014), 'Implementation of a photovoltaic floating cover for irrigation reservoirs', *Journal of Cleaner Production* **66**, 568–570.

SINTEF Ocean (2014), 'Towing Tank', https://www.sintef.no/en/all-laboratories/towing-tanks/. Accessed on 12.04.2018.

Stansberg, C. T. (1993), 'Propagation-dependent spatial variations observed in wave trains generated in a long wave tank', *Data Report* **490030.01**.

Steen, S. (2014), *Experimental Methods in Marine Hydrodynamics*, revised edn, NTNU - Department of Marine Technology, Trondheim.

Trapani, K. & Millar, D. L. (2013), 'Proposing offshore photovoltaic (PV) technology to the energy mix of the Maltese islands', *Energy Conversion and Management* **67**, 18–26.

Trapani, K., Millar, D. L. & Smith, H. C. (2013), 'Novel offshore application of photovoltaics in comparison to conventional marine renewable energy technologies', *Renewable Energy* **50**, 879–888.

Trapani, K. & Redón Santafé, M. (2015), 'A review of floating photovoltaic installations: 2007-2013', *Progress in Photovoltaics: Research and Applications* **23**(4), 524–532.

United Nations (2015), 'Paris Agreement', https://treaties.un.org/Pages/ViewDetails.aspx?src=TREATY&mtdsg_no=XXVII-7-d&chapter=27&clang=_en. Accessed on 25.06.2018.

Xu, T.-J., Dong, G.-H., Zhao, Y.-P., Li, Y.-C. & Gui, F.-K. (2011), 'Analysis of hydrodynamic behaviors of gravity net cage in irregular waves', *Ocean Engineering* **38**, 1545–1554.

APPENDIX A

Information From Test Setup

This chapter contains additional information about the model setup.

A.1   Floating Collar Specifications

Specifications of floating collar provided by SINTEF Ocean.

1.1 Flytekrage

Modellen av flytekragen er bygd opp av 2 indre kjerner av PVC bolt med korrekt bøyestivhet. Utenpå boltene ble korte stykker av spesialbygde flytelegemer med riktig diameter og oppdrift tredd. Små avstandsstykker ble innsatt mellom hvert flytelegeme for å hindre kontakt ved bøying og derved endring av bøyestivheten.

Spesialtilpassede klammer ble bygd i plast og holdt de 2 flyterørene sammen med riktig avstand. Oppå hvert klammer ble det limt vertikale stolper med føringer for en tynn slange. En fleksibel slange ble tredd igjennom hver stolpe for å simulere rekkverk. Selve rekkverks-slangen inngikk ikke i noen form for hydrodynamisk modellering, og ble bare satt på av visuelle hensyn. Det ble valgt helt slakt for ikke å bidra til noen form for bøyestivhet. Flytekragen har for disse testene totalt 40 klammer. Notposen var innfestet til hvert av de modellerte klamrene.

Den spesifikke flyteevnen til hvert av flyte-rørene var 0.20, dvs. tørrvekten målt i forhold til oppdriften av fullt neddykket rør. Detaljer av prototyp- og modell-dataene er vist i Tabell 3.1.

Bilde av flyteringen som modellert er vist på Figur 3.3.
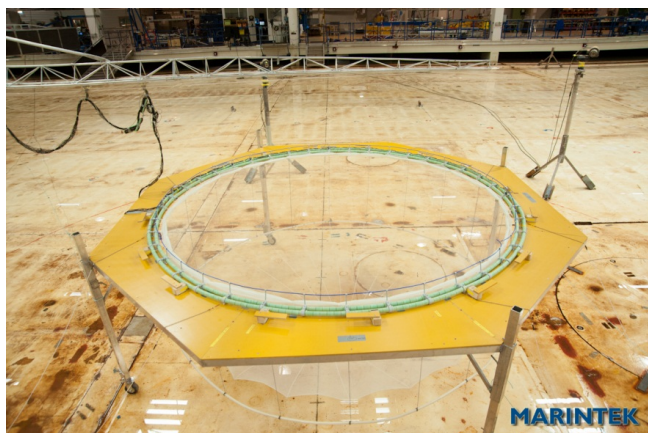
Figur 3.3: Oversiktsbilde av flyteringen.

Bilde av detalj av flyteringen er vist på Figur 3.4.

Figur 3.4: Detalj av flyteringen.

Table 3.1:   Merd-dimensjoner, fullskala og modell.

Merd-del	Symbol	Enhet	Spesifisert FS verdi	Spesifisert MS verdi	Modellert verdi
Flytering:					
Diameter, indre	D_{Horis}	m	62.5	3.125	3.13
Omkrets, innvendig	O_{innv}	m	196.25	9.813	9.81
Rør-diameter	$D_{Rør}$	mm	630	32.5	32.5
Veggtykkelse rør	t	mm	35.5		
Diameter / veggtykkelse	SDR	-	17.6		
Materiale	HDPE	-			
Elastisitetes-modul	E-modul	MPa	1100		
Bøyestivhet	EI	Nm^2	3 375 479	1.0	1.7
Flyteevne			0.2	0.2	0.2

Innvendig omkrets er 9.81 m

40 klammer ->

Avstand mellom hvert

klammer er 0.245m

Høyden på rekkverket fra toppen av flyteringen

er 80 mm
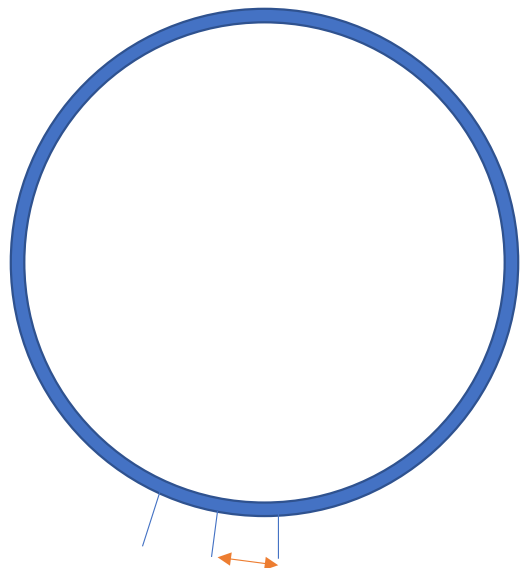
A.2 Marker Placement
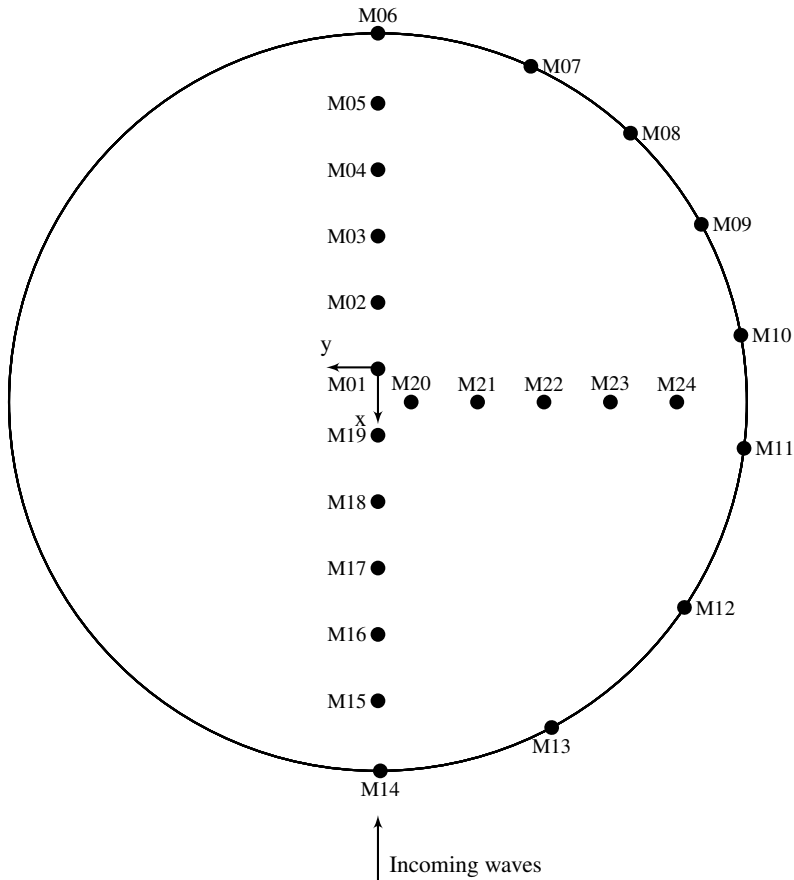
Figure A.1: *Test 2000. Approximate location of markers for test 2000, where the model had no panels. Exact coordinates presented in Table A.1.*

Table A.1: *x- and y-coordinates of markers in test 2000, see locations in Figure A.1*

Marker	(x,y) [m]	Marker	(x,y) [m]	Marker	(x,y) [m]
M01	Origo: (0,0)	M09	(-0.61,-1.37)	M17	(0.89,0.00)
M02	(-0.30,-0.01)	M10	(-0.14,-1.54)	M18	(0.59,-0.01)
M03	(-0.60,0.00)	M11	(0.33,-1.54)	M19	(0.29,0.00)
M04	(-0.90,-0.01)	M12	(1.01,-1.28)	M20	(0.14,-0.15)
M05	(-1.21,-0.01)	M13	(1.52,-0.74)	M21	(0.14,-0.44)
M06	(-1.42,0.00)	M14	(1.70,-0.01)	M22	(0.15,-0.74)
M07	(-1.27,-0.64)	M15	(1.49,0.00)	M23	(0.14,-1.05)
M08	(-0.99,-1.07)	M16	(1.19,0.00)	M24	(0.14,-1.35)
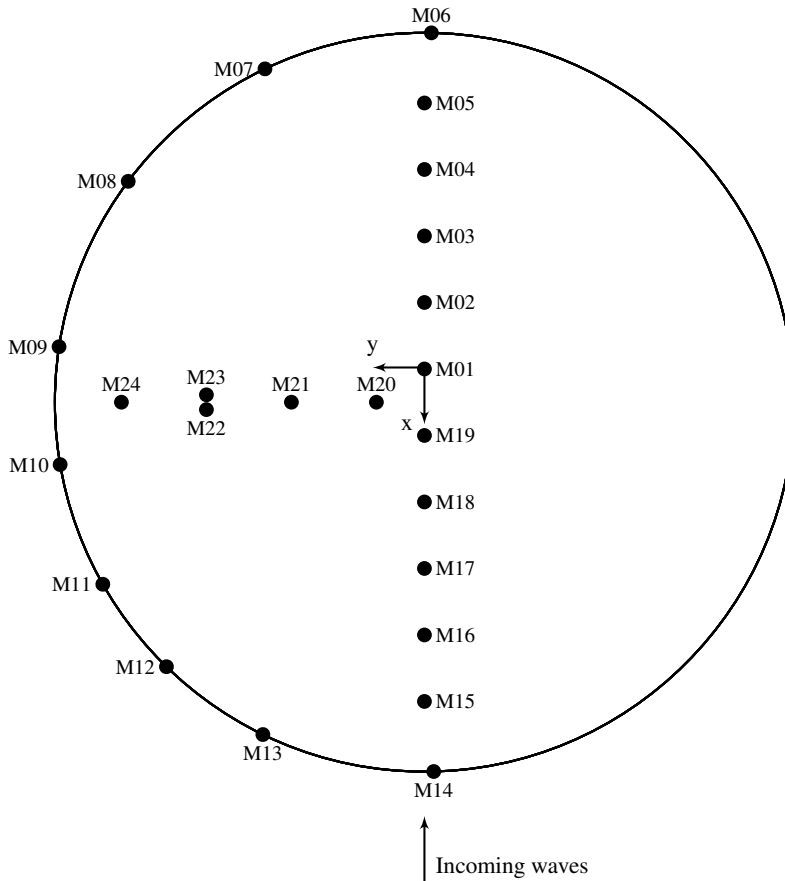
Figure A.2: *Test 3000. Approximate location of markers for test 3000, where the model had panels. Exact coordinates presented in Table A.2.*

Table A.2: *x- and y-coordinates of markers in test 3000, see locations in Figure A.2. Origo is located at the position of marker M01.*

Marker	(x,y) [m]	Marker	(x,y) [m]	Marker	(x,y) [m]
M01	Origo: (0,0)	M09	(-0.05,1.49)	M17	(0.84,-0.01)
M02	(-0.24, 0.00)	M10	(0.43,1.49)	M18	(0.59,-0.00)
M03	(-0.49, 0.01)	M11	(0.93,1.33)	M19	(0.35,-0.00)
M04	(-0.73,0.01)	M12	(1.27,1.06)	M20	(0.24,0.14)
M05	(-0.97,0.01)	M13	(1.54,0.67)	M21	(0.24,0.50)
M06	(-1.39,-0.03)	M14	(1.72,-0.04)	M22	(0.29,0.85)
M07	(-1,22,0.67)	M15	(1.32,-0.01)	M23	(0.20,0.86)
M08	(-0.74,1.23)	M16	(1.08,-0.01)	M24	(0.25,1.21)
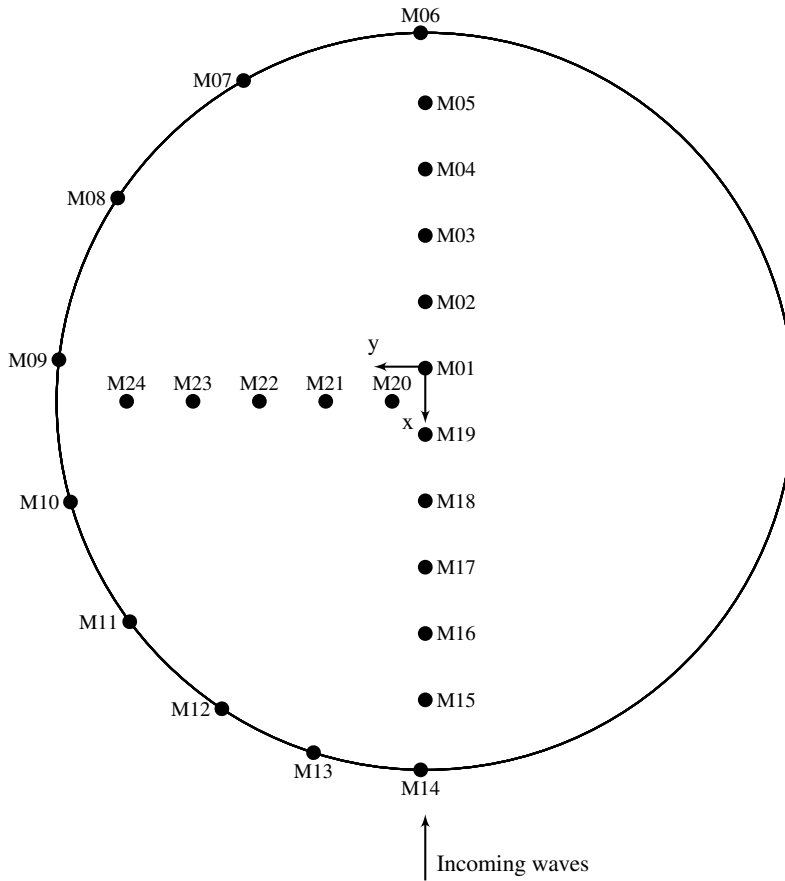
Figure A.3: *Test 4000. Approximate location of markers for test 4000, where the model had panels that where rotated 30 degrees. Exact coordinates presented in Table A.3.*

Table A.3: *x- and y-coordinates of markers in test 4000, see locations in Figure A.3*

Marker	(x,y) [m]	Marker	(x,y) [m]	Marker	(x,y) [m]
M01	(0,0)	M09	(0.03,1.56)	M17	(0.99,0.04)
M02	(-0.28-0.00,)	M10	(0.64,1.52)	M18	(0.71,0.04)
M03	(-0.57,-0.01)	M11	(1.16,1.26)	M19	(0.42,0.04)
M04	(-0.85,-0.01)	M12	(1.53,0.87)	M20	(0.18,0.33)
M05	(-1.13,-0.01)	M13	(1.71,0.47)	M21	(0.18,0.58)
M06	(-1.35,0.02)	M14	(1.77,0.02)	M22	(0.19,0.83)
M07	(-1.16,0.78)	M15	(1.55,0.05)	M23	(0.18,1.08)
M08	(-0.67,1.32)	M16	(1.27,0.05)	M24	(0.19,1.31)

A.3   Channel Lists

This section contains the full channel list for each test.

A.3.1   Test 2000

Table A.4: *Channel list for test 2000 (see Table 2.5).*

Channel name	Sample frequency [Hz]	Explanation
DAQ time stamps	50	Time stamps for 50/25 Hz measurements
DAQ time stamps SR2	200	Time stamps for 200 Hz measurements
DAQ time stamps absolute	50	Total time passed
DAQ time stamps absolute SR2	200	Total time passed
bm_upper_ctrl	50	Signal to upper wavemaker flap
bm_lower_ctrl	50	Signal to lower wavemaker flap
bm_upper_meas	50	Position of wavemakers upper flap
bm_lower_meas	50	Position of wavemakers lower flap
wave_probe_1	50	Measured water level at wave probe 1
wave_probe_2	50	Measured water level at wave probe 2
acq_status	50	Data acquisition status
start_stop_pulse	50	Start pulse for measurements
acq_time	50	Data acquisition time
framenumber	50	No of frames for Oqus
errorcode	50	Oqus error code
x01-x24	50	x-position of markers M01-M24
y01-y24	50	y-position of markers M01-M24
z01-z24	50	z-position of markers M01-M24
res01-res24	50	Residual for markers M01-M24
NTP time stamps QX	50	Time stamp for sampling rate 1
pos_carriage_analog_GV	200	Carriage position in towing tank
speed_carriage_analog_GV	200	Carriage speed
acqstatus	200	Data acquisition status
speed_carriage	200	Carriage speed
NTP time stamps QX SR2	200	Time stamp for sampling rate 2
WAVE_01	200	Wave probe 1 in front of model
line0_Z8758	200	Tension fore mooring line
line90_Z8759	200	Tension left mooring line
line180_Z8760	200	Tension aft mooring line
line270_Z8763	200	Tension right mooring line

A.3.2 Tests 3000, 4000 and 5000

Table A.5: *Channel list for tests 3000 4000 and 5000 (see Table 2.5).*

Channel name	Sample frequency [Hz]	Explanation
DAQ time stamps	25	Time stamps for 50/25 Hz measurements
DAQ time stamps SR2	200	Time stamps for 200 Hz measurements
DAQ time stamps absolute	25	Total time passed
DAQ time stamps absolute SR2	200	Total time passed
bm_upper_ctrl	200	Signal to upper wavemaker flap
bm_lower_ctrl	200	Signal to lower wavemaker flap
bm_upper_meas	200	Position of wavemakers upper flap
bm_lower_meas	200	Position of wavemakers lower flap
wave_probe_1	200	Measured water level at wave probe 1
wave_probe_2	200	Measured water level at wave probe 2
acq_status	200	Data acquisition status
start_stop_pulse	200	Start pulse for measurements
acq_time	200	Data acquisition time
framenumber	25	No of frames for Oqus
errorcode	25	Oqus error code
x01-x24	25	x-position of markers M01-M24
y01-y24	25	y-position of markers M01-M24
z01-z24	25	z-position of markers M01-M24
res01-res24	25	Residual for markers M01-M24
NTP time stamps QX	25	Time stamp for sampling rate 1
pos_carriage_analog_GV	25	Carriage position in towing tank
speed_carriage_analog_GV	25	Carriage speed
acqstatus	200	Data acquisition status
speed_carriage	200	Carriage speed
NTP time stamps QX SR2	200	Time stamp for sampling rate 2
WAVE_01	25	Wave probe 1 in front of model
WAVE_02	25	Wave probe 2 next to WAVE_01
line0_Z8758	200	Tension fore mooring line
line90_Z8759	200	Tension left mooring line
line180_Z8760	200	Tension rear mooring line
line270_Z8763	200	Tension right mooring line
B_0	200	Back panel strain gage 0°
B__45	200	Back panel strain gage -45°
B_45	200	Back panel strain gage 45°
M_0	200	Middle panel strain gage 0°
M__45	200	Middle panel strain gage -45°
M_45	200	Middle panel strain gage 45°
S_0	200	Side panel strain gage 0°
S__45	200	Side panel strain gage -45°
S_45	200	Side panel strain gage 45°
F_0	200	Front panel strain gage 0°
F__45	200	Front panel strain gage -45°
F_45	200	Front panel strain gage 45°
FA_0	200	Front aluminum panel strain gage 0°
FA__45	200	Front aluminum panel strain gage -45°
FA_45	200	Front aluminum panel strain gage 45°

A.3.3 Test 8000

Table A.6: *Channel list for test 8000 (see Table 2.5).*

Channel name (Sample frequency [Hz])	Explanation	
DAQ time stamps SR2	200	Time stamps for 200 Hz measurements
DAQ time stamps absolute SR2	200	Total time passed
bm_upper_ctrl	200	Signal to upper wavemaker flap
bm_lower_ctrl	200	Signal to lower wavemaker flap
bm_upper_meas	200	Position of wavemakers upper flap
bm_lower_meas	200	Position of wavemakers lower flap
acq_status	200	Data acquisition status
NTP time stamps QX SR2	200	Time stamp for sampling rate 2
pos_carriage_analog_GV	200	Carriage position in towing tank
speed_carriage_analog_GV	200	Carriage speed
acqstatus	200	Data acquisition status
speed_carriage	200	Carriage speed
WAVE_01	200	Wave probe 1 in front of model
WAVE_02	200	Wave probe 2 at model position

A.4   Sensor calibration

A.4.1   Wave Probe Calibration
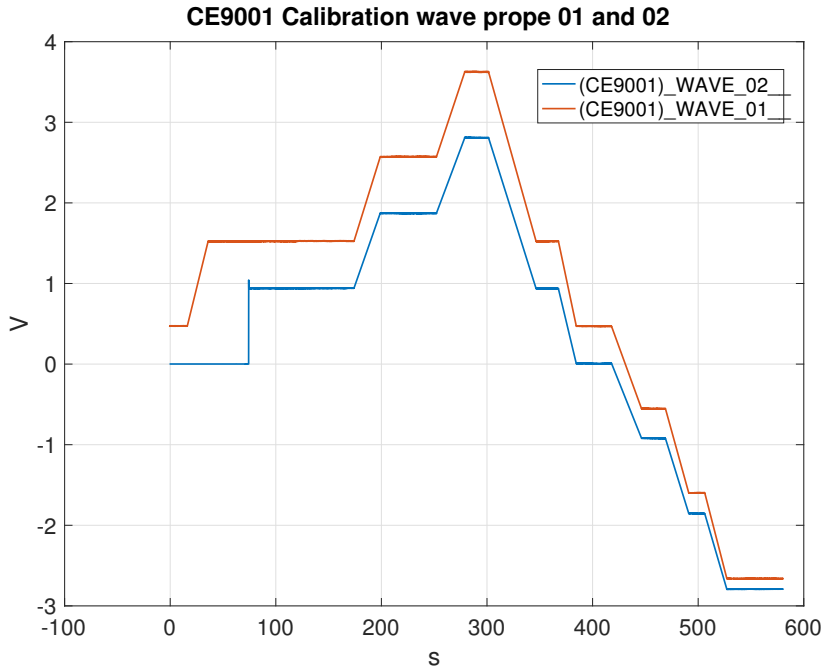
Figure A.4: *Calibration of wave probes 01 and 02. The probes are submerged to known submergence levels, and the voltage output is saved. The calibration factors are decided based on the calibration curve.*

(a) *Calibration factor check 1.*

(b) *Calibration factor check 2.*
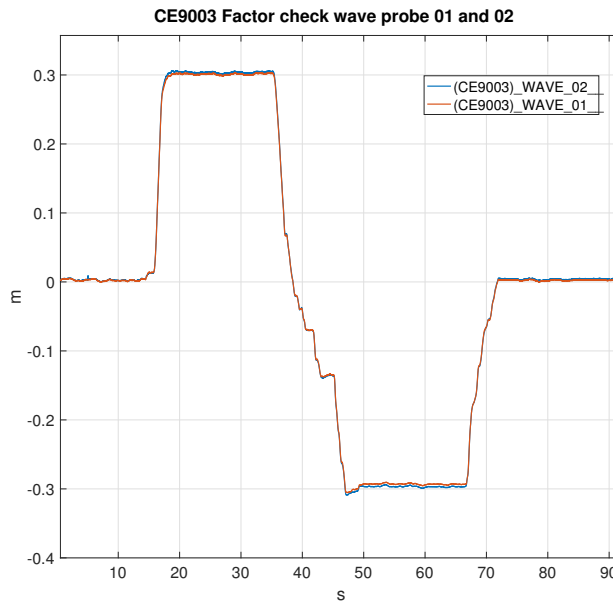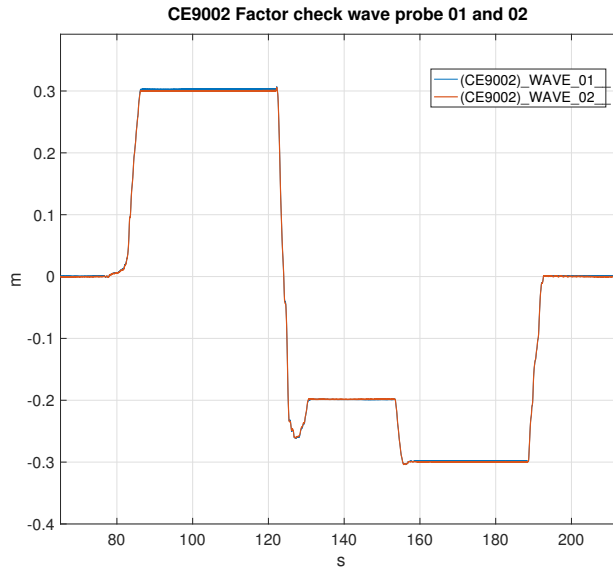
Figure A.5: *Check of calibration factor after calibration (A.5a), and after -1% correction of factor (A.5b).*

A.4.2 Load Cell Calibration
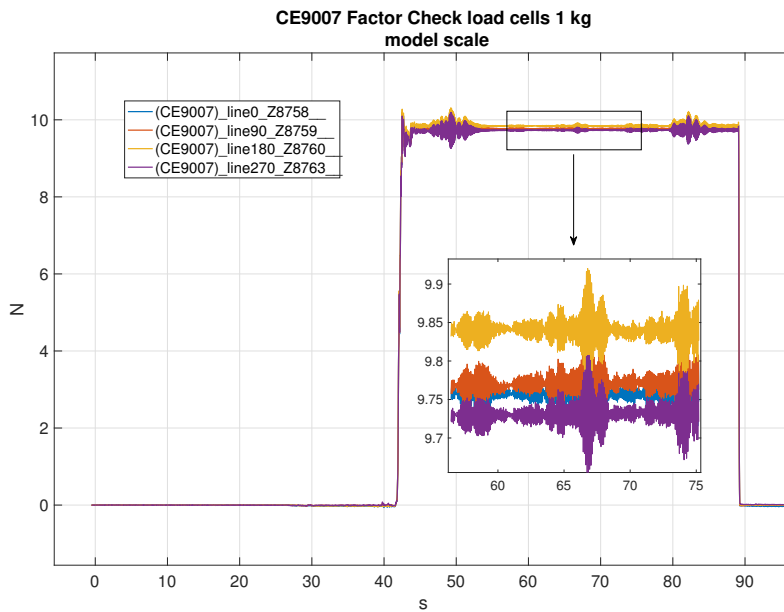
Figure A.6: *Check of calibration factors for load cells on the four mooring lines positioned on 0°, 90°, 180° and 270°. Plot shows less than ± 1% error in measurements.*

APPENDIX B

Model Test

B.1 Test Log

This chapter contains the log for the full experiment log and the logged temperatures for each day. Some measurements are considered irrelevant by the author and are left out from the log. Temperatures were only logged while running tests, this is the reason for intervals with no measurements.

Table B.1: *Test log from model tests. Some measurements are considered irrelevant by the author and are left out of this log.*

Date	Time	Test No	Comment
26.02.2018	12:48	9001	Calibration of wave probes
	14:10	9002	Factor check
	14:27	9003	Factor check after correction
	15:33	8010	Regular wave H2.3 T8.6
	1600	8020	Regular wave H2.0 T8.0
			Water temperature 13.9°C
	16:40	8030	Regular wave H1.5 T6.9
	16:55	8080	Regular wave H0.3 T3.3
			Water temperature 13.7°C
	17:26	8070	Regular wave H0.4 T3.6
	17:44	8060	Regular wave H0.5 T4.0
			Water temperature 13.4°C
	17:57	8050	Regular wave H0.7 T4.6
	18:12	8040	Regular wave H1.0 T5.7
			Water temperature 13.4°C
	18:28	8160	Regular wave H0.6 T3.3

Date	Time	Test No	Comment
26.02.2018	18:44	8150	Regular wave H0.7 T3.6
			Water temperature 12.7°C
	19:00	8140	Regular wave H0.8 T4.0
	19:20	8130	Regular wave H1.1 T4.6
			Water temperature 13.9°C
	19:38	8120	Regular wave H1.7 T5.7
	19:53	8110	Regular wave H2.5 T6.9
			Water temperature 13.8°C
	20:12	8100	Regular wave H3.3 T8.0
	20:27	8090	Regular wave H3.9 T8.6
			Water temperature 13.1°C
	20:42	8170	Regular wave H7.7 T8.6
27.02.18	08:07		Water temperature 13.0°C
	08:12	8240	Regular wave H1.1 T3.3
			Very unstable measurements
	08:27	8230	Regular wave H1.3 T3.6
			Very unstable measurements
	08:32	-	Water temperature 13.1°C
	08:45	8220	Regular wave H1.7 T4.0
	09:00	8210	Regular wave H2.2 T4.6
	09:12	-	Water temperature 12.9°C
	09:16	8200	Regular wave H3.3 T5.7
	09:29	8190	Regular wave H5.0 T6.9
	09:47	-	Water temperature 13.0°C
	09:56	8180	Regular wave H6.7 T8.0
	10:14	-	Water temperature 13.3°C
	10:56	8520	Irregular wave Hs2.5 Tp6.0 G2.0 RN9
	11:44	-	Water temperature 13.6°C
	11:46	8530	Irregular wave Hs1.5 Tp4.5 G2.0 RN9
	12:53	-	Set up model configuration 2000
	15:15	9007	Factor check load cells
	16:25	-	Test Oqus system
	16:59	-	Water temperature 13.0°C
	17:15	9010	Pre-tension mooring lines
	17:31	2010	Regular wave H2.3 T8.6
	17:49	2020	Regular wave H2.0 T8.0
	18:09	2030	Regular wave H1.5 T6.9
	18:26	2040	Regular wave H1.0 T5.7
	18:31	-	Water temperature 13.8°C
	18:42	2050	Regular wave H0.7 T4.6
	18:58	2060	Regular wave H0.5 T4.0
			Unstable run
	19:12	-	Water temperature 13.9°C
	19:16	2070	Regular wave H0.4 T3.6
	19:33	2080	Regular wave H0.3 T3.3

Date	Time	Test No	Comment
27.02.2018	19:39	-	Water temperature 13.3°C
	19:47	2090	Regular wave H3.9 T8.6
28.02.2018	07:25	-	Water temperature 14.5°C
	07:26	2100	Regular wave REG H3.3 T8.0
	07:45	2110	Regular wave H2.5 T6.9
	08:00	-	Water temperature 14.1°C
	08:04	2120	Regular wave H1.7 T5.6
	08:20	2130	Regular wave H1.1 T4.6
	08:33	-	Water temperature 13.6°C
	08:35	2140	Regular wave H0.8 T4.0
			Unstable due to water not calm enough
	0852	2150	Regular wave H0.7 T3.6
			More visible flapping in membrane
	09:04	-	Water temperature 13.8°C
	09:07	2160	Regular wave H0.6 T3.3
	09:26	2170	Regular wave H7.7 T8.6
			Freeboard stopped over-topping
	09:33	-	Water temperature 13.3°C
	09:43	2180	Regular wave H6.7 T8.0
			Freeboard stopped over-topping
	10:00	2190	Regular wave H5.0 T6.9
			Water washing over on first wave (2200ml)
	10:12	-	Water temperature 12.9°C
	10:21	2200	Regular wave H3.3 T5.7
			Water washing over on first wave (620ml)
	10:40	2210	Regular wave H2.2 T4.6
			Water washing over on first wave (770ml)
	11:01	-	Water temperature 13.5°C
	11:13	2220	Regular wave H1.7 T4.0
	11:48	2061	Regular wave H0.5 T4.0
			Repetition run 2060, more stable
	12:10	2230	Regular wave H1.3 T3.6
			Tried less steep wave, still unstable
	12:37	2141	Regular wave H0.8 T4.0
			Repetition run 2140, more stable
	13:00	9011	Test of wave probes
			Added wave probe 2 next to wave probe 1
	13:21	2062	Regular wave H0.5 T4.0
			Repetition run 2060
	13:56	2530	Irregular wave Hs1.5 Tp4.5 G2.0 RN9
			Water washing over (2520ml)
			Problems with Oqus
	14:55	-	Water temperature 13.0°C
	16:01	2063	Regular wave H0.5 T4.0
			Repetition run 2060
	16:20	-	Water temperature 14.0°C

Date	Time	Test No	Comment
28.02.2018	16:24	2520	Irregular wave Hs2.5 Tp6.0 G2.0 RN9
			Problems with wave maker
01.03.2018	09:00	-	Wave maker fixed
	10:30	-	Communication test
	10:53	2064	Regular wave H0.5 T4.0
			Repetition run 2060
	11:04	-	Water temperature 13.9°C
	11:19	2082	Regular wave H0.3 T3.3
			Repetition run 2080
	11:43	2531	Irregular wave Hs1.5 Tp4.5 G2.0 RN9
			Repetition run 2531
			Water washing over (2100ml)
	12:08	-	Oqus failure
	12:41	-	Water temperature 13.2°C
	13:27	2523	Irregular wave Hs2.5 Tp6.0 G2.0 RN9
			Repetition run 2520
			Water washing over (14220ml)
	14:09	-	Start process of changing model configuration
	15:08	-	Change measurement frequency from 50 to 25 Hz
	19:38	-	Model with panels, 3000, in place
02.03.2018	08:00	-	Set up Oqus and strain gages
	08:30	-	Water temperature 14.5°C
	08:40	-	Test of Oqus
	09:03	3010	Regular wave H2.3 T8.6
			Oqus failure, need rerun
	09:22	3011	Regular wave H2.3 T8.6
	09:47	3020	Regular wave H2.0 T8.0
	10:03	-	Water temperature 14.2°C
	10:10	3030	Regular wave H1.5 T6.9
			Strain gages drift
	10:13	9017	Check strain gage drift
	10:33	3140	Regular wave H0.8 T4.0
	10:56	3150	Regular wave H0.7 T3.6
			Smaller motions that without panels
	11:18	3530	Irregular wave Hs1.5 Tp4.5 G2.0 RN9
			Water washing over (1340ml)
	13:26	-	Water temperature 14.0°C
	13:41	3080	Regular wave H0.3 T3.3
			Water temperature 13.3°C
	1402	3070	Regular wave H0.4 T3.6
			Water temperature 12.6°C
	14:23	3060	Regular wave H0.5 T4.0
			Water temperature 13.7°C
	14:50	3050	Regular wave H0.7 T4.6
			Water temperature 13.8°C

Date	Time	Test No	Comment
02.03.2018	15:12	3040	Regular wave H1.0 T5.7
			Water temperature 13.8°C
	15:39	3160	Regular wave H0.6 T3.3
			Water temperature 13.8°C
	15:41	9018	Check drift in strain gages
	16:01	3130	Regular wave H1.1 T4.6
			Water temperature 13.4°C
	16:24	3120	Regular wave H1.7 T5.7
	16:47	3110	Regular wave H2.5 T6.9
			Water temperature 14.0°C
	17:14	3100	Regular wave H3.3 T8.0
	17:38	3090	Regular wave H3.9 T8.6
			Water temperature 14.0°C
	18:07	3170	Regular wave H7.7 T8.6
03.03.2018	10:24	3220	Regular wave H1.7 T4.0
			Water temperature 14.5°C
			Water washing over on first wave (1610ml)
	10:58	3210	Regular wave H2.2 T4.6
			Water temperature 13.8°C
	11:23	3200	Regular wave H3.3 T5.7
			Water temperature 13.3°C
			Water washing over on first wave (1000ml)
	11:56	3190	Regular wave H5.0 T6.9
			Water washing over on first wave (2300ml)
			Much local wave action in membrane
	12:30	3180	Regular wave H6.7 T8.0
			Water temperature 13.2°C
	13:01	3141	Regular wave H0.8 T4.0
			Water temperature 13.1°C
			Repetition run 3140
	13:24	3142	Regular wave H0.8 T4.0
			Water temperature 13.4°C
			Repetition run 3140
	13:51	3143	Regular wave H0.8 T4.0
			Water temperature 13.°C
			Repetition run 3140
	14:21	3144	Regular wave H0.8 T4.0
			Water temperature 13.8°C
			Repetition run 3140
	14:41	3145	Regular wave H0.8 T4.0
			Water temperature 13.5°C
			Repetition run 3140
	15:05	3520	Irregular wave Hs2.5 Tp6.0 G2.0 RN9
			Water temperature 13.5°C
	16:58	-	Model rotated 30°, test 4000

Date	Time	Test No	Comment
05.03.2018	18:14	-	Set up Oqus
	09:00	4080	Regular wave H0.3 T3.3
			Two defect strain gages disabled
			Water temperature 14.5°C
	09:23	4070	Regular wave H0.4 T3.6
			Water temperature 13.4°C
	09:47	4060	Regular wave H0.5 T4.0
			Water temperature 14.0°C
	10:16	4050	Regular wave H0.7 T4.6
	10:38	4040	Regular wave H1.0 T5.7
			Water temperature 14.5°C
	11:05	4030	Regular wave H1.5 T6.9
			Water temperature 14.5°C
	11:30	4020	Regular wave H2.0 T8.0
			Water temperature 14.2°C
	11:58	4010	Regular wave H2.3 T8.6
			Water temperature 13.9°C
	12:29	4160	Regular wave H0.6 T3.3
			Water temperature 14.0°C
	12:56	4150	Regular wave H0.7 T3.6
			Water temperature 14.1°C
	13:21	4140	Regular wave H0.8 T4.0
			Water temperature 13.1°C
	13:43	4130	Regular wave H1.1 T4.6
			Water temperature 14.3°C
	14:08	4120	Regular wave H1.7 T5.7
			Water temperature 13.9°C
	14:32	4110	Regular wave H2.5 T6.9
			Water temperature 14.4°C
	15:08	4100	Regular wave H3.3 T8.0
			Water temperature 14.1°C
	15:38	4090	Regular wave H3.9 T8.6
	16:09	4220	Regular wave H1.7 T4.0
			Water washing over on last wave (880ml)
	16:35	4210	Regular wave H2.2 T4.6
			Water temperature 13.9°C
			Water washing over on first wave (330ml)
	17:02	4200	Regular wave H3.3 T5.7
			Water temperature 13.9°C
			Water washing over on first wave (420ml)
	17:29	4190	Regular wave H5.0 T6.9
			Water temperature 13.8°C
			Water washing over on first wave (3420ml)
	17:58	4180	Regular wave H6.7 T8.0
			Water temperature 13.8°C

Date	Time	Test No	Comment
05.03.2018	18:24	4170	Regular wave H7.7 T8.6
			Wave crests hit the side bridge on the carriage
	18:53	4530	Irregular wave Hs1.5 Tp4.5 G2.0 RN9
			Water temperature 13.7°C
			Water washing over (3250ml)
	19:54	4520	Irregular wave Hs2.5 Tp6.0 G2.0 RN9
			Water washing over (9000ml)
06.03.2018	08:28	4211	Regular wave H2.2 T4.6
			Repetition run 4210
			Water temperature 14.8°C
	08:53	4212	Regular wave H2.2 T4.6
			Repetition run 4210
			Water temperature 14.1°C
	09:17	4213	Regular wave H2.2 T4.6
			Repetition run 4210
			Water temperature 13.9°C
			Water washing over on last waves (900ml)
	09:50	4214	Regular wave H2.2 T4.6
			Repetition run 4210
			Water washing over on last waves (780ml)
	10:09	9019	Measure pre-tension before towing test
			0°: 45.38N, 90°: 10.23N
			180°: 44.60N, 270°: 11.42N
	10:38	5010	Towing, 1 and 2 knots
			Strange measurements
	10:50	5011	Towing, 1 and 2 knots. Repetition run 5010.
			Strange measurements
	11:01	5012	Towing, 1 and 2 knots. Repetition run 5010.
			Strange measurements. Pulley friction
	11:12	5020	Towing 2 and 3 knots.
	11:21	5021	Towing 2 and 3 knots. Repetition run 5020
	12:17	-	Start tidying up

B.2   Temperature Log
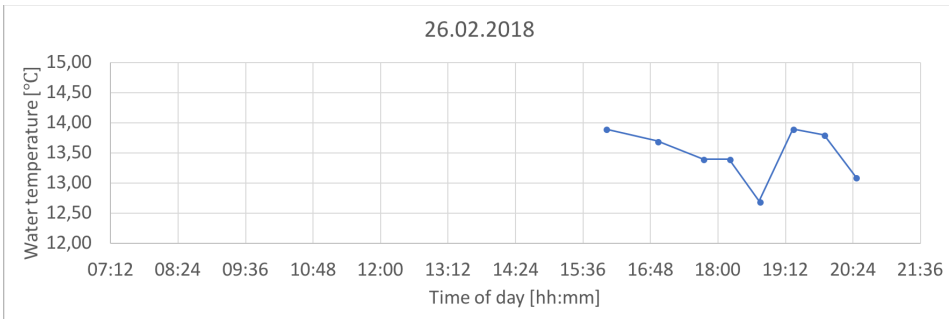
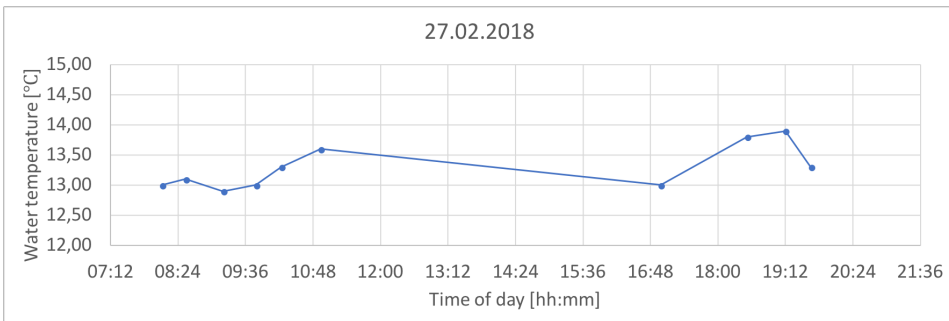**Figure B.1:** *Logged water temperatures 26.02.2018*

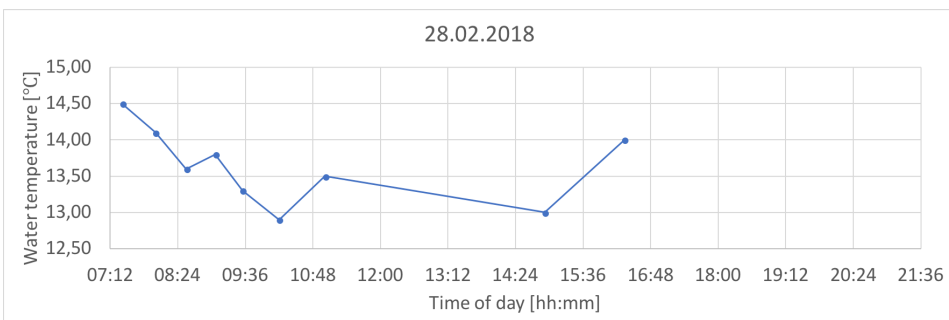**Figure B.2:** *Logged water temperatures 27.02.2018*
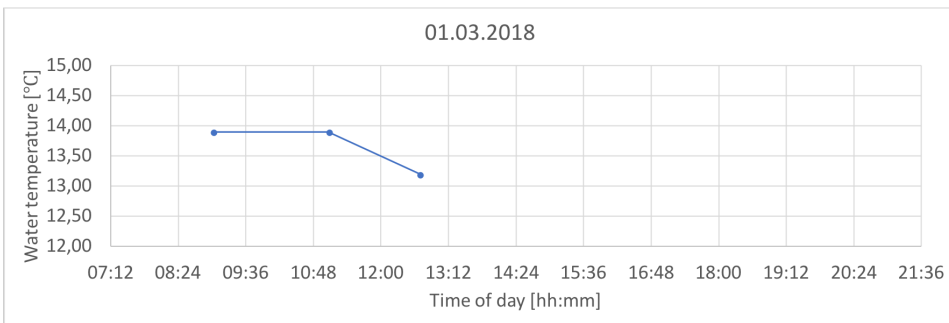

Figure B.3: *Logged water temperatures 28.02.2018*
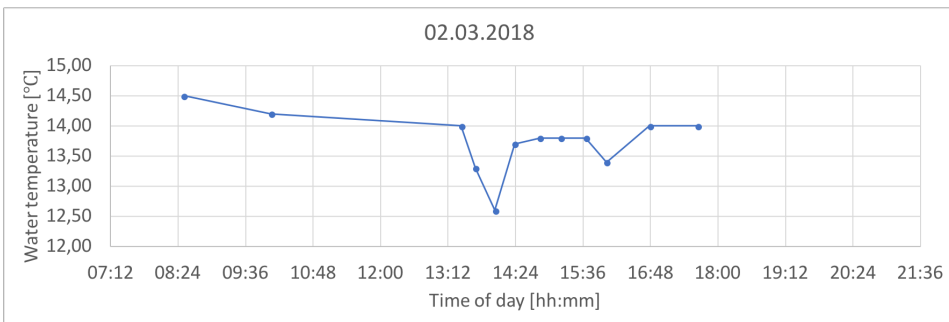
Figure B.4: *Logged water temperatures 01.03.2018*
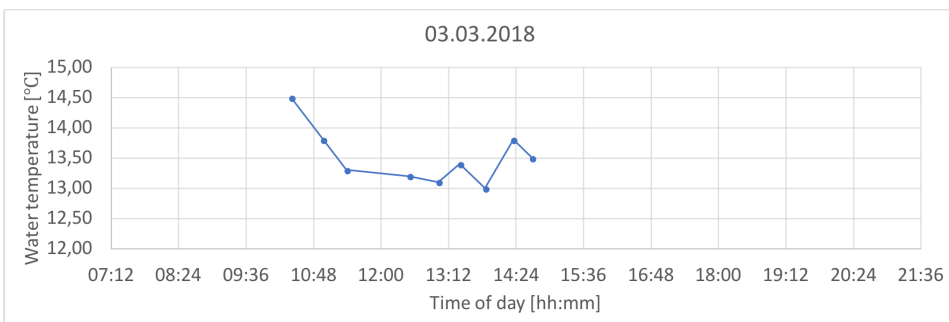

Figure B.5: *Logged water temperatures 02.03.2018*
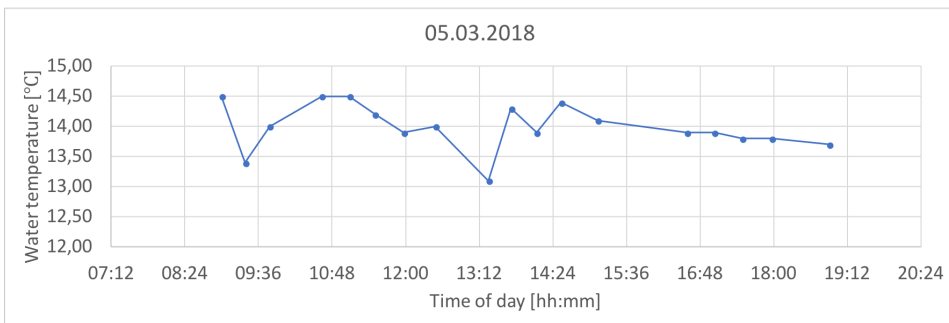

Figure B.6: *Logged water temperatures 03.03.2018*
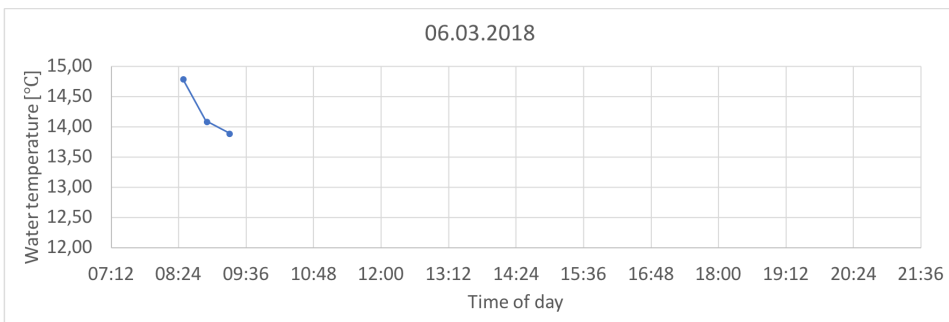
Figure B.7: *Logged water temperatures 05.03.2018*

Figure B.8: *Logged water temperatures 06.03.2018*

APPENDIX C

Additional Results

This chapter contains additional results referred to in the report.
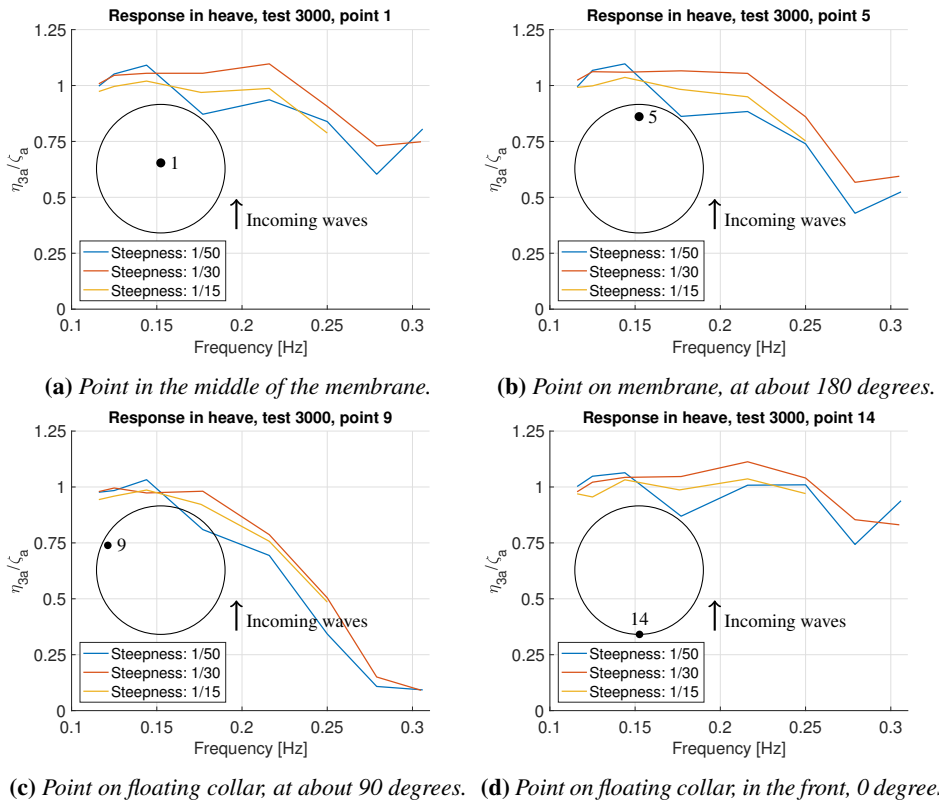
C.1 Steepness Comparisons

(a) *Point in the middle of the membrane.*

(b) *Point on membrane, at about 180 degrees.*

(c) *Point on floating collar, at about 90 degrees.*

(d) *Point on floating collar, in the front, 0 degrees.*

Figure C.1: *Response plot in heave showing the variations with wave steepness for run 3000. Positions of markers are described in Figure 2.9.*

(a) *Point in the middle of the membrane.*

(b) *Point on membrane, at about 180 degrees.*

(c) *Point on floating collar, at about 90 degrees.*

(d) *Point on floating collar, in the front, 0 degrees.*
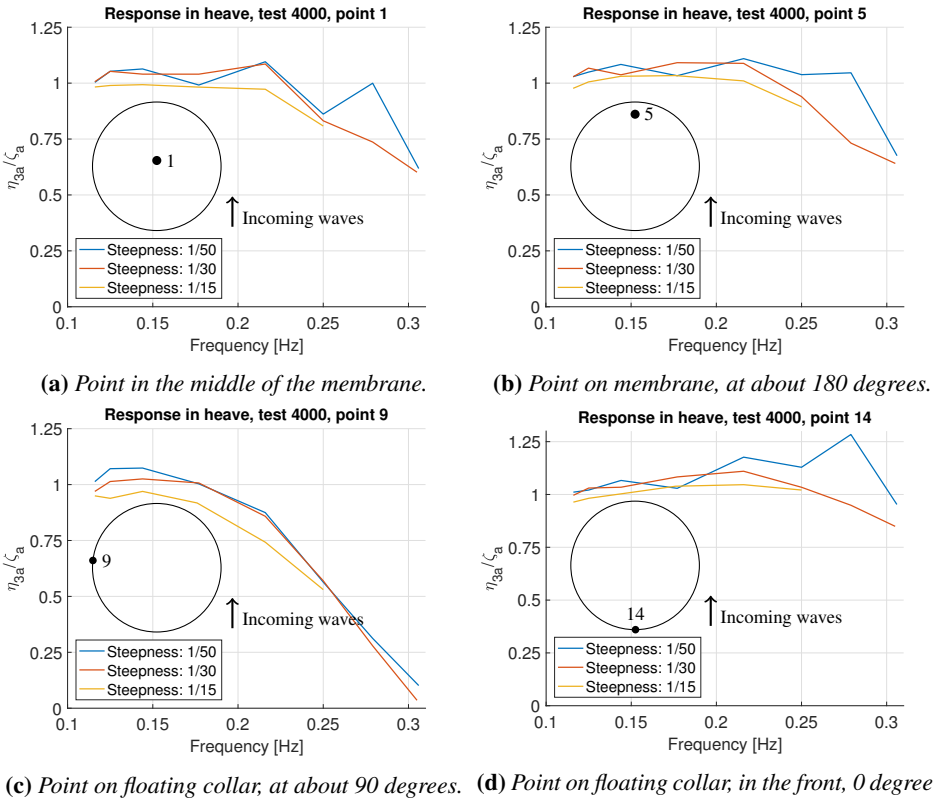
Figure C.2: *Response plot in heave showing the variations with wave steepness for run 4000. Positions of markers are described in Figure 2.9.*
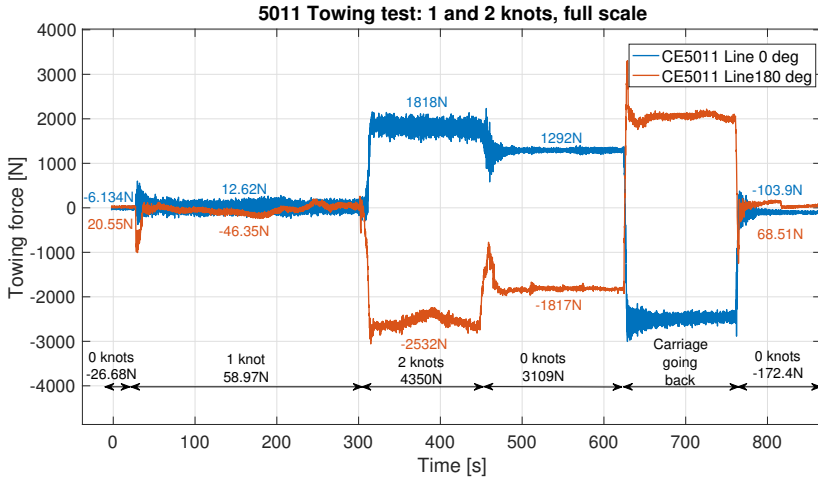
C.2 Towing Test

Figure C.3: *Towing test to find resistance at 1 and 2 knots. Full scale resistance values for each velocity is mean towing force for the current speed.*
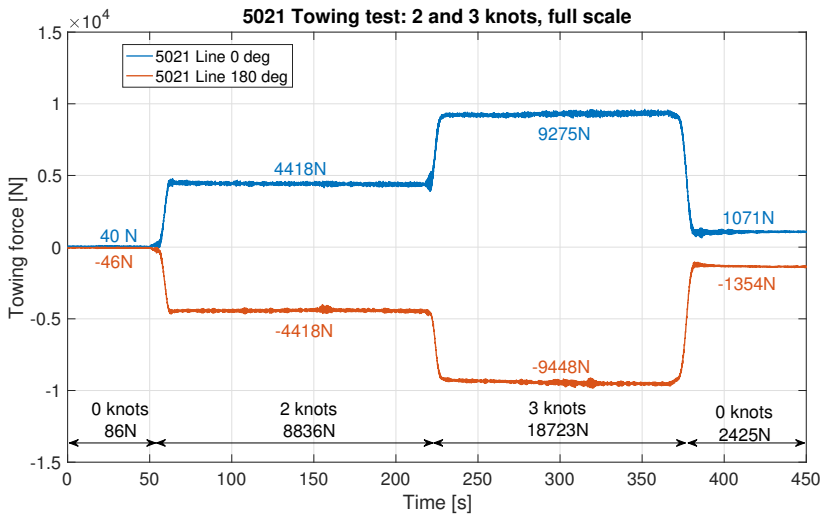

Figure C.4: *Towing test to find resistance at 2 and 3 knots. Full scale resistance values for each velocity is mean towing force for the current speed.*

C.3 Wave Spectra Comparison

(a) *Run 2010/3010.*

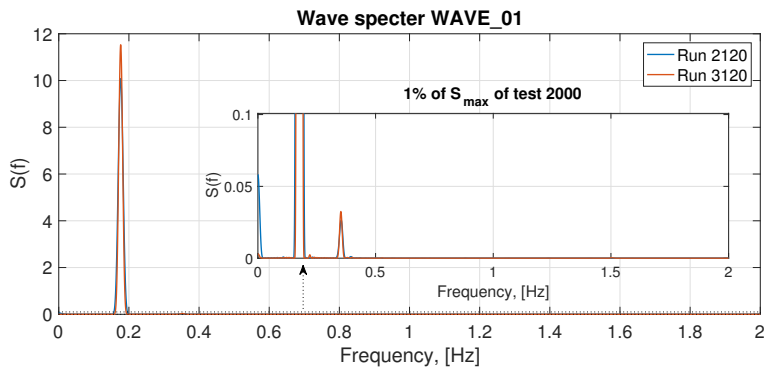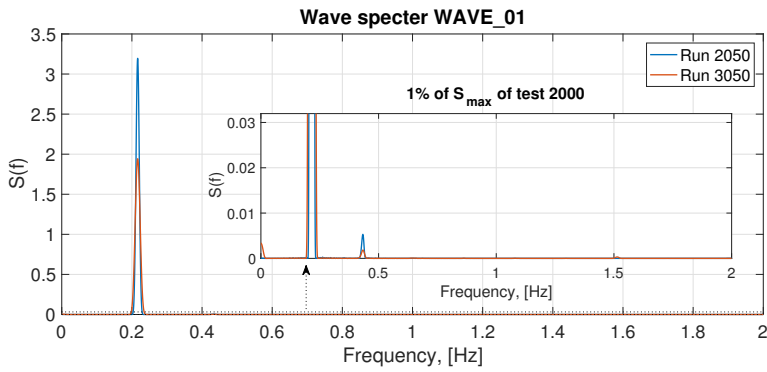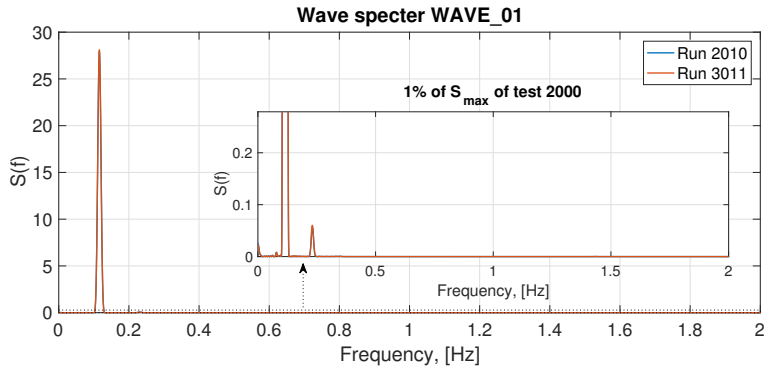**(b)** *Run 2050/3050.*

(c) *Run 2120/3120.*

Figure C.5: *Wave spectrum comparisons for waves sampled at different frequencies. Each plot has one wave sampled at 200Hz and one at 25Hz, plotted for different wave lengths and heights. Both are measurements from wave probe 1 (WAVE_01), which is placed in front of the model. The box shows a zoomed version of the spectra, only showing 1% of the maximum spectrum value of the wave from test 2000.*